Transport Phenomena for Chemical Reactor Design

New Ideas and Corrections by Chapter (Errata and Corrigenda)

Preface

Page xxii 3 lines up from the bottom, remove the comma after Damköhler number

Part 1
Elementary Topics in Chemical Reactor Design

(1) Multiple Chemical Reactions in PFR's & CSTR's

Page#4 2nd sentence of the 2nd paragraph; Which of the following alternatives is more desirable when the inlet molar flowrate of ammonia is 1 g-mol/min; a stoichiometric (1:1) feed of ethylene oxide and ammonia enters the reactor, or a 3:1 molar ratio of ethylene oxide to ammonia enters the reactor? Consider economics qualitatively. Provide support for your answer by calculating ...

Page#7 Equation (1-15) needs script R-sub-j; use old English font for R in (1-15)

Page#10 2 lines above Table 1-1; insert the following paragraph and graphical solution

It is much more desirable to use an excess of ethylene oxide in the feed stream because ethylene oxide participates in all three chemical reactions. An excess of NH_3 will deplete ethylene oxide in the first reaction. This is counter-productive because there will not be a significant amount of ethylene oxide remaining, which is required to generate the desired product in the third reaction. At 325K, 5 atmospheres total pressure, and a 3:1 feed ratio of ethylene oxide to ammonia, a total reactor volume of 75 Litres will yield a desired product (i.e., tri-ethanolamine) molar flowrate of approximately 0.75 g-mol per minute as summarized quantitatively in Table 1-1 and the accompanying figure. For comparison to illustrate the effect of total pressure on reaction kinetics at 325K, an decrease in total pressure from 5 atm. to 3 atm. together with a 3:1 feed ratio of ethylene oxide to ammonia yields the same outlet molar flowrate of tri-ethanolamine when the total reactor volume is 200 Litres. Since the *overall* chemical reaction can be described as 3 moles of ethylene oxide and 1 mole of ammonia producing one mole of tri-ethanolamine, the 3:1 feed ratio of ethylene oxide to ammonia yields an *equilibrium* outlet molar flowrate of 1 g-mol/minute for tri-ethanolamine when reactor volume is exceedingly large.

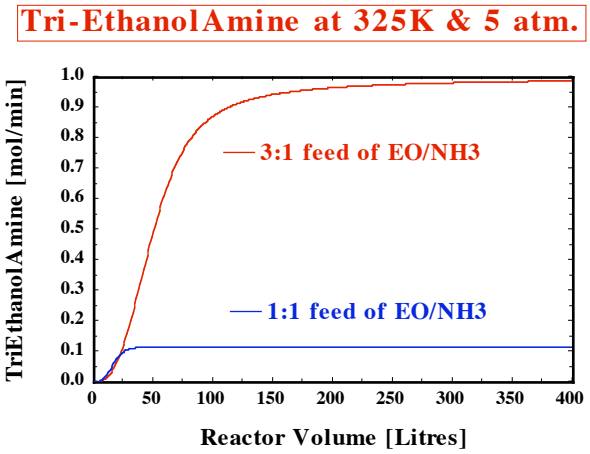

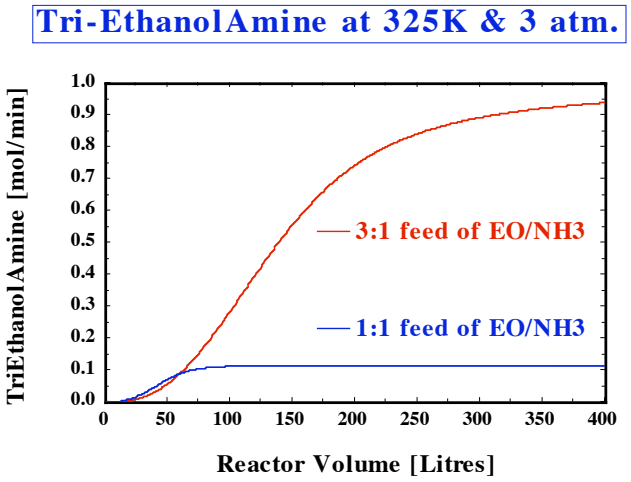

Page#10 caption to Table 1-1; gas-phase PFR operating at 325K and 5 atmospheres total pressure [a]

Page#12 add the word "then" after "other reactions, then" 2 lines above equation (1-26)

Page#12 bottom line; j is not required, then the extent of reaction ξ is analogous to ...

Page#13 first component on the left side of reaction (1-32) should be $C_6H_4Cl_2$

Page#18 middle of the page; reactive intermediate C, *then* it is possible to verify the molar density ratio, C/A, which is given in the problem statement.

Page#19 bottom line of text; irreversible, *then* the generic form of each rate law is

Page#25 near the bottom of the page, after CSTR design strategy#2

Numerical verification of this strategy is summarized graphically for third-order irreversible chemical kinetics, when the rate law depends on the molar densities of reactants A and B. The appropriate objective statement and system of equations required to prove this design strategy are outlined below;

Objective statement

Consider the generic liquid-phase chemical reaction where one mole of key limiting reactant A and two moles of reactant B combine to form products;

$$A + 2B \overset{k_{3,forward,C}(T)}{\Rightarrow} products$$

The reaction is *elementary and irreversible*, and the feed stream to a liquid-phase isothermal CSTR is stoichiometric in reactants A and B (i.e., 1:2). The time constant for convective mass transfer through the reactor is $\tau = V_{CSTR}/q$, and λ is the time constant for 3rd-order irreversible chemical reaction [i.e., $\lambda = (C_{A,inlet})^{1-n}/k_{n,forward,C}$, with n=3].

Generate numerical results that support the important reactor design strategy which can be stated as follows; *"under conditions of a liquid phase volumetric flow rate that is the same for both examples, the reactor volume required to achieve a specified final conversion of reactant A in the exit stream of one CSTR is larger and economically less attractive than the overall reactor volume required to achieve the same final conversion in the exit stream of the last CSTR in a series configuration of 3 equi-sized reactors"*. Demonstrate that the initial (i.e., capital) cost for the train of 3 CSTRs is 10-fold less expensive than the initial cost for 1 CSTR when τ/λ for the 1-CSTR-problem is on the order of 1000. Produce one graph of $\log(\tau/\lambda)$ for both configurations vs. conversion $\chi_{A,final}$ in the exit stream of the last reactor that proves this important strategy.

Verification of this reactor design strategy

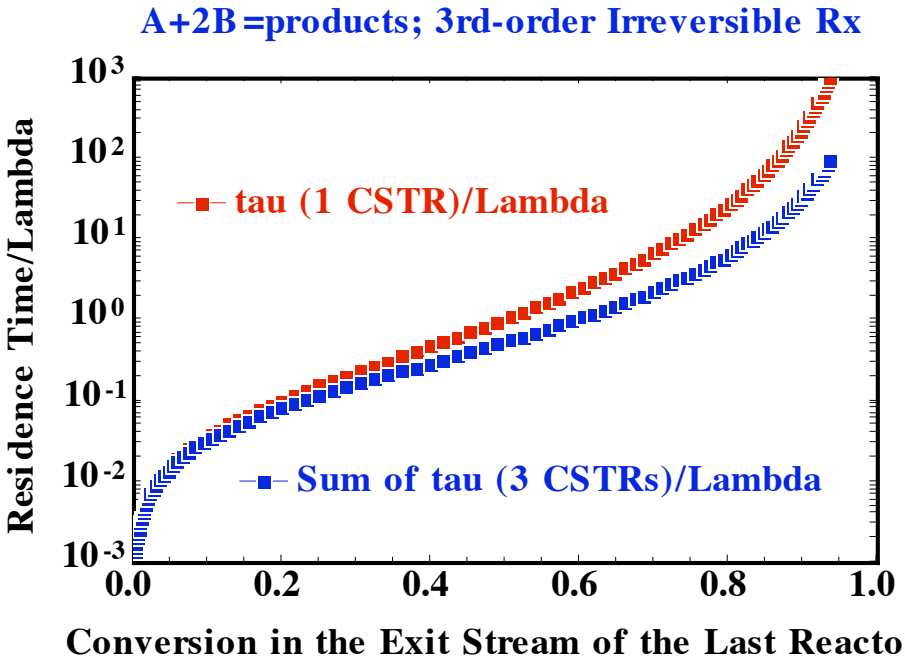

Calculate the conversion of reactant A in the exit stream of **one** liquid-phase CSTR. The elementary irreversible chemical reaction is described above. Conversion of reactant A is determined from the cubic CSTR design equation. The kinetics are first-order with respect to reactant A, and second-order with respect to reactant B.

$\{\tau_{1CSTR}/\lambda\}(1-\chi_{1CSTR})(\Theta_B+\upsilon_B\chi_{1CSTR})^2-\chi_{1CSTR}=0$	mass balance for **one** CSTR
$\Theta_B=2$	inlet feed ratio parameter for reactant B
$\upsilon_B=-2$	stoichiometric coefficient for reactant B

Now, consider a train of 3 equi-sized CSTRs operating at the same temperature and feed conditions such that the chemical reaction time constant λ for each reactor in series is the same as λ for the one-reactor configuration. The overall objective is to demonstrate that $\tau_1+\tau_2+\tau_3=\tau_{3CSTRs}<\tau_{1CSTR}$ when conversion of reactant A in the exit stream of the third CSTR, χ_3, is the same as χ_{1CSTR} and $\tau_1=\tau_2=\tau_3=\tau_{3CSTRs}/3$. Three sequential CSTR design equations are required to analyze the performance of the train.

$\{\tau_{3CSTRs}/3\lambda\}(1-\chi_1)(\Theta_B+\upsilon_B\chi_1)^2-(\chi_1-0)=0$ mass balance for the 1st CSTR in the train
$\{\tau_{3CSTRs}/3\lambda\}(1-\chi_2)(\Theta_B+\upsilon_B\chi_2)^2-(\chi_2-\chi_1)=0$ mass balance for the 2nd CSTR in the train
$\{\tau_{3CSTRs}/3\lambda\}(1-\chi_3)(\Theta_B+\upsilon_B\chi_3)^2-(\chi_3-\chi_2)=0$ mass balance for the 3rd CSTR in the train

final conversion is the same for both configurations

$\chi_3=\chi_{1CSTR}$

Page#25 bottom of the page after CSTR design strategy#4.

Analytical verification of strategy#4 for first-order irreversible chemical reaction. This problem can be analyzed as restricted optimization if the total reactor volume is limited. Hence, $\tau_1+\tau_2 = \tau_{total}$ = constant. Construct the steady state mass balance on species *i* in the k^{th}-CSTR. The important mass transfer rate processes are convection and chemical reaction, where the rate law is first-order and depends only on the molar density of reactant A. Hence, if the k^{th}-reactor operates at temperature T_k, then;

$$\frac{dN_{i,k}}{dt} = qC_{i,k-1} - qC_{i,k} + \upsilon_i k_1(T_k)C_{A,k}V_{k^{th}CSTR} = 0$$

Application of the stoichiometric relation for constant-density systems, with residence time $\tau_k = V_k/q$ and characteristic time constant for 1st-order irreversible chemical reaction $\lambda_k = \{k_1(T_k)\}^{-1}$, yields the following recurrence formula;

$$C_{i,k} = C_{A0}\{\Theta_i + \upsilon_i\chi_k\}$$

$$C_{i,k-1} - C_{i,k} = \upsilon_i C_{A0}\{\chi_{k-1} - \chi_k\} = -\upsilon_i \frac{\tau_k}{\lambda_k} C_{A0}\{1-\chi_k\}$$

$$\{\chi_{k-1} - \chi_k\} = \{1-\chi_k\} - \{1-\chi_{k-1}\} = -\frac{\tau_k}{\lambda_k}\{1-\chi_k\}$$

$$1-\chi_k = \frac{\lambda_k}{\lambda_k+\tau_k}\{1-\chi_{k-1}\}$$

Now, apply the recurrence formula for two CSTRs in series with first-order irreversible chemical kinetics;

$$1-\chi_1=\left\{\frac{\lambda_1}{\lambda_1+\tau_1}\right\}(1-\chi_0)=\frac{\lambda_1}{\lambda_1+\tau_1}$$

$$1-\chi_2(\tau_1)=\left\{\frac{\lambda_2}{\lambda_2+\tau_2}\right\}(1-\chi_1)=\left\{\frac{\lambda_2}{\lambda_2+\tau_{total}-\tau_1}\right\}\left\{\frac{\lambda_1}{\lambda_1+\tau_1}\right\}$$

Maximize χ_2 by minimizing $1-\chi_2$ with respect to τ_1 at constant τ_{total}, T_1, and T_2. Since the chemical reaction time constants are truly constants when the temperature in each CSTR does not change;

$$\frac{\partial}{\partial\tau_1}\{1-\chi_2(\tau_1)\}=\left\{\frac{\lambda_2}{\lambda_2+\tau_{total}-\tau_1}\right\}\left\{\frac{-\lambda_1}{(\lambda_1+\tau_1)^2}\right\}+\left\{\frac{\lambda_1}{\lambda_1+\tau_1}\right\}\left\{\frac{\lambda_2}{(\lambda_2+\tau_{total}-\tau_1)^2}\right\}=0$$

$$\frac{1}{\lambda_2+\tau_{total}-\tau_1}-\frac{1}{\lambda_1+\tau_1}=0$$

$$\tau_1=\frac{1}{2}\{\tau_{total}+\lambda_2-\lambda_1\}$$

The following reactor design strategy will maximize the conversion of reactant A in the exit stream of the second CSTR in series. If both reactors operate at the same temperature, then $T_1=T_2$ and both chemical reaction time constants should be the same. Under these conditions, the residence time for each CSTR should be 50% of the total residence time. Hence, $\tau_1=\tau_2$. This theorem applies only when the kinetics are first-order and irreversible. If the first CSTR operates at higher temperature, then $T_1>T_2$ and $\lambda_1<\lambda_2$, because chemical reaction time constants decrease at higher temperature. Now, $\tau_1>\tau_2$, which suggests that the first CSTR should be larger. If the second CSTR operates at higher temperature, then $T_1<T_2$ and $\lambda_1>\lambda_2$. Now, τ_1 should be less than τ_2. In general, the reactor that operates at higher temperature should have a longer residence time, and this theorem is applicable to any type of n^{th}-order kinetic rate law when $n>0$.

Page#26 *Answer to Problem#1:*

Combine the first and fourth strategies outlined above.

The smaller reactor that operates at 30°C should be first in the train.

The larger reactor that operates at 70^{0}C should be last in the train.
Numerical verification of this combination of strategies is illustrated graphically below, via the solution of coupled nonlinear algebraic equations.

$\tau_1 R_1 - C_{A,inlet}(\chi_1 - \chi_0)=0$	design equation for the first CSTR
$\tau_2 R_2 - C_{A,inlet}(\chi_2 - \chi_1)=0$	design equation for the second CSTR
$R_1 = k_{forward}(T_1)\{C_{A,inlet}(1-\chi_1)\}^n$	n^{th}-order kinetics in the first CSTR at T_1
$R_2 = k_{forward}(T_2)\{C_{A,inlet}(1-\chi_2)\}^n$	n^{th}-order kinetics in the second CSTR at T_2
$\tau_1+\tau_2=50$ minutes	restricted optimization
$k_{forward}(T_1)=0.1$ (L/mol)$^{n-1}$/min	reaction time constant is 10 min. at T_1
$k_{forward}(T_2)=0.5$ (L/mol)$^{n-1}$/min	reaction time constant is 2 min. at $T_2 > T_1$
$\chi_0=0$	no conversion in the inlet stream to 1st CSTR
$C_{A,inlet}=1$ g-mol/Litre	molar density of reactant A; inlet to 1st CSTR
$n=3$	third-order kinetics, where $R = f(C_A) = k_n(C_A)^n$

Effect of Temp. & tau on Conversion; 2 CSTRs; 3rd-Order Rx.

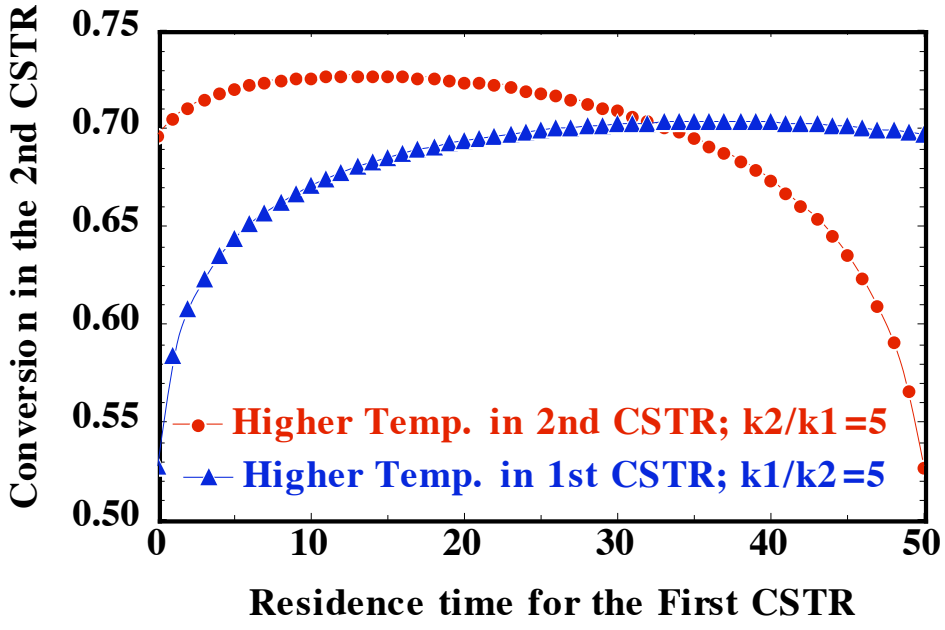

If the kinetics are first-order and irreversible (i.e., n=1), such that $R = k_1 C_A$, then the residence time should be longer for the reactor that operates at higher temperature, but it does not matter whether the hotter or colder reactor is first in the train.

Effect of Temp. & tau on Conversion; 2 CSTRs; 1st-Order Rx.

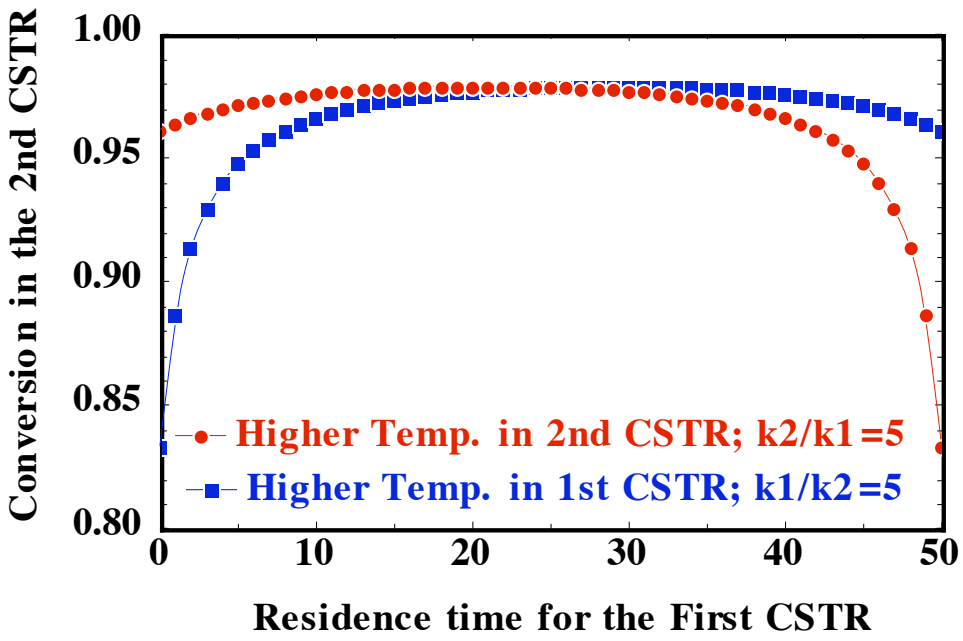

Page#29 Problem 1-7; pre-exponential (i.e., 6 lines up from the bottom of the page)

Page#30 ***Answer to Problem 1-7;***

The following sequence of coupled nonlinear algebraic equations must be solved to address this restricted optimization problem with one degree of freedom (i.e., either τ_1 or τ_2);

$\tau_1 R_1 - C_{A,inlet}(\chi_1 - \chi_0)=0$	CSTR mass balance in the 1st CSTR w/ one chemical reaction
$\tau_2 R_2 - C_{A,inlet}(\chi_2 - \chi_1)=0$	CSTR mass balance in the 2nd CSTR w/ one chemical reaction
$R_1=k_{r1}\{(C_{A1})^n-(C_{B1})^n/K_{Eq\#1}\}$	reversible rate law for nth-order kinetics in the 1st CSTR
$R_2=k_{r2}\{(C_{A2})^n-(C_{B2})^n/K_{Eq\#2}\}$	reversible rate law for nth-order kinetics in the 2nd CSTR
$C_{A1}=C_{A,inlet}(1-\chi_1)$	molar density of reactant A in the exit stream of 1st CSTR
$C_{A2}=C_{A,inlet}(1-\chi_2)$	molar density of reactant A in the exit stream of 2nd CSTR
$C_{B1}=C_{A,inlet}(\Theta_B+\upsilon_B\chi_1)$	molar density of product B in the exit stream of 1st CSTR
$C_{B2}=C_{A,inlet}(\Theta_B+\upsilon_B\chi_2)$	molar density of product B in the exit stream of 2nd CSTR
$K_{Eq\#1}=\exp(A+B/T_1)$	thermodynamic equilibrium constant in the first reactor
$K_{Eq\#2}=\exp(A+B/T_2)$	thermodynamic equilibrium constant in the second reactor
$A\approx\Delta S^0_{Rx,298K}/R_{gas}$	standard state entropy change for reaction at 298K
$B\approx-\Delta H^0_{Rx,298K}/R_{gas}$	standard state enthalpy change for reaction at 298K
$k_{r1}=k_\infty\exp\{-E_{Activation}/(R_{gas}T_1)\}$	Arrhenius kinetic rate constant in the first reactor
$k_{r2}=k_\infty\exp\{-E_{Activation}/(R_{gas}T_2)\}$	Arrhenius kinetic rate constant in the second reactor
T_1=350K to 370K	temperature in the first reactor
T_2=350K to 370K	temperature in the second reactor
$\chi_0=0$	conversion of reactant A in the inlet stream to the 1st CSTR
$\tau_1+\tau_2$=1000 minutes	restricted optimization; total residence time is limited

$C_{A,inlet}$=0.4 mol/Litre	molar density of reactant A in the inlet stream; 1st CSTR
Θ_B=0	inlet molar density ratio; product B/reactant A; 1st CSTR
υ_B=+0.5	stoichiometric coefficient of product B, when υ_A = −1
k_∞=1*x*10^9 (L/mol)$^{n-1}$/min.	pre-exponential factor for the Arrhenius kinetic rate constant
$E_{Activation}$=17 kcal/mol	Arrhenius activation energy for the forward reaction
$\Delta H^0_{Rx,298K}$ = −9 kcal/mol	standard state enthalpy change for reaction at 298K
$\Delta S^0_{Rx,298K}$ = −15 cal/mol	standard state entropy change for reaction at 298K (2 moles of reactant A produce 1 mole of product B)
R_{gas}=1.987 cal/mol-K	universal gas constant
n=3	3rd-order forward and backward chemical kinetics

Operate both CSTRs at the highest possible temperature; 370K

τ_1 ≈ 400 minutes; τ_2 ≈ 600 minutes

Reversible Exothermic Reaction in 2 CSTRs

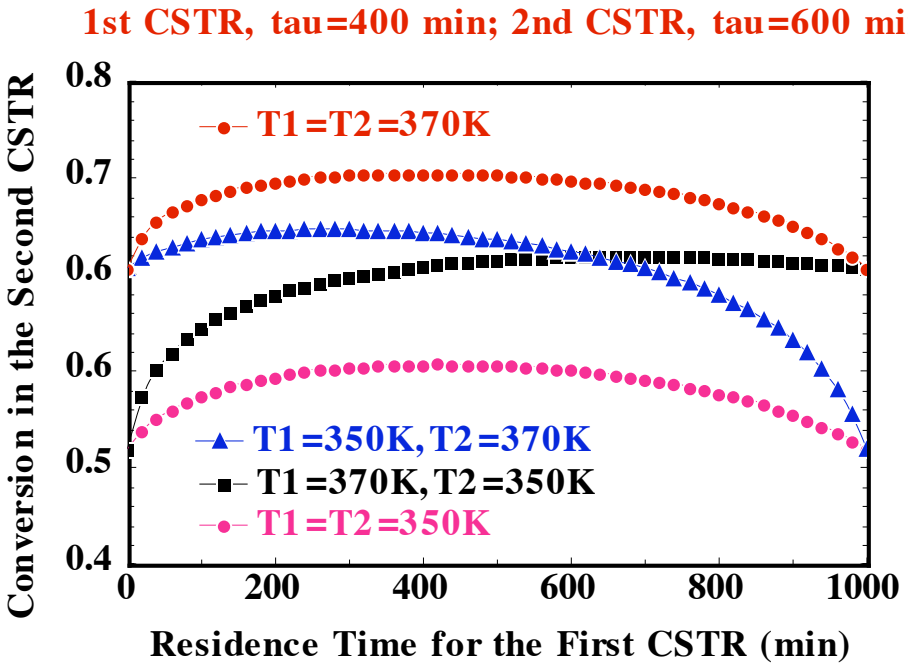

Page#31 ***Answer to Problem 1-8;***

The following sequence of coupled linear and nonlinear algebraic equations is required to address these CSTR optimization problems with multiple chemical reactions and one degree of freedom (i.e., reactor temperature T);

$\xi_1 = \tau R_1$	CSTR design equation for the first reaction
$\xi_2 = \tau R_2$	CSTR design equation for the second reaction
$C_A = C_{A,inlet} - \xi_1$	molar density of reactant A, mol/Litre
$C_B = C_{B,inlet} + \xi_1 - \xi_2$	molar density of intermediate product B, mol/Litre

$C_C = C_{C,inlet} + \xi_2$	molar density of final product C, mol/Litre
$R_1 = k_1(T)\{C_A\}^n$	kinetic rate law for the first chemical reaction
$R_2 = k_2(T)\{C_B\}^n$	kinetic rate law for the second chemical reaction
$k_1(T) = k_{1\infty}\exp\{-E_{Activation\#1}/(R_{gas}T)\}$	Arrhenius kinetic rate constant; 1st reaction
$k_2(T) = k_{2\infty}\exp\{-E_{Activation\#2}/(R_{gas}T)\}$	Arrhenius kinetic rate constant; 2nd reaction
$k_{1\infty} = 1x10^7$ (Litre/mol)$^{n-1}$/sec.	Arrhenius pre-exponential factor; 1st reaction
$k_{2\infty} = 4x10^6$ (Litre/mol)$^{n-1}$/sec.	Arrhenius pre-exponential factor; 2nd reaction
$E_{Activation\#1}$ = 15 kcal/mol	Arrhenius activation energy; 1st reaction
$E_{Activation\#2}$ = 12 kcal/mol	Arrhenius activation energy; 2nd reaction
R_{gas} = 1.987 cal/mol-Kelvin	universal gas constant
$Volume_{CSTR}$ = 100 Litres	reactor volume
FlowRate = 0.250 kg/sec.	mass flowrate through the CSTR
$q = FlowRate/\rho$	volumetric flowrate, Litres/sec.
ρ = 1 kg/Litre	overall density of the reactive mixture
$\tau = Volume_{CSTR} / q$	average residence time for the CSTR, seconds
$C_{A,inlet}$ = 1 or 2 mol/Litre	inlet molar density of reactant A
$C_{B,inlet} = 0$	intermediate B is not present in the feed
$C_{C,inlet} = 0$	final product C is not present in the feed
$\lambda_{Rx\#1} = \{C_{A,inlet}\}^{1-n}[k_1(T)]^{-1}$	time constant for the first chemical reaction
$\lambda_{Rx\#2} = \{C_{A,inlet}\}^{1-n}[k_2(T)]^{-1}$	time constant for the second chemical reaction
n = 1 or 2	order of both irreversible chemical reactions
$S_{B/C} = C_B / C_C$	selectivity of intermediate B vs. product C
$Yield_B = \{C_B - C_{B,inlet}\}/C_{A,inlet}$	yield of intermediate B wrt feed of reactant A

Answer to Problem 1-8 (a_1);

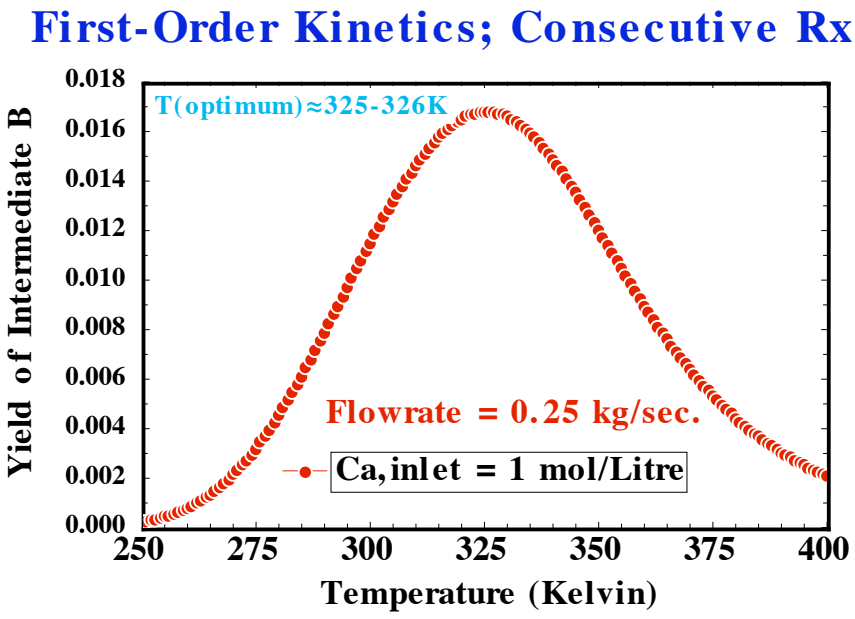

Answer to Problem 1-8 (a_2);

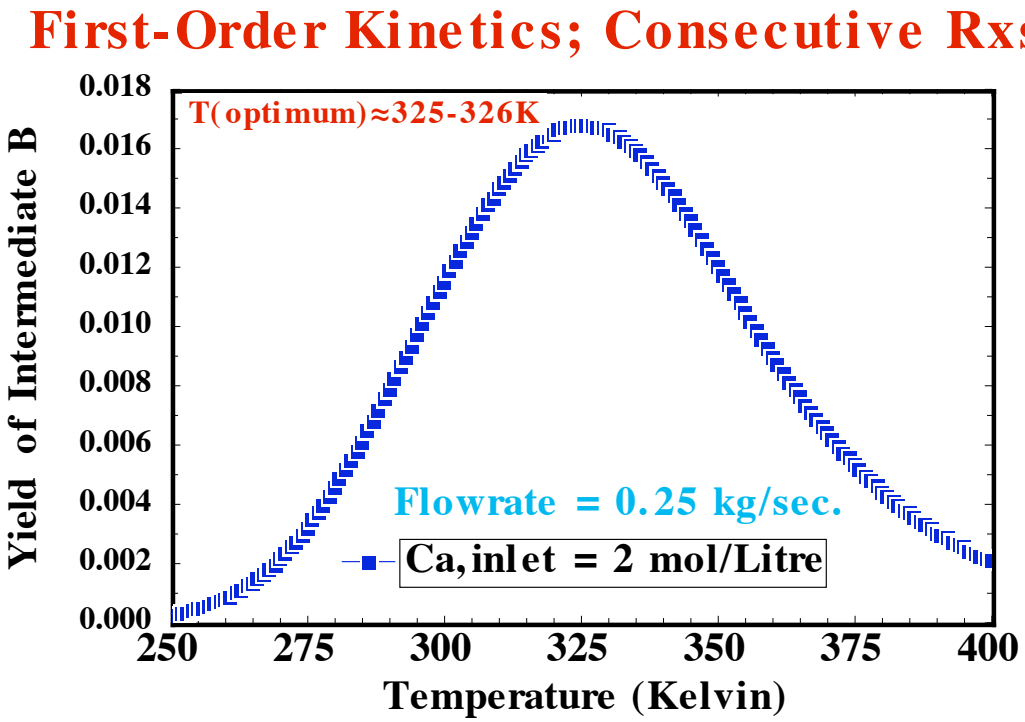

Answer to Problem 1-8 (b_1 and b_2);

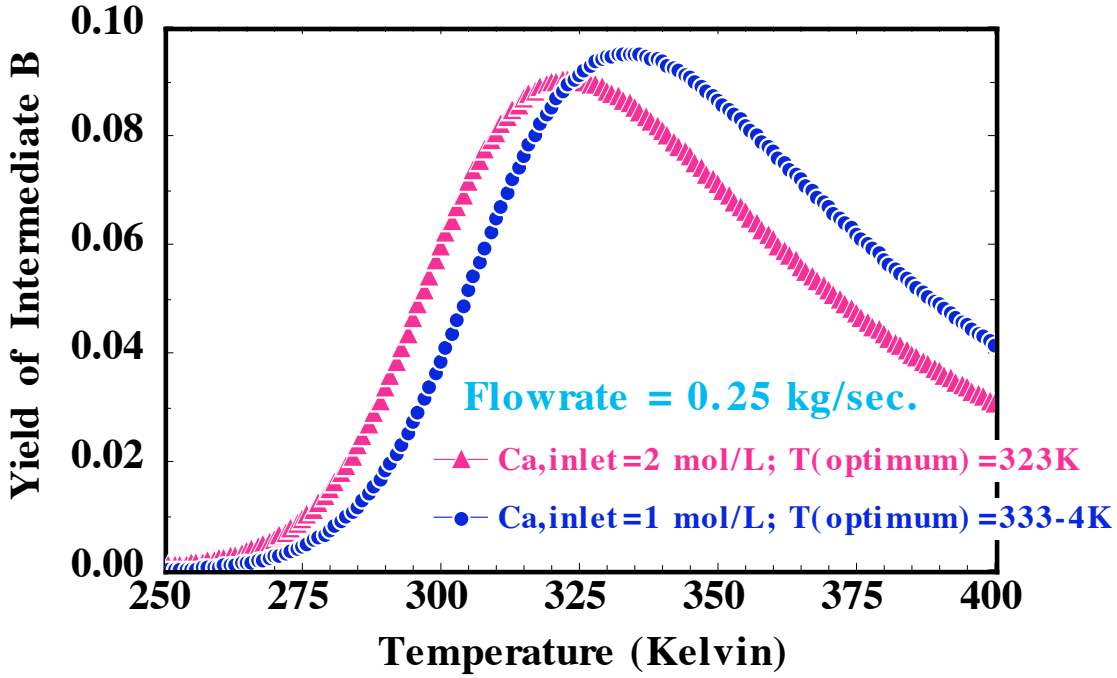

Answer to Problem 1-8 (c);

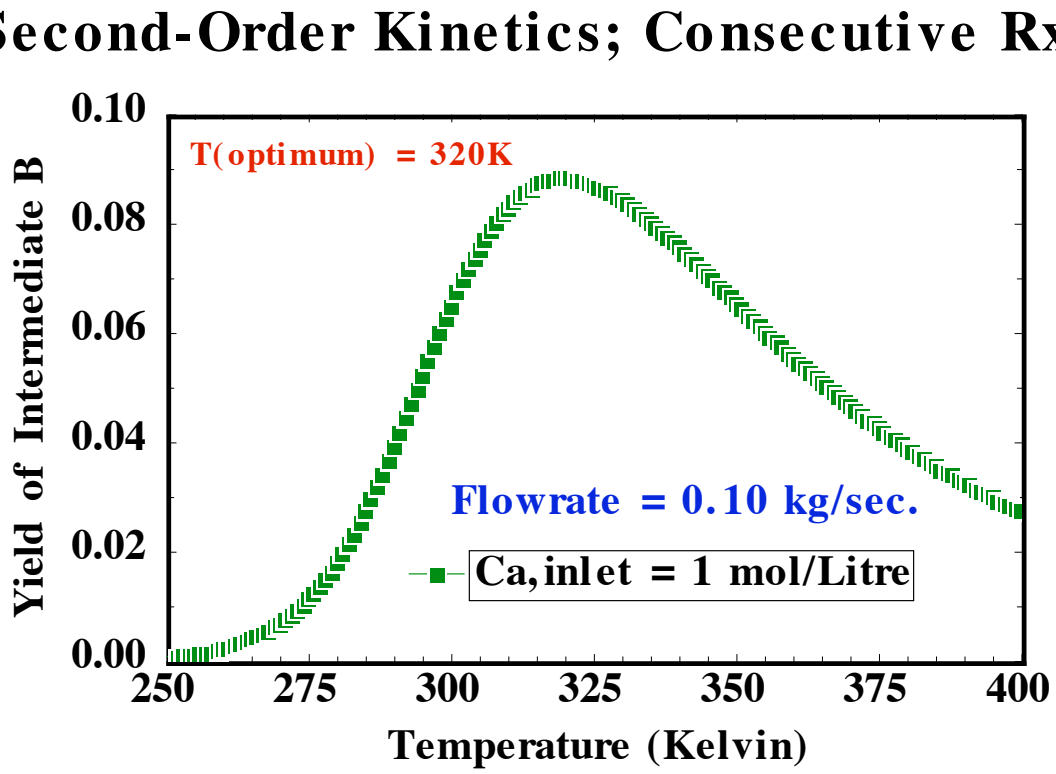

(2d) *Why is the optimum reactor temperature the same for ($2a_1$) and ($2a_2$), but the optimum reactor temperature for ($2b_1$) is higher than that for ($2b_2$)?*

Answer:
In all four simulations under consideration, the CSTR residence time is 400 seconds (i.e., V_{CSTR} = 100 Litres, q = 0.25 Litre/sec.). The yield of intermediate product B is optimized at temperatures where the time constant for the first reaction λ_1 is longer than residence time τ, so that the system dwells on producing B via the first reaction instead of depleting B via the second reaction. The second reaction proceeds slowly when intermediate B is not very abundant. For first-order kinetics, the characteristic molar density of reactant A in the feed stream does not affect chemical reaction time constants. Optimum conditions occur when $\lambda_1 \approx$ 1200 seconds at 325-326K in example ($2a_1$) and ($2a_2$). When the kinetics are second-order, reaction time constants scale inversely with the characteristic molar density of reactant A in the feed stream. Now, the optimum conditions occur when $\lambda_1 \approx$ 700 seconds. Hence, at higher feed concentrations of reactant A (i.e., now λ_1 decreases), it is necessary to operate at lower temperature (i.e., 323K in $2b_2$ vs. 333K in $2b_1$) to decrease kinetic rate constants and counterbalance the increase in $C_{A,inlet}$ such that $\lambda_1 \approx$ 700 seconds. In part (2c) where the flowrate decreases and the residence time increases to τ = 1000 seconds with

second-order kinetics, optimum CSTR operation occurs at lower temperature (i.e., 320K) to achieve a chemical reaction time constant for the first reaction (i.e., λ_1 > 1700 seconds) that is significantly longer than τ.

(2) Start-up Behaviour of a CSTR Train

Page#46 **Problem 2-2**

Startup behaviour of a CSTR train with multiple chemical reactions

How many coupled ordinary differential equations must be solved to analyze the complete transient response of a train of 2 CSTRs in series when 5 components participate in 3 independent chemical reactions in the 1st tank and 4 independent chemical reactions in the 2nd tank? A catalyst in the 2nd tank is responsible for the fact that an additional reaction occurs in the 2nd tank, but this catalyst is not present in the 1st tank.

(3) Non-Isothermal Adiabatic Plug Flow Tubular Reactors

Page#62 **Problem 3-1;** just below the chemical reaction illustrating the hydrogenation of benzene; ... replace *and a catalyst is not required,* by "over a supported-nickel catalyst (i.e., 58% Ni). The appropriate gas-phase thermodynamic data are provided ...

Page#64 **Problem 3-3.**

Analyze the production of methanol from a stoichiometric feed of carbon monoxide and hydrogen in an adiabatic gas phase tubular reactor when the specific heat of the 3-component mixture exhibits dependence on temperature and conversion. Do not average the specific heat of each component over a reasonable range of operating temperatures, as illustrated on pages 48-49, and do not neglect the dependence of $C_{P,mixture}$ on the conversion of CO, as discussed on pages 50-51. Include flexibility for reactor performance at various pressures and inlet temperatures, as well as the use of an inert gas such as argon in the feed stream. In the absence of argon, demonstrate that an inlet feed temperature of 350K and an operating pressure of 2 atmospheres yield slightly higher CO conversion in an adiabatic tubular reactor that is at least 10-fold smaller than the simulations suggest in Figure 3-1 on page#61. **Hint:** Do not assume that non-equilibrium reactor temperature and CO conversion exhibit linear relations given by equations (3-41) and (3-42). Coupled heat and mass transfer in adiabatic gas phase tubular reactors are described by equations (3-38) and (3-39). Based on your more accurate simulations in the solution to this problem, are the approximations invoked in Chapter#3 justified?

(4) **Coupled Heat and Mass Transfer in Non-Isothermal Liquid Phase Tubular Reactors with Strongly Exothermic Chemical Reaction; Thermal Runaway, Parametric Sensitivity & Multiple Stationary States**

Page#91 illustrative problems at the top of the page

(a) Describe qualitatively why thermal runaway occurs when the flowrate of the cocurrent endothermic cooling fluid is too FAST. In other words, **thermal runaway occurs when $\Psi > 0.65$** (see Figures 4-8 and 4-9).

Answer:

If the cooling fluid flowrate is too fast and its residence time is too short relative to the time constant for endothermic chemical reaction in the cooling fluid, then the conditions are not appropriate to remove much thermal energy from the reactive fluid in the inner tube. The cooling fluid does not remain in the double-pipe heat exchanger long enough to function as a sink of thermal energy via endothermic chemical reaction. Hence, thermal runaway occurs in the reactive fluid within the inner tube.

(b) Describe qualitatively why thermal runaway occurs when the flowrate of the cocurrent endothermic cooling fluid is too SLOW. In other words, **thermal runaway occurs when $\Psi < 0.15$** (see Figures 4-10 and 4-11).

Answer:

If the cooling fluid flowrate is too slow and its residence time is much longer than the time constant for endothermic chemical reaction in the cooling fluid, then near-equilibrium conditions occur in the cooling fluid before it exits the double-pipe heat exchanger. Hence, thermal runaway occurs in the reactive fluid near the tube outlet because the cooling fluid has "equilibrated" and it is not available to remove much thermal energy from the reactive fluid when τ_{Rx} is between 25 sec and 30 sec.

Page#104 **Problem#4-3**

Analyze the performance of an exothermic plug-flow tubular reactor with countercurrent cooling in a concentric double-pipe configuration that is not insulated from the surroundings. Three coupled ordinary differential equations, split boundary conditions, and numerical values for all of the important parameters are summarized in Table#4-7 on page#98. Consider the specific situations where the outlet temperature of the cooling fluid is 310 K, the flowrate ratio parameter $\psi = 3$, and the time constant for heat transfer to the surroundings across the outer wall of the configuration is 10 seconds instead of 2500 seconds. Radius ratios of the double-pipe configurations (i.e., $\kappa = R_{Inside}/R_{Outside}$) range from 0.50 to 0.75. Interestingly enough, reactive and

cooling fluid temperature profiles in these double-pipe reactors are physically disallowed in the absence of chemical reaction when the outer wall is adiabatically insulated from the surroundings. If κ = 0.5, then does the same behaviour occur (i) when the average velocity of both fluids is the same, such that ψ = 1 and values for τ_{Rx} on the horizontal axis (i.e., $0 \le \tau_{Rx} \le 15$ sec) represent the same axial position z in the double-pipe reactor for each fluid, and (ii) when no chemical reaction occurs within the inner tube? Explain why the temperature profiles change drastically in the presence of chemical reaction, with ψ = 3 when the radius ratio κ = 0.78, relative to the previous values of κ that were investigated above. *Note: These anomalous effects that are revealed by computer simulations for countercurrent flow are not predicted when the cooling fluid flows cocurrently with respect to the reactive fluid.*

Page#104 **Problem#4-4**

Repeat the formalism in *Section 4-1.3* for the ***Thermodynamics of multicomponent mixtures*** and obtain Equation (4-31) for the total differential of specific enthalpy *h* of an N-component mixture in the presence of multiple chemical reactions;

$$dh = \left\langle C_{p,mixture} \right\rangle dT + \frac{1}{\rho}\left(1 - \alpha T\right)dp + \frac{dV_{PFR}}{\rho q}\sum_{jRx's} R_j \sum_{i=1}^{N} \upsilon_{ij}\,\overline{H_i}$$

In this case, start from the *extensive* enthalpy H which, in agreement with the phase rule for single phase behaviour of simple systems where all chemical reactions have not equilibrated (i.e., there are N+1 degrees of freedom), depends on the following N+2 independent variables; T, p, M_1, M_2, ..., M_N, where T represents temperature, p is pressure, and M_i corresponds to the mass of species i in this reactive mixture. The stipulation of *simple systems* implies that there are no strong external fields, like electric and magnetic fields, which introduce addition degrees of freedom to characterize the field strength.

Answer:

Since *extensive* enthalpy H exhibits dependence on total system mass, $M_{total} = \Sigma_{1 \le i \le N} M_i$, the problem statement suggests the following functional dependence of H on N+2 independent variables, which yields it total differential as;

$$H\left(T, p, M_1, M_2, M_3, ..., M_N\right)$$

$$dH = \left\{\frac{\partial H}{\partial T}\right\}_{p,composition} dT + \left\{\frac{\partial H}{\partial p}\right\}_{T,composition} dp + \sum_{i=1}^{N}\left\{\frac{\partial H}{\partial M_i}\right\}_{T,p,all\_M_j[j \ne i]} dM_i$$

Expressing H in terms of temperature T and pressure p guarantees that (i) the total differential of H contains temperature changes (i.e., dT) as required to generate temperature profiles via the differential thermal energy balance in plug-flow tubular reactors, and (ii) the temperature coefficient of H at constant pressure and composition yields an extensive heat capacity of the mixture, defined by;

$$C_{p,Extensive} = \left\{\frac{\partial H}{\partial T}\right\}_{p,composition}$$

The *gymnastics* of differential thermodynamic relations, including one Maxwell relation from the Gibbs free energy based on the fact that reversing the order of second-mixed partial differentiation of thermodynamic state functions (i.e., exact differentials) does not affect the final result, yields an expression for the pressure coefficient of H at constant temperature and composition;

$$dH = TdS + Vdp + composition - dependent - terms\left\{i.e., \sum_{i=1}^{N} \mu_i dN_i\right\}$$

$$\left\{\frac{\partial H}{\partial p}\right\}_{T,composition} = T\left\{\frac{\partial S}{\partial p}\right\}_{T,composition} + V$$

$$\left\{\frac{\partial S}{\partial p}\right\}_{T,composition} = -\left\{\frac{\partial V}{\partial T}\right\}_{p,composition} = -V\alpha$$

The "chemical reaction contribution" to the total differential of extensive enthalpy is embedded in the species concentration dependence of H at constant temperature, pressure, and composition of all other species in the reactive mixture. This is expressed using partial molar enthalpies, or partial specific enthalpies, which are defined as follows;

$$\left\{\frac{\partial H}{\partial M_i}\right\}_{T,p,all\_M_j[j\neq i]} = \left\{\frac{\partial H}{\partial N_i}\right\}_{T,p,all\_N_j[j\neq i]} \left\{\frac{\partial N_i}{\partial M_i}\right\}_{T,p,all\_M_j[j\neq i]} = \frac{\overline{H_i}}{MW_i}$$

where mole numbers for species i are represented by N_i, MW is molecular weight, and the overbar identifies a *partial molar property.* The next step in this development relates extensive enthalpy H to specific enthalpy *h* via division of dH by total system mass, M_{total}, which remains constant at steady state. Hence, it is justified to divide by M_{total} inside the differential operators, particularly for dH and dM_i. Division of system volume $V = V_{PFR}$ by

M_{total} yields specific volume, or the inverse of the overall density of the mixture ρ, and division of M_i by M_{total} identifies the mass fraction of species i, ω_i. One obtains the following expression for the total differential of specific enthalpy in multicomponent mixtures with multiple chemical reactions;

$$\frac{1}{M_{total}} dH = dh = C_{p,\text{int}ensive} dT + \frac{1}{\rho}(1 - \alpha T) dp + \sum_{i=1}^{N} \frac{\overline{H_i}}{MW_i} d\omega_i$$

This analysis of the thermodynamics of multicomponent mixtures is employed in the plug-flow thermal energy balance to generate temperature profiles for tubular reactors that operate nonisothermally due to the endothermic or exothermic nature of the chemical reactions. The *coupling between heat and mass transfer* is invoked to introduce an expression for the differential change of species mass fraction $d\omega_i$ via the plug-flow mass balance for flow reactors with multiple chemical reactions. This is accomplished via a simple relation between mass fraction ω_i and molar flowrate F_i for species i that includes the total mass flowrate ρq which remains constant at steady state with one inlet stream and one outlet stream. Hence, if no material escapes from the tubular reactor across the impermeable boundary at the tube wall (i.e., $r=R_{PFR}$), then (i) the plug-flow mass balance for ideal PFRs with multiple chemical reactions, and (ii) the relation between ω_i and F_i are;

$$\frac{dF_i}{dV_{PFR}} = \sum_{jRx's} \upsilon_{ij} R_j$$

$$\omega_i = \frac{MW_i F_i}{\rho q}$$

$$d\omega_i = \frac{MW_i}{\rho q} dF_i = \frac{MW_i dV_{PFR}}{\rho q} \sum_{jRx's} \upsilon_{ij} R_j$$

The *chemical reaction* contribution to the total differential of specific enthalpy is manipulated as follows when multiple chemical reactions occur. It is straightforward to include only the first term in the summation (i.e., over index j) for one chemical reaction;

$$\sum_{i=1}^{N} \frac{\overline{H_i}}{MW_i} d\omega_i = \frac{dV_{PFR}}{\rho q} \sum_{i=1}^{N} \overline{H_i} \sum_{jRx's} \upsilon_{ij} R_j = \frac{dV_{PFR}}{\rho q} \sum_{jRx's} R_j \sum_{i=1}^{N} \upsilon_{ij} \overline{H_i}$$

The *stoichiometric-coefficient-weighted* sum of partial molar enthalpies for all species that participate in the j^{th}-chemical reaction, given by the last summation on the extreme right

side of the previous equation, is an exact expression for the molar enthalpy change $\Delta H_{Rx,j}$ that considers nonideal effects, such as heats of mixing and possible ionic interactions, in addition to the making and breaking of chemical bonds. Hence, thermodynamic formalism for the specific enthalpy *h* of mixtures of N-components that participate in several chemical reactions reveals that the chemical reaction contribution to thermal energy effects requires a sum of products of kinetic rate laws and the corresponding molar enthalpy change for each reaction. If the intensive heat capacity of the mixture, $C_{p,Extensive}/M_{total}$, is averaged over the complete temperature range of operation, then the final expression for *dh* in the steady state plug-flow thermal energy balance and the first law of thermodynamics for open systems reduces to;

$$dh = \left\langle C_{p,mixure} \right\rangle dT + \frac{1}{\rho}\left(1 - \alpha T\right)dp + \frac{dV_{PFR}}{\rho q}\sum_{jRx's} R_j \Delta H_{Rx,j}$$

Page#104 **Problem#4-5**

Use the final result from *Problem#4-4* together with the first law of thermodynamics for open systems to obtain an ODE that is useful for steady state analysis of temperature profiles in ideal plug-flow tubular reactors with multiple chemical reactions that is the same as Equation (4-33).

Answer:

Define the system as an N-component reactive mixture within differential control volume, $\pi R^2 dz$. There is one inlet stream at position z and one outlet stream at z+dz. The reactor wall at r=R is impermeable to mass, but it is not impermeable to radial conduction of thermal energy. The rate of thermal energy transfer into the system across the diathermal wall is described by $\{dQ/dt\}_{input}$. The rate at which the surroundings perform mechanical work on the system via *moving solid surfaces* is given by $\{dW/dt\}_{moving}$, which does not include pV-work across the inlet and outlet planes. If U represents extensive internal energy, then the first law for open systems, with dimensions of energy per time, can be stated as;

$$\frac{dU}{dt} = \left\{\frac{dQ}{dt}\right\}_{input} + \left\{\frac{dW}{dt}\right\}_{moving} + \left\{h\frac{dm}{dt}\right\}_{input@z} - \left\{h\frac{dm}{dt}\right\}_{output@z+dz}$$

Specific enthalpy *h* in the previous equation conveniently accounts for the convective flux of internal energy and pV-work acting across the inlet and outlet planes. There are two important consequences of steady state operation in ideal PFRs with one inlet and one outlet stream; (1) the left side of the previous equation vanishes, (2) the total mass flowrates (i.e., ρq) across the inlet and outlet planes, at positions z and z+dz respectively, are equivalent via the overall macroscopic mass balance. Since there are no moving solid

surfaces that perform mechanical work on the system, the first law for open systems reduces to;

$$\rho q\left\{h_{output@z+dz} - h_{input@z}\right\} = \rho q\{dh\} = \left\{\frac{dQ}{dt}\right\}_{input}$$

Now, one combines this simplified version of the first law with the final result from *Problem 4-4* for the total differential of specific enthalpy in multicomponent reactive systems to obtain the following ODE that is useful to predict plug-flow temperature profiles in ideal reactors;

$$\rho q\{dh\} = \rho q\left\langle C_{p,mixure}\right\rangle dT + q(1-\alpha T)dp + \left\{\sum_{jRx's} R_j \Delta H_{Rx,j}\right\} dV_{PFR} = \left\{\frac{dQ}{dt}\right\}_{input}$$

(5) Multiple Stationary States in CSTR's

Page#110 15 lines down from the top; T_{lower} = 301K, χ = 0.14% (reduce χ by factor of 10)

Page#117 ***Problem 5-2:*** *second line of the problem statement*
at 440K under steady state conditions, with assistance from a PID controller (i.e., proportional, integral, and differential control) because the mid-range operating point is intrinsically unstable.

Page#120 ***Problem 5-2(c);***

(c_1) Design the length of the 1.5-cm-diameter cooling coil to accomplish this task.

(c_2) How much conversion of reactants to products occurs in this CSTR?

(c_3) Predict the outlet temperature of the cooling fluid in the exit stream of the cooling coil.

Answers:

(c_1) $L_{CoolingCoil}$ = 412 cm

(c_2) 59% final conversion of reactants to products is achieved in this CSTR

(c_3) Use Equation 5-26 on page#109 of *Transport Phenomena for Chemical Reactor Design,* with z = $L_{CoolingCoil}$ = 412 cm. and T = T_{CSTR} = 440K, to predict the outlet temperature of the cooling fluid;

$$T_{cool,outlet} = T_{CSTR} - \left(T_{CSTR} - T_{cool,inlet}\right)\exp\{-CoolFactor\} = 366K$$

$$CoolFactor = \frac{\pi D_{CoolingCoil} U_{Overall} L_{CoolingCoil}}{\rho_{Cool} q_{Cool} \left\langle C_{p,cool}\right\rangle}$$

(6) Coupled Heat & Mass Transfer in Batch Reactors

Page#130 next to last sentence should include, “then PFRs yield higher conversion than CSTRs when the kinetics are n^{th}-order and irreversible, with n>0. Equation (6-36) ...”

Page#138 **Problem#6.2(b)**
... whereas thermodynamic data are sufficient to calculate $\Delta T_{adiabatic}$ if only one reaction occurs and that reaction achieves equilibrium conversion.

Page#138 **Problem#6-3**
Conversion vs. time for variable-pressure batch reactors that produce methanol in the gas phase at constant T and V

Problem statement: A stoichiometric feed (i.e., 1:2) of carbon monoxide (C≡O) and hydrogen (H_2) in an inert carrier gas (i.e., Argon) is injected into a cylindrical stainless steel batch reactor (i.e., diameter = 25 cm; height = 50 cm) to an initial operating pressure of 200 torr. A cooling coil within the reactor counterbalances the thermal energy generated from this exothermic reaction such that isothermal operation at 300K is guaranteed. The molar ratio of argon to C≡O in the feed is 4 (i.e., Θ_{Argon} = 4). **How much time is required to achieve 60% conversion of carbon monoxide?**

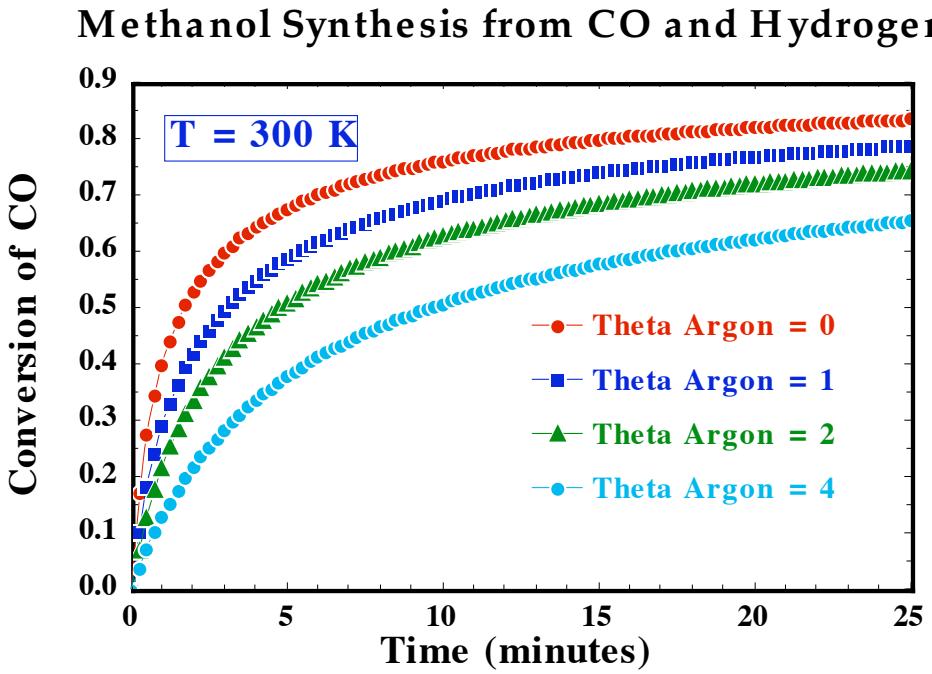

Answer: ***≈17 minutes.*** *Use the isothermal aspects of the methodology outlined in Section 6-4 and integrate the unsteady state constant-volume batch reactor mass balance. The graphical simulations illustrated above and below summarize the transient behaviour of CO conversion and total reactor pressure for three different inert (i.e., Argon) fractions in the feed.*

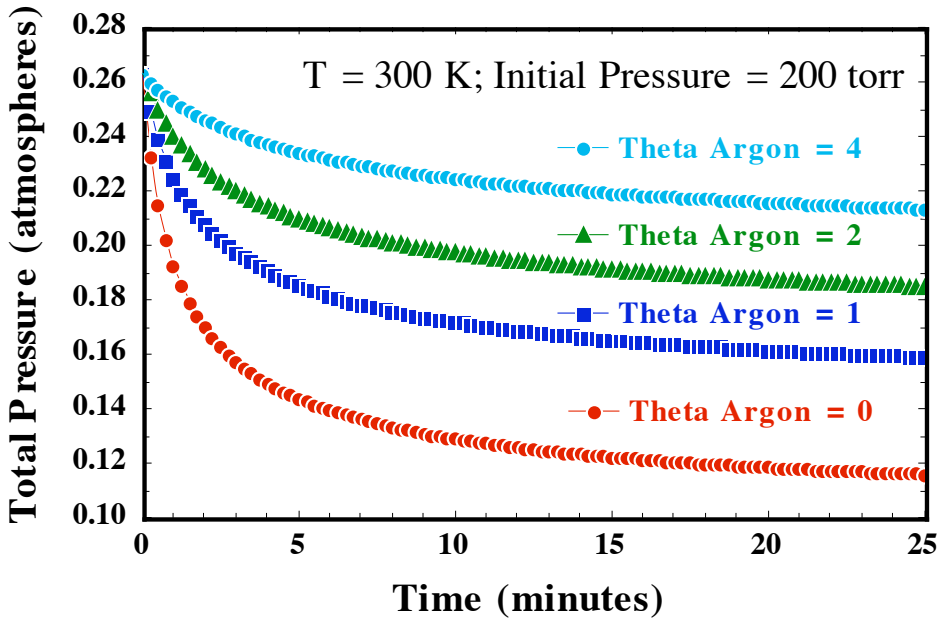

Page#138 **Problem#6-4**

Part (a): The following irreversible chemical reaction, A+2B ⇒ 3D, is carried out in a liquid-phase batch reactor at constant temperature, using a stoichiometric feed of A and B. The objective is to produce an average of 500 grams per hour of product D. Hence, the average mass of product D that is generated in the batch reactor on a per unit time basis is designated by β_D.

$$\beta_D = \frac{1}{t_{final} - t_{initial}} \int_{t_{initial}}^{t_{final}} \left\{ \frac{dm_D}{dt} \right\} dt = \frac{m_D\left(t_{final}\right) - m_D\left(t_{initial}\right)}{t_{final} - t_{initial}} = 500 grams/hr$$

Use the integral form of the constant-volume batch reactor design equation for t_{final} during each cycle of operation and obtain an expression for the required volume of the batch reactor to produce 500 grams per hour of product D. Your answer should contain the homogeneous kinetic rate law **R** and the final conversion $\chi_{A,final}$ of reactant A that is achieved during each cycle of operation.

Answer:

Relate the molar densities of reactant A and product D via stoichiometry and the conversion of reactant A in constant-volume systems;

$$\frac{1}{\upsilon_D}\left\{C_D(t)-C_D(t=0)\right\}=\frac{1}{\upsilon_A}\left\{C_A(t)-C_A(t=0)\right\}\overset{\upsilon_A=-1}{\Rightarrow}\chi_A C_A(t=0)$$

Now, convert the molar density of product D into the mass of product D that is generated by the reaction when the reactor operates for time t_{final}, yielding $\chi_{A,final}$, as follows;

$$\beta_D\left\{t_{final}-t_{initial}\right\}=m_D\left(t_{final}\right)-m_D\left(t_{initial}\right)$$

$$=\left\{C_D\left(t_{final}\right)-C_D\left(t_{initial}\right)\right\}MW_D V_{\underset{\text{Reactor}}{Batch}}=\upsilon_D\chi_{A,final}C_A(t=0)MW_D V_{\underset{\text{Reactor}}{Batch}}$$

Use the integral form of the classic batch reactor design equation for t_{final} and rearrange the previous expression to evaluate the required reactor volume;

$$t_{final}-t_{initial}=C_A(t=0)\int_0^{\chi_{A,final}}\frac{d\chi_A}{R(T,\chi_A)}$$

$$V_{\underset{\text{Reactor}}{Batch}}=\frac{\beta_D\left\{t_{final}-t_{initial}\right\}}{\upsilon_D\chi_{A,final}C_A(t=0)MW_D}=\frac{\beta_D}{3\chi_{A,final}MW_D}\int_0^{\chi_{A,final}}\frac{d\chi_A}{R(T,\chi_A)}$$

Part (b): If reactant B is present in excess and; A+2B ⇒ 3D, represents an elementary step, then evaluate the previous expression for the batch reactor volume required to produce an average of 500 grams per hour of product D.

Answer:

For third-order irreversible chemical kinetics with an excess of reactant B, one writes the rate law in terms of the conversion of reactant A as follows;

$$A+2B\overset{k_3(T)}{\Rightarrow}3D$$

$$R(T,\chi_A)=k_3(T)C_A C_B^2\approx k_3(T)\left\{C_B(t=0)\right\}^2 C_A(t=0)\left\{1-\chi_A(t)\right\}$$

Substitution of this kinetic rate expression into the final answer for $V_{BatchReactor}$ from part (a) yields the desired result;

$$V_{\substack{Batch\\ \text{Re}actor}} = \frac{\beta_D}{3\chi_{A,final}MW_D}\int_0^{\chi_{A,final}} \frac{d\chi_A}{R(T,\chi_A)} = \frac{\beta_D \int_0^{\chi_{A,final}} \frac{d\chi_A}{1-\chi_A}}{3\chi_{A,final}MW_D k_3(T)\{C_B(t=0)\}^2 C_A(t=0)}$$

$$= \frac{\beta_D\left[-\ln\left(1-\chi_{A,final}\right)\right]}{3\chi_{A,final}MW_D k_3(T)\{C_B(t=0)\}^2 C_A(t=0)}$$

Page#138 **Problem#6-5**

Consecutive gas-phase reactions in constant-volume batch reactors; optimizing the production of di-ethanolamine

Consecutive reactions that involve ethylene oxide are carried out in a constant-volume batch reactor under isothermal conditions at 325K. Three possible reactions can occur, and **the overall objective of this exercise is to maximize the production of diethanolamine**, which is generated in the second reaction. The reaction scheme is described below. All reactions are elementary, irreversible, and occur in the gas phase. In the 1st reaction, cyclic ethylene oxide and ammonia combine to form mono-ethanolamine via a ring-opening mechanism;

$$CH_2CH_2O + NH_3 \xrightarrow{k_1(325K)=0.05\frac{Litre}{mol-\min}} HOCH_2CH_2NH_2$$

At 325K, the kinetic rate constant for the 1st reaction is 0.05 Litre per gram-mole per minute. In the 2nd reaction, ethylene oxide and mono-ethanolamine combine to form the desired product, di-ethanolamine, via another ring-opening reaction;

$$CH_2CH_2O + HOCH_2CH_2NH_2 \xrightarrow{k_2(325K)=0.1\frac{Litre}{mol-\min}} \left(HOCH_2CH_2\right)_2NH$$

At 325K, the kinetic rate constant for the 2nd reaction is 0.10 Litre per gram-mole per minute. In the 3rd reaction, ethylene oxide reacts with the desired product, di-ethanolamine, to generate tri-ethanolamine via the third ring-opening reaction;

$$CH_2CH_2O + \left(HOCH_2CH_2\right)_2NH \xrightarrow{k_3(325K)=0.07\frac{Litre}{mol-\min}} N\left(CH_2CH_2OH\right)_3$$

At 325K, the kinetic rate constant for the 3rd reaction is 0.07 Litre per gram-mole per minute. The constant-volume batch reactor is initially charged with a 1:1 molar ratio of ethylene oxide and ammonia. Provide graphs and/or data tables to support your answers to the following questions.

(1) If the initial molar density of ethylene oxide is 1 mole per Litre, how long should the reaction mixture remain in the batch reactor to maximize the production of di-ethanolamine? After this length of time, the contents of the reactor are quenched, the desired product is recovered via a sequence of separation processes, and the batch reactor is re-charged with fresh reactants (ethylene oxide and ammonia) to produce more di-ethanolamine.
Hint: Qualitatively consider economics to help you identify the operating point for the batch reactor.

Answer:
30-50 minutes, no maximum is observed for the molar density of di-ethanolamine vs. time (see graph below).

(2) Is it advantageous to use an excess of ethylene oxide, or an excess of ammonia? Remember, that the overall goal is to produce larger amounts of di-ethanolamine as quickly as possible.

Answer:
An excess of ethylene oxide is advantageous (i.e., 10:1 is better than 5:1, see graph below) because ethylene oxide participates in all three chemical reactions. An excess of NH_3 will deplete ethylene oxide in the first reaction. This is counter-productive because there will not be a significant amount of ethylene oxide remaining, which is required to generate the desired product in the second reaction.

(3) When the feed is stoichiometric (i.e., 1:1) and the initial molar density of ethylene oxide is 1 mole per Litre, your task is to design a fixed-volume batch reactor that produces di-ethanolamine "continuously" at an average rate of 500 grams per hour. At the end of the production cycles in the batch reactor, 25 pounds of this intermediate product, di-ethanolamine, should be recovered via a sequence of unit operations. Identify the operating point of the batch reactor by considering, qualitatively, the initial and operating costs associated with reactor volume and the total number of cycles.
Hint: If di-ethanolamine is species D in the 5-component mixture, then the appropriate design equations are;

$$\dot{m}_D = \frac{1}{t_{final} - t_{initial}} \int_{t_{initial}}^{t_{final}} \left\{ \frac{dm_D}{dt} \right\} dt = \frac{m_D\left(t_{final}\right) - m_D\left(t_{initial}\right)}{t_{final} - t_{initial}} = 500\, grams/hr$$

$$\dot{m}_D \left\{ t_{final} - t_{initial} \right\} = \left\{ C_D\left(t_{final}\right) - C_D\left(t_{initial}\right) \right\} MW_D V_{Batch\,\mathrm{Re}actor}$$

Do you know how to *out-smart* ODE solvers and force them to "divide by zero"?

One possible answer to produce 25 pounds of di-ethanolamine is:
$t_{final} \approx 50$ minutes
$V_{BatchReactor} \approx 20$ Litres
27 cycles

Graphical answer to part (1);

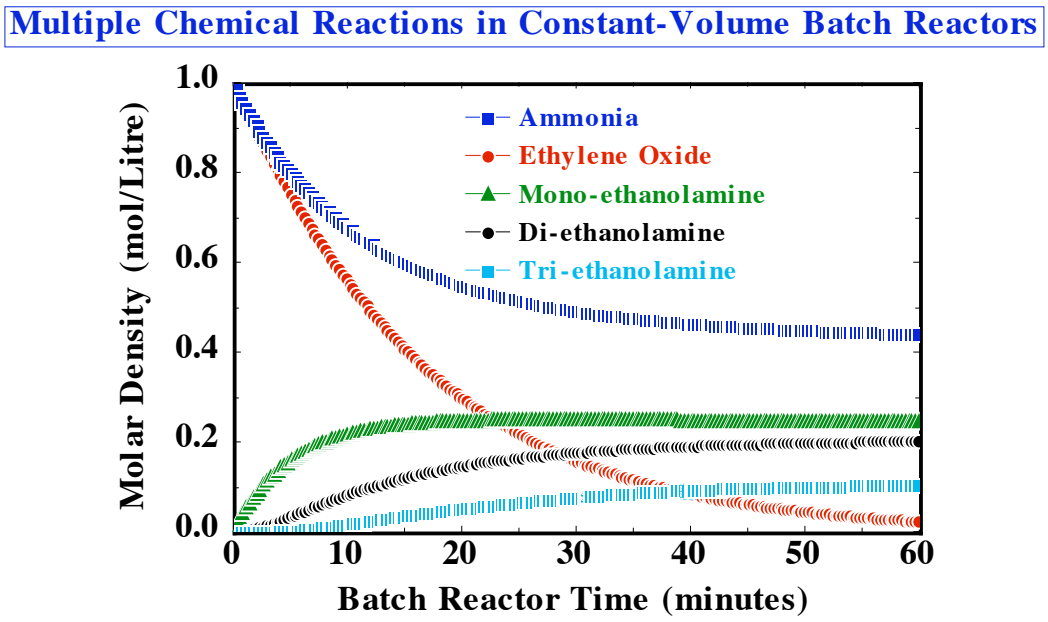

Graphical answer to part (2);

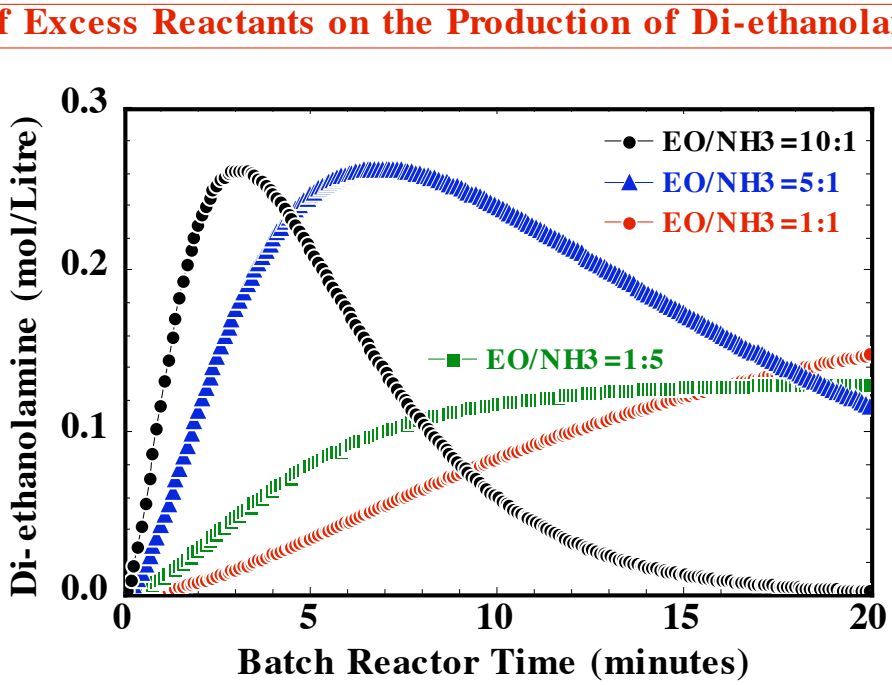

Page#138 **Problem#6-6**
Parallel the developments in Sections 6-1 and 6-3, respectively, to obtain the equations that describe isothermal and adiabatic operation of a *semi-batch* reactor with feed in the presence of one strongly exothermic chemical reaction.

(7) Total Pressure Method of Reaction Rate Data Analysis

Page#145 just below equation (7-34b); value of the intercept c, *then* the linear least-
Page#147 In 3 places, add a space between the left parenthesis of the bond energy and N_2, H-H, and N-H; 9 lines up from the bottom of the page
Page#148 6 lines from the top; If the gas mixture does not behave ideally at this high pressure, *then* it might seem reasonable to replace partial pressures by fugacities in the kinetic rate law.

Page#152 **Problem#7-13**
Reactant A is consumed by two parallel reactions in a constant-volume batch reactor. The kinetic rate laws depend only on the molar density of reactant A. For example, species A is

consumed by first-order irreversible chemical kinetics in the presence of an excess of reactant B;

$$A + B \overset{k_1}{\Rightarrow} \text{Products}$$

$$Rate_1 = k_1 C_A$$

Species A is also consumed by n^{th}-order irreversible chemical kinetics (i.e., n > 1) in the presence of an excess of reactant D;

$$A + D \overset{k_n}{\Rightarrow} \text{Products}$$

$$Rate_n = k_n C_A^n$$

The unsteady state constant-volume batch reactor mass balance on the moles of species A can be written in terms of N_A (= moles of A) or C_A (= molar density of A = $N_A/V_{BatchReactor}$). Hence;

$$\frac{dN_A}{dt} = -V_{Batch\,Reactor}\left\{Rate_1 + Rate_n\right\}$$

$$\frac{dC_A}{dt} = -k_1 C_A - k_n C_A^n$$

The analytical laboratory has provided N discrete data points for the time dependence of C_A (i.e., C_A vs. time *t*) in the constant volume batch reactor. Devise a linear least squares procedure to determine the reaction order *n* and both kinetic rate constants (i.e., k_1 and k_n) via the *Differential Method of Reaction Rate Data Analysis.*

Helpful hints: Divide the previous equation by C_A and take its time derivative. It is not possible to take the *logarithm* of a negative number.

Solution

Begin with the unsteady state constant volume batch reactor mass balance in terms of the molar density of reactant A, and divide the equation by C_A;

$$-\frac{1}{C_A}\frac{dC_A}{dt} = -\frac{d\ln C_A}{dt} = k_1 + k_n C_A^{n-1}$$

Take the time derivative of the previous equation, assuming that both kinetic rate constants are time-independent;

$$-\frac{d^2 \ln C_A}{dt^2} = (n-1) k_n C_A^{n-2} \frac{dC_A}{dt}$$

Now, take the logarithm (i.e., Log) of the previous equation and rearrange terms such that it is possible to identify the dependent and independent variables of a first-order polynomial;

$$Log\left\{\frac{d^2 \ln C_A}{dt^2}\right\} - Log\left\{-\frac{dC_A}{dt}\right\} = Log(n-1) + Log(k_n) + (n-2) Log\{C_A\}$$

The polynomial model is; $y(x) = a_0 + a_1 x$

The dependent variable *y* is;

$$y = Log\left\{\frac{d^2 \ln C_A}{dt^2}\right\} - Log\left\{-\frac{dC_A}{dt}\right\}$$

The independent variable is; $x = Log\{C_A\}$. One obtains the reaction order *n* from the first-order coefficient a_1, or the slope;

$$a_1 = n - 2$$
$$n = a_1 + 2$$

One obtains the n^{th}-order kinetic rate constant k_n from the zeroth-order coefficient, a_0, or the intercept;

$$a_0 = Log(n-1) + Log(k_n)$$

$$Log(k_n) = a_0 - Log(a_1+1)$$

It is necessary to reformulate this analysis if the first-order coefficient $a_1 = -1$, which yields $n = 1$. In this case, both rate laws are first-order with respect to the molar density of reactant A, and one should not take the time derivative of the unsteady state constant volume batch reactor mass balance after division by C_A. If the kinetics of one of the reactions is not first-order, then the previous linear least squares analysis provides an estimate of the reaction order *n* and the corresponding kinetic rate constant k_n for the process that is not first-order. Then, the following rearrangement of the mass balance yields a prediction of the kinetic rate constant k_1 for the first-order irreversible chemical reaction using a zeroth-order polynomial model [i.e., $y(x) = b_0$, with zero slope];

$$-\frac{d\ln C_A}{dt} - k_n C_A^{n-1} = k_1$$

Once the reaction order *n* and kinetic rate constant k_n have been determined, the dependent variable *y* is;

$$y = -\frac{d\ln C_A}{dt} - k_n C_A^{n-1}$$

If there are N data pairs, then the linear least squares prediction of the best intercept, b_0, is given by;

$$b_0 = k_1 = \frac{1}{N}\sum_{i=1}^{N} y_i = \frac{1}{N}\sum_{i=1}^{N}\left\{-\frac{d\ln C_A}{dt} - k_n C_A^{n-1}\right\}_{@t_i}$$

Part 2
Transport Phenomena: Fundamentals & Applications

(8) Applications of the Equations of Change in Fluid Dynamics

Page#162 3 lines above the matrix representation of $\rho\mathbf{vv}$ (8-6); change is to are.

Page#163 5 lines above equation (8-7); matrix (8-6), then the three entries ...

Page#174 just below equation (8-47); where d**r** is a differential position vector that is tangential to closed path C in the direction of integration, and **n** is a unit normal vector that emanates from surface S in region R, directed in the right-handed screw sense obtained by following closed path C along the integration contour. There are many closed paths in region R ...

Page#223 just below expression (b); The balance on overall fluid mass is obtained by equating expressions (a) and (b) ...

Page#236 just above part (c) of problem 8-16; The $\Theta\Theta$-component of τ reduces to μA.

Page#239

Part (e); *Solution*

The symmetry condition on v_z at r=0 represents the fourth boundary condition required to determine all four integration constants, A, B, C, and D. The fact that viscous shear stress vanishes and v_z achieves its maximum value, via Newton's law of viscosity, at the centerline of the tube is reasonable because r=0 is the symmetry axis. Telescoping cylindrical shells of infinitesimally small radii near the centerline of the tube do not *slide by each other* and create frictional forces due to viscous shear, because v_z is maximum with zero slope at the symmetry axis.

Part (f); Solution

Rigorously, it is only necessary that integration constant A vanishes (i.e., A=0), to insure that the stream function ψ vanishes at r=0, because $r^2 ln r$ tends toward zero as r approaches zero via l'Hopital's rule. Hence;

$$\psi(r) = Br^2 + Cr^2 \ln r + Dr^4$$

Now, one should obtain the velocity profile from the previous expression for the stream function and invoke symmetry at the centerline of the tube (i.e., r=0). For example;

$$v_z(r) = \frac{1}{r}\frac{d\psi}{dr} = 2B + C + 2C\ln r + 4Dr^2$$

$$\left\{\frac{dv_z}{dr}\right\}_{r=0} = \left\{2C\frac{1}{r} + 8Dr\right\}_{r=0} = 0$$

Either of these expressions reveals that integration constant C=0 because both v_z and τ_{rz} must be well-behaved functions with no singularities at r=0. Even though there is no rigorous boundary condition on the stream function itself which suggests that integration constant C must vanish, because $r^2 ln r$ is presumably *well-behaved* at r=0, the singularity in *ln*r at the symmetry axis becomes apparent when one evaluates v_z and τ_{rz} at r=0.

Page#250 Need a closing parenthesis at the end of problem statement 8-31; $\langle v_z \rangle$).

(9) Derivation of the Mass Transfer Equation

(10) Dimensional Analysis of the Mass Transfer Equation

(11) Laminar Boundary Layer Mass Transfer Around Solid Spheres, Gas Bubbles and Other Submerged Objects

Page#313 Change *solid-liquid* to *gas-liquid,* 2 lines and 10 lines below Section 11-7.
Page#360 just above part (c) and last line on the page; change “scales at” to “scales as”

(12) Dimensional Analysis of the Equations of Change for Fluid Dynamics within the Mass Transfer Boundary Layer

(13) Diffusion & Chemical Reaction Across Spherical Gas-Liquid Interfaces

Page#371 The sentence above equation (13-10) should be modified because the equation is not truly dimensionless. Hence, remove the word “dimensionless” above equation (13-10) so that the sentence is; “Now, the mass transfer equation for $\Psi_A(\eta)$ exhibits constant coefficients”.

Part 3
Kinetics and Elementary Surface Science

(14) Kinetic Mechanisms and Rate Expressions for Heterogeneous Surface-Catalyzed Chemical Reactions

Include this reference for the volume of activation;

Activation and reaction volumes in solution. 3
Drljaca A, Hubbard CD, van Eldik R, Asano T, Basilevsky MV, le Noble WJ
Chemical Reviews, **98** (6), 2167-2289 (1998)

Page#392 2 lines above equation (14-35); K_i, with units of inverse atmospheres. This equilibrium constant for species i in a mixture is the same as that for pure gas i exposed to the same high-surface-area catalyst. Identification of the same adsorption/desorption equilibrium constant for pure gas i and species i in a mixture is analogous to the fact that the equilibrium constant for a chemical reaction, constructed from the stoichiometric difference between free energies of formation of products and reactants in their standard states, is not affected by the number of chemical reactions that occur. The net rate of adsorption for component i ...

Add the following reference on page 392:

Myers, AL; & Prausnitz, JM; **Thermodynamics of Mixed-Gas Adsorption**, *AIChE Journal,* **11** (1), 121 (1965).

Page#395 add examples (4) and (5) for dual-site adsorption below the second and third examples near the top of the page (i.e., below line 12);

(4) When NO adsorbs on ruthenium, dissociation occurs preferentially at edge dislocations. Rates of dissociative adsorption can be several orders of magnitude higher in the vicinity of the defects. This effect is supported by scanning tunneling microscope images that reveal a higher concentration of nitrogen near defects on the ruthenium surface. This example is consistent with the general trend that favours enhanced catalytic activity where individual metal atoms are further apart on “stretched” surfaces, relative to defect-free regions. Hence, catalyst “turnover” rates are dominated by dissociative adsorption on defect sites, and these sites are essentially responsible for the entire reactivity of metallic nanoparticles.

(5) When NO adsorbs on copper, the frequency at which dissociative adsorption occurs increases by more than 3 orders of magnitude if it is vibrationally excited relative to the ground state. Results that support this claim appear in *Science,*

284, 1647 (1999). NO molecules were "pumped" into the 13th vibrational state and directed toward the 111-surface of copper. At the time when this research was performed, no theory existed to explain the interactions of vibrationally excited molecules with surfaces.

Page#423 just below equation (14-182); This result corresponds to free translation of the activated complex over the barrier with activation energy denoted by ΔG^*, or a very low energy vibration of the activated complex due to weak bonding, which causes it to dissociate into products. Envision the distortion of a chemical bond along a *normal coordinate mode of vibration,* with vibrational energy $h_{Planck}\upsilon_{infrared}$, in the transformation from reactants to products. Estimates of the lifetime of the activated complex in the transition state are inversely proportional to kinetic theory calculations of molecular velocities with thermal energy $k_{Boltzmann}T$. Now, equate the vibrational energy of the distorted bond in the activated complex to the thermal energy of this intermediate as it translates *through the transition state.* This simplistic picture of the activated complex allows one to identify the pre-exponential factor in equation (14-182), $k_{Boltzmann}T/h_{Planck} \approx 10^{13}$ sec^{-1}, as the stretching frequency $\upsilon_{infrared}$ of the distorted chemical bond that cleaves to form products. As expected, the stretching frequency of this low-energy distorted bond is found in the far-infrared region of the spectrum;

$$\upsilon_{infrared} \approx \frac{k_{Boltzmann}T}{h_{Planck}} = \frac{c_{Light}}{\lambda}$$

$$\lambda^{-1} \approx \frac{k_{Boltzmann}T}{h_{Planck}c_{Light}} = \frac{\left(1.38x10^{-23}\,Joule/K\right)\left(298K\right)}{\left(6.63x10^{-34}\,Joule-\sec\right)\left(3x10^{10}\,cm/\sec\right)} \approx 200cm^{-1}$$

Furthermore, $\{\upsilon_{infrared}\}^{-1} \approx 10^{-13}$ sec. provides a crude estimate of the lifetime of the activated complex in the transition state, which is consistent with the use of femtosecond spectroscopy (i.e., on the order of 10^{-15} sec.) to probe sub-molecular events in the transformation from reactants to products. If the reaction mechanism does not change and the same chemical bond must dissociate, then better catalysts stabilize the intermediate and lower the energy barrier ΔG^* between reactants and products, but lifetimes of the distorted complex moving through the transition state with thermal energy $k_{Boltzmann}T$ should not change appreciably. Hence catalysts function by lowering the activation energy, but not necessarily the pre-exponential factor, where the latter for first-order kinetics can be viewed as the low-energy vibrational frequency of a distorted chemical bond in the activated complex that cleaves to form products. Another viewpoint of the effect of catalysts on lifetimes in the

transition state experienced by activated complexes focuses on the savings in thermal energy, due the fact that the barrier is lowered, and utilization of this energy reserve to increase molecular velocities and the pre-exponential factor. The pressure dependence of $k_{forward}$ ...

Page#446 **Problem 14-27** (bottom of page)
N data pairs characterize the discrete temperature dependence of kinetic rate constants k_{Rx} for gas-phase chemical reactions; $k_{Rx,i}$ vs. T_i, $1 \le i \le N$. It is desired to generalize the transition state model, given by Equation (14-182), such that the generic function of temperature T in the pre-exponential factor is $g(T) = AT^n$, where *A* is a temperature-independent constant and the exponent *n* is not necessarily equal to unity. Develop a *linear least squares* strategy to evaluate the pre-exponential constant *A,* the exponent *n,* and the transition state activation energy $E_{act,TST} = \Delta G^*$, where ΔG^* is the difference between molar Gibbs free energies of the activated complex in the transition state and all of the reactants in their standard states. In other words, use all N data pairs ($k_{Rx,i}$,T_i; $1<i<N$) and develop three coupled linear algebraic equations to determine the three parameters in the following function for $k_{Rx}(T)$;

$$k_{Rx}(T) = AT^n \exp\left\{-\frac{E_{act,TST}}{R_{gas}T}\right\}$$

Answer:
Begin by taking the natural *logarithm* of the previous equation prior to identifying the independent and dependent variables in the function y(x) that contains three constants, a_0, a_1, and a_2, which must be related to the three parameters of interest in $k_{Rx}(T)$. Hence, for temperatures T that are greater than zero, one obtains;

$$\ln(k_{Rx}) = \ln(A) + n\ln(T) - \frac{E_{act,TST}}{R_{gas}T}$$

$$y(x) = a_0 + a_1\ln(x) + \frac{a_2}{x}$$

The following correspondences are appropriate;

(i) The independent variable, x = T (degrees Kelvin)
(ii) The dependent variable, $y = \ln(k_{Rx})$
(iii) The zeroth-order coefficient, $a_0 = \ln(A)$
(iv) The coefficient of ln(x) is, $a_1 = n$
(v) The coefficient of x^{-1} is, $a_2 = -E_{act,TST}/R_{gas}$

Now, construct the Error via the formalism of *Linear Least Squares Analysis,* and simultaneously minimize the Error with respect to a_0, a_1, and a_2, yielding three coupled linear algebraic equations for these three constants. Using all of the data, one constructs the sum of squares of the difference between y_i and $y(x_i)$;

$$Error = \sum_{i=1}^{N} \left\{ y(x_i) - y_i \right\}^2 = \sum_{i=1}^{N} \left\{ a_0 + a_1 \ln(x_i) + \frac{a_2}{x_i} - y_i \right\}^2$$

Partial differentiation of the *Error* with respect to a_0, a_1, and a_2 provides three equations that must vanish to minimize the square of the differences between y_i and $y(x_i)$ for all data points. By default, one is guaranteed to locate the minimum, and not a maximum, in the *Error* by solving the following three equations simultaneously;

$$\left(\frac{\partial Error}{\partial a_0} \right)_{a_1, a_2} = \sum_{i=1}^{N} 2 \left\{ a_0 + a_1 \ln(x_i) + \frac{a_2}{x_i} - y_i \right\} (1) = 0$$

$$\left(\frac{\partial Error}{\partial a_1} \right)_{a_0, a_2} = \sum_{i=1}^{N} 2 \left\{ a_0 + a_1 \ln(x_i) + \frac{a_2}{x_i} - y_i \right\} \left[\ln(x_i) \right] = 0$$

$$\left(\frac{\partial Error}{\partial a_2} \right)_{a_0, a_1} = \sum_{i=1}^{N} 2 \left\{ a_0 + a_1 \ln(x_i) + \frac{a_2}{x_i} - y_i \right\} \left[\frac{1}{x_i} \right] = 0$$

Rearrangement and division of each equation by 2 yields the desired result below, maintaining the same order with respect to partial differentiation. All three unknown constants a_0, a_1, and a_2, appear on the left side of each linear equation;

$$N a_0 + a_1 \sum_{i=1}^{N} \ln(x_i) + a_2 \sum_{i=1}^{N} \frac{1}{x_i} = \sum_{i=1}^{N} y_i$$

$$a_0 \sum_{i=1}^{N} \ln(x_i) + a_1 \sum_{i=1}^{N} \left\{ \ln(x_i) \right\}^2 + a_2 \sum_{i=1}^{N} \frac{\ln(x_i)}{x_i} = \sum_{i=1}^{N} y_i \ln(x_i)$$

$$a_0 \sum_{i=1}^{N} \frac{1}{x_i} + a_1 \sum_{i=1}^{N} \frac{\ln(x_i)}{x_i} + a_2 \sum_{i=1}^{N} \frac{1}{x_i^2} = \sum_{i=1}^{N} \frac{y_i}{x_i}$$

Since activation energies that characterize a barrier are greater than zero, a_2 must be negative. If the exponent on temperature T in the pre-exponential factor (i.e., AT^n) is

greater than zero, then a_1 must be positive. One expects that $a_1 = n$ should be close to unity, in agreement with the final form of kinetic rate constants from transition state theory.

Page#446 **Problem 14-28**

Prove that Arrhenius activation energies are always larger than activation energies for the generalized transition state model, if the exponent n on temperature in the pre-exponential factor is positive.

Answer:

Equate temperature-dependent kinetic rate constants for both models, take the natural logarithm and then the temperature derivative. For example;

$$k_\infty \exp\left\{-\frac{E_{act,Arrhenius}}{R_{gas}T}\right\} = AT^n \exp\left\{-\frac{E_{act,TST}}{R_{gas}T}\right\}$$

$$\ln\left(k_\infty\right) - \frac{E_{act,Arrhenius}}{R_{gas}T} = \ln\left(A\right) + n\ln\left(T\right) - \frac{E_{act,TST}}{R_{gas}T}$$

Upon taking the temperature derivative of the previous equation, one obtains a relation between temperature-dependent terms that contain the activation energies and the exponent *n* on temperature in the pre-exponential factor. The pre-exponential constants, k_∞ and A, do not affect the relation between Arrhenius and transition-state activation energies. The final result is;

$$\frac{E_{act,Arrhenius}}{R_{gas}T^2} = \frac{n}{T} + \frac{E_{act,TST}}{R_{gas}T^2}$$

$$\frac{E_{act,Arrhenius}}{R_{gas}} = \frac{E_{act,TST}}{R_{gas}} + nT$$

Hence, Arrhenius activation energies are greater than transition-state activation energies if the exponent *n* on temperature in the pre-exponential factor is greater than zero.

Part 4
Mass Transfer & Chemical Reaction in Isothermal Catalytic Pellets

(15) Diffusion & Heterogeneous Chemical Reaction in Catalytic Pellets

Page#450 just above (15-3); Hence, Laplace's equation

Page#450 just below (15-3); replace "is the simplified mass transfer equation for" by "must be solved to analyze steady state diffusion within the internal pores, ..."

(16) Diffusion & Zeroth-Order Chemical Reactions in Catalytic Pellets

Page#468 First sentence of section 16-4; change "challange" to "challenge".

Page#471 (last problem in the Chapter)

Problem#16-3

How large must the intrapellet Damkohler number be for reactant A such that one can use the analytical relation (i.e., equation 16-8) between $\eta_{critical}$ and Λ_A with confidence for flat-slab porous-wafer catalysts to estimate the fraction of the central core of spherical catalysts that are void of reactants when the pellet operates above the critical value of the intrapellet Damkohler number (i.e., $\Lambda^2_{critical} = 6$ when $L = R_{sphere}$)?

(17) Diffusion & First-Order Chemical Reactions in Catalytic Pellets

(18) Numerical Solutions for Diffusion & n^{th}-Order Chemical Reactions in Isothermal Catalytic Pellets

page#486 just above equation (18-13), add the noun "one" in front of (1). Or, remove the s at the end of each verb which follows (1) begin ..., (2) calculate ..., (3) multiply ..., and (4) evaluate ...

(19) Numerical Solutions for Diffusion and Hougen-Watson Chemical Kinetics in Isothermal Catalytic Pellets

page#500 equation#19-43 needs a closing parenthesis; script R*(all $\Psi_{i,surface}$)

(20) Effectiveness Factor Correlations

Page#532 8 lines up from the bottom of the page; $\Psi_A = 1$ at $\eta = 1$; change n to η

Page#535 just above Problem 20-9; ... where $\varepsilon \leq 10^{-5}$. A more elegant solution to part (b) involves the use of equation (20-47a) for the effectiveness factor in catalysts with rectangular symmetry, based on volumetric averaging of the kinetic rate law for simple n^{th}-order chemical reaction (i.e., n = 2). If the dimensionless molar density of reactant A at the center of the catalyst is the same as it is on

the external surface of the catalyst [i.e., $\Psi_A(\eta=0) = \Psi_A(\eta=1) = 1$], then the concentration profile is constant throughout the catalyst and $\Psi_A \neq f(\eta)$ in the reaction-controlled regime where the rate of reactant diffusion into the catalyst is much greater than the rate of chemical reaction. Under these conditions, integration of equation (20-47a) is trivial, as illustrated below;

$$E = \int_0^1 \left\{\Psi_A(\eta;\Lambda)\right\}^n d\eta = \int_0^1 \{1\}^2 d\eta = 1$$

Page#536 True/false question 20-14 (b) might be phrased ambiguously

(21) Effective Diffusion Coefficients & Intrapellet Damkohler Numbers within the Internal Pores of Catalytic Pellets

Page#543 4 lines below equation (21-19); ... Brownian motion in three dimensions. A rigorous approach provided by G Chen in *Nanoscale Energy Transport and Conversion,* Oxford (2005), pp. 412-416, reveals that diffusion coefficients can be calculated from the velocity autocorrelation function. This includes a factor of 1/3 via the Green-Kubo equation on p.#503 of Chen's textbook for three-dimensional particle dynamics, where mobility is the inverse of the friction coefficient. In many cases, ...

Page#545 just below the parametric values required in equation (21-24); As mentioned in the previous section, binary molecular diffusion coefficients can be expressed in terms of the velocity autocorrelation function via the Green-Kubo equation. Hence, if $v_x(t')$ is the x-component of a particle's velocity vector prior to any collision with its neighbors and $v_x(t)$ represents the corresponding x-component of the same particle's velocity after the collision, then random Brownian motion in three-dimensional space implies that autocorrelation functions for all three scalar components of the velocity vector are equivalent. Under these conditions, the Green-Kubo equation, which agrees with predictions of transport coefficients via Enskog's solution of the linearized Boltzmann equation, reduces to;

$$D_{AB} \approx \int_0^\infty \left\langle v_x(t) v_x(t') \right\rangle d(t-t') = \frac{1}{3}\int_0^\infty \left\langle \underline{v}(t) \bullet \underline{v}(t-\tau) \right\rangle d\tau = \frac{1}{3}\int_0^\infty \left\langle \underline{v}(t+\tau) \bullet \underline{v}(t) \right\rangle d\tau$$

The time difference before and after collisions is $\tau = t - t'$, and the scalar dot product of the particle velocity vectors yields a factor of $\cos\chi$, where χ is the

angle of deflection in a collision. An analogous expression for shear viscosity μ that is consistent with two-dimensional particle motion in the xy-plane, prior to and after a collision, contains the autocorrelation function of the product $v_x v_y$. Hence;

$$\mu \approx \int_0^\infty \left\langle v_x(t) v_y(t) v_x(t') v_y(t') \right\rangle d(t - t') = \int_0^\infty \left\langle v_x(t+\tau) v_y(t+\tau) v_x(t) v_y(t) \right\rangle d\tau$$

Integral calculus, symmetry of the convective momentum flux tensor, and tedious algebra reveal that this expression for μ can be written in terms of the square of the scalar dot product of velocity vectors before and after a collision, yielding a factor of $\cos^2\chi$ [see, Resibois, P; & de Leener, M; *Classical Kinetic Theory of Fluids,* Wiley (1977), pp. 141-2, 372-3].

Part 5
Isothermal Chemical Reactor Design

(22) Heterogeneous Packed Catalytic Tubular Reactors

Page579 The title of section 22-4 should be **"Design of Non-Ideal Heterogeneous Packed Catalytic Tubular Reactors with Interpellet Axial Dispersion"**. Hence, change "intrapellet" to "interpellet" in the title and in the header from pages 579 to 591. Also, make the same change on page xiv of the Table of Contents for the title of section 22-4.

Page#580 immediately after equation (22-59);

which was also employed by Irving Langmuir [*Journal of the American Chemical Society,* **30**, 1742 (1908)]. One arrives at equation (22-59) by invoking continuity of the rate of mass transfer of reactant A at $\zeta = 0^-$ and $\zeta = 0^+$, where interpellet axial dispersion exists within the packed bed, but not upstream from the inlet where the catalytic pellets are absent and no chemical reaction occurs. Realizing that the cross-sectional area for fluid flow decreases abruptly at the inlet, due to the presence of the catalytic pellets, continuity of the rate of mass transfer for reactant A at z=0 yields;

$$qC_{A,BulkGas\,\mathrm{Re}al}\left(z=0^{-}\right)=qC_{A,BulkGas\,\mathrm{Re}al}\left(z=0^{+}\right)-D_{A,\mathrm{int}erpellet}\left\{\frac{d}{dz}C_{A,BulkGas\,\mathrm{Re}al}\right\}_{z=0^{+}}\pi R_{PFR}^{2}\varepsilon_{p,\mathrm{int}erpellet}$$

$$q=\pi R_{PFR}^{2}\left\langle v_{z}\right\rangle_{\mathrm{sup}erficial}=\varepsilon_{p,\mathrm{int}erpellet}\pi R_{PFR}^{2}\left\langle v_{z}\right\rangle_{\mathrm{int}erstitial}$$

The characteristic molar density required for dimensional analysis is $C_{A,BulkGasReal}(z=0^{-})$, and $z = \zeta L_{PFR}$. Even though chemical reaction occurs beyond the inlet, but it is absent prior to the inlet, division of the steady state balance for reactant A at z=0 by the product of the volumetric flowrate q and $C_{A,BulkGasReal}(z=0^{-})$ yields the required Danckwerts boundary condition at the inlet, where the mass transfer Peclet number contains the interstitial fluid velocity and the interpellet axial dispersion coefficient. Hiby (1962, p. 312) has ...

Page#580 after the last line on the page, add; (see the solution to Problem 30-12).

Page#583 7th line from the top, after; PFR [see Problem 22-13 (f)], but reactor ...

Page#591 1st line of section 22-4.3; This is an unprecedented novel idea when the kinetics are not zeroth-order that allows one to compare $\Psi_A(\zeta=1,RTD)$ ...

Page#591 between equations (22-70) and (22-71); subject to $\Psi_A=1$ at $\zeta=0$, which yields;

Page#592 just above ***Problem.*** ... in the PFR exit stream. For example, when the chemical kinetics are second-order irreversible, the product of the catalyst filling factor, the effectiveness factor, and the interpellet Damkohler number is 5, and the mass transfer Peclet number is 10, numerical results in Table 22-1 reveal that non-ideal packed catalytic tubular reactors achieve 30% final conversion of reactants to products when the Danckwerts boundary condition in the exit stream (i.e., $d\Psi_A/d\zeta \Rightarrow 0$ when $\zeta=1$) is satisfied. One predicts 32% final conversion in the same non-ideal reactor when the dimensionless reactant concentration gradient in the exit stream is –2/9th, which agrees with equation (22-76) for ideal reactors with n=2.

Page#595 5th line from the top, “fundamental basis of their existence”

Page#600 In steps 19 and 20, spell “Coefficient” completely and begin with capital C

Last True/False problem at the end of Chapter#22;

Problem 22-13 (f);

When the kinetic rate law is simple nth-order, irreversible, and only a function of the molar density of one reactant, with n>0, one achieves higher conversion of reactants to products under ideal conditions in plug flow tubular reactors (PFRs) relative to continuous stirred tank reactors (CSTRs). PFRs represent the extreme of no mixing, whereas CSTRs correspond to the other extreme of complete mixing. Hence, it is reasonable that when axial diffusion or interpellet axial dispersion is included in the nonideal PFR differential design equation, one achieves less conversion of reactants to products relative to ideal PFR predictions because diffusion or dispersion introduces mixing ahead of and behind the “plug”. In order of

decreasing outlet conversion of reactants to products, the following trend is observed; (i) ideal PFRs with no axial mixing, (ii) real PFRs with some axial mixing, and (iii) ideal CSTRs with complete mixing throughout the reactor. The mass transfer Peclet number and the reactor type govern the extent of mixing, where smaller values of Pe_{MT} correspond to more mixing. **Are all of these statements TRUE or FALSE?**

Note: The ideal design equations for PFRs and CSTRs predict equivalent performance for zeroth-order chemical kinetics. However, one is not guaranteed that the analysis of both types of nonideal reactors (i.e., PFRs vs. CSTRs) will yield equivalent predictions of reactant conversion for zeroth-order reaction. A more in-depth analysis of the difference between real and ideal PFR performance for zeroth-order chemical kinetics is provided by *Problem#12* at the end of Chapter 30 (as described near the end of this document).

(23) Heterogeneous Catalytic Reactors with Metal Catalyst Coated on the Inner Walls of the Flow Channels

Page#613 first sentence of the last paragraph: 1) Fluid flow within ... (replace *with* by *within*)

Page#615 immediately after the last sentence of the first paragraph: *The aspect ratio of the rectangular channel is $A_r = a/b$ and the eigenvalues are $M_n = (2n+1)\pi/2$.*

The derivation of equation (23-2) proceeds as follows [see C Jarusiripot, PhD thesis, Colorado State University (2006)]. Consider fully developed one-dimensional laminar flow of incompressible Newtonian fluids through straight horizontal channels with rectangular cross-section. There are stationary solid boundaries at $x = \pm a$ and $y = \pm b$, where channel width a is much larger than its height b (i.e., $A_r = a/b > 1$). The origin of the Cartesian coordinate system coincides with the center of the channel at the inlet plane. Gravity forces affect fluid pressure vertically (i.e., y-direction), but there are no gravitational contributions to the x- and z-components of the Equation of Motion. The Equation of Continuity for one-dimensional flow, $\nabla \bullet \mathbf{v} = \partial v_z/\partial z = 0$, reveals that the z-component of the fluid velocity vector v_z does not depend on axial position z, measured in the direction of flow from the inlet. Since there is no transverse flow in the x- and y-directions, the unimportant components of the Equation of Motion (i.e., x- and y-components) yield the following information about dynamic pressure P, which is the sum of fluid pressure p and gravitational energy per unit volume;

x-component: $0 = -\partial P/\partial x$, therefore $P \neq f(x)$

y-component: $0 = -\partial P/\partial y$, therefore $P \neq f(y)$

These results imply that dynamic pressure is only a function of z at steady state. Now, the important component of the Equation of Motion in terms of velocity gradients for incompressible Newtonian fluids yields a 2nd-order partial differential equation which allows one to calculate $v_z(x,y)$;

z-component: $$0 = -\frac{dP}{dz} + \mu\left\{\frac{\partial^2 v_z}{\partial x^2} + \frac{\partial^2 v_z}{\partial y^2}\right\}$$

If fluid flow is driven only by a fluid pressure drop in the z-direction, then $g_z = 0$ and one can replace the dynamic pressure gradient dP/dz in the previous equation by the fluid pressure gradient, dp/dz. Separation of variables yields $dp/dz = -\Delta p/L$, where Δp represents the positive fluid pressure drop from inlet to outlet. The general solution for $v_z(x,y)$ can be represented as the sum of homogeneous $\{v_z(x,y)\}_{Homogeneous}$ and particular $\{v_z(x,y)\}_{Particular}$ solutions. The appropriate equation for $\{v_z(x,y)\}_{Homogeneous}$, based on the z-component of the Equation of Motion, is;

$$\left\{\frac{\partial^2}{\partial x^2} + \frac{\partial^2}{\partial y^2}\right\} v_{z,Homogeneous} = 0$$

One postulates the following *separation of variables* solution to the previous equation;

$$\left\{v_z(x,y)\right\}_{Homogeneous} = X(x)Y(y)$$

Substitution of the postulated homogeneous solution into the z-component of the Equation of Motion and division by $v_{z,Homogeneous}$ yields;

$$\frac{1}{X}\frac{d^2X}{dx^2} = -\frac{1}{Y}\frac{d^2Y}{dy^2} = \lambda^2$$

where λ^2 is the *separation constant.* The previous equation is *separated* into two 2nd-order linear ordinary differential equations:

$$\frac{d^2X}{dx^2} - \lambda^2 X = 0; \frac{d^2Y}{dy^2} + \lambda^2 Y = 0$$

Solutions to these frequently occurring 2nd-order ODEs depend on the *sign* of the coefficient of the zeroth-derivative term (i.e., $-\lambda^2$ and $+\lambda^2$). If λ is real and λ^2 is greater than zero, then

X(x) is expressed in terms of hyperbolic sines and cosines, whereas Y(y) contains trigonometric sines and cosines. Hence;

$$X(x) = A\cosh(\lambda x) + B\sinh(\lambda x)$$
$$Y(y) = C\cos(\lambda y) + D\sin(\lambda y)$$

The particular solution to;

$$\left\{\frac{\partial^2}{\partial x^2} + \frac{\partial^2}{\partial y^2}\right\} v_{z,Particular} = \frac{1}{\mu}\frac{dP}{dz} = -\frac{\Delta p}{\mu L} < 0$$

is a one-dimensional quadratic function with respect to either x or y, such that the Laplacian of $v_{z,Particular}$ yields a negative constant (i.e., $-\Delta p/\mu L$). The result is;

$$v_{z,Particular}(y) = -\frac{\Delta p}{2\mu L} y^2 + Ey + F$$

The quadratic with respect independent variable y has been chosen because this is the important functional dependence of v_z that survives for channels with very large aspect ratios (i.e., $A_r = a/b \Rightarrow \infty$). Hence, the final result for $v_z(x,y)$ reduces to $v_z(y) \approx F - y^2\Delta p/2\mu L$ when the stationary walls at $x=\pm a$ have an insignificant effect on the one-dimensional viscous flow profile. The general solution for the z-component of the fluid velocity vector is;

$$v_z(x,y) = \{v_z(x,y)\}_{Particular} + \{v_z(x,y)\}_{Homogeneous}$$
$$= -\frac{\Delta p}{2\mu L} y^2 + Ey + F + \{A\cosh(\lambda x) + B\sinh(\lambda x)\}\{C\cos(\lambda y) + D\sin(\lambda y)\}$$

Focus on the upper right-hand quadrant of the flow cross-section in the positive xy-plane and invoke no-slip at the stationary solid boundaries (i.e., x=a, y=b) together with symmetry at the midplanes (i.e., x=0, y=0). Hence, the previous general solution for $v_z(x,y)$ must satisfy the following boundary conditions;

$$v_z(x=a, y) = v_z(x, y=b) = 0$$
$$\left(\frac{\partial v_z}{\partial x}\right)_{x=0} = \left(\frac{\partial v_z}{\partial y}\right)_{y=0} = 0$$

Symmetry at both midplanes requires that B=D=E=0, because all *odd* functions of x and y with respect to x=0 and y=0 [i.e., Ey, Bsinh(λx), Dsin(λy)] must be discarded from the general solution, yielding the following simplified result for v_z;

$$v_z(x,y) = -\frac{\Delta p}{2\mu L}y^2 + F + G\cosh(\lambda x)\cos(\lambda y)$$

where integration constant G = AC. Since F and G cannot be functions of x or y, no-slip at y=b allows one to calculate F and define the eigenvalues for this problem;

$$F = \frac{b^2\Delta p}{2\mu L}; \lambda_n b = (2n+1)\frac{\pi}{2}; n = 0,1,2,3...$$

$$v_z(x,y) = \frac{\Delta p}{2\mu L}\left\{b^2 - y^2\right\} + \sum_{n=0}^{\infty} G_n \cosh(\lambda_n x)\cos(\lambda_n y)$$

The no-slip boundary condition at x=a yields the following infinite series that defines $G_n\cosh(\lambda_n a)$ as Fourier cosine coefficients of a simple quadratic function. For example;

$$\sum_{n=0}^{\infty} G_n \cosh(\lambda_n a)\cos(\lambda_n y) = -\frac{\Delta p}{2\mu L}\left\{b^2 - y^2\right\}$$

$$\sum_{n=0}^{\infty} G_n \cosh(\lambda_n a)\int_0^b \cos(\lambda_n y)\cos(\lambda_m y)dy = -\frac{\Delta p}{2\mu L}\int_0^b \left\{b^2 - y^2\right\}\cos(\lambda_m y)dy$$

With assistance from integral tables, it can be shown that all terms in the *sum of integrals* vanish except when summation index n=m, due to the orthogonality relations of the cosine functions. For example, when n≠m;

$$\int_0^b \cos(\lambda_n y)\cos(\lambda_m y)dy = \left[\frac{\sin\{(\lambda_n - \lambda_m)y\}}{2(\lambda_n - \lambda_m)} + \frac{\sin\{(\lambda_n + \lambda_m)y\}}{2(\lambda_n + \lambda_m)}\right]_{y=0}^{y=b}$$

$$\frac{b}{2\pi}\left[\frac{\sin\left\{(n-m)\pi\frac{y}{b}\right\}}{(n-m)} + \frac{\sin\left\{(n+m+1)\pi\frac{y}{b}\right\}}{(n+m+1)}\right]_{y=0}^{y=b} = 0$$

The only term that survives in the sum of integrals, when n=m, is;

$$\int_0^b \cos(\lambda_m y)\cos(\lambda_m y)dy = \left[\frac{y}{2} + \frac{\sin(2\lambda_m y)}{4\lambda_m}\right]_{y=0}^{y=b} = \frac{b}{2} + \frac{b}{2}\left[\frac{\sin\left\{(2m+1)\pi\frac{y}{b}\right\}}{(2m+1)\pi}\right]_{y=0}^{y=b} = \frac{b}{2}$$

The appropriate Fourier cosine coefficients in the infinite series solution for $v_z(x,y)$ are;

$$\sum_{n=0}^{\infty} G_n \cosh(\lambda_n a)\int_0^b \cos(\lambda_n y)\cos(\lambda_m y)dy = \sum_{n=0}^{\infty} G_n \frac{b}{2}\delta_{mn}\cosh(\lambda_n a)$$

$$= \frac{1}{2}bG_m \cosh(\lambda_m a) = -\frac{\Delta p}{2\mu L}\int_0^b \left\{b^2 - y^2\right\}\cos(\lambda_m y)dy$$

The right side of the previous equation is evaluated with assistance from integral tables;

$$b^2\int_0^b \cos(\lambda_m y)dy = \frac{b^2}{\lambda_m}\left[\sin\left\{(2m+1)\frac{\pi y}{2b}\right\}\right]_{y=0}^{y=b} = (-1)^m\frac{b^2}{\lambda_m}$$

$$\int_0^b y^2\cos(\lambda_m y)dy = \frac{1}{\lambda_m^3}\left[\lambda_m y\left\{2\cos(\lambda_m y) + \lambda_m y\sin(\lambda_m y)\right\} - 2\sin(\lambda_m y)\right]_{y=0}^{y=b}$$

$$= \frac{1}{\lambda_m^3}\left[\lambda_m b\left\{2\cos\left\{(2m+1)\frac{\pi}{2}\right\} + \lambda_m b\sin\left\{(2m+1)\frac{\pi}{2}\right\}\right\} - 2\sin\left\{(2m+1)\frac{\pi}{2}\right\}\right] = \frac{(-1)^m}{\lambda_m^3}\left[(\lambda_m b)^2 - 2\right]$$

The general expression for the coefficients in the infinite series for $v_z(x,y)$ is;

$$\frac{1}{2}bG_m\cosh(\lambda_m a) = -\frac{\Delta p}{2\mu L}\int_0^b \left\{b^2 - y^2\right\}\cos(\lambda_m y)dy = -\frac{\Delta p}{2\mu L}\left\{(-1)^m\frac{b^2}{\lambda_m} - \frac{(-1)^m}{\lambda_m^3}\left[(\lambda_m b)^2 - 2\right]\right\}$$

$$= (-1)^{m+1}\frac{\Delta p}{\mu L\lambda_m^3}$$

$$G_m = (-1)^{m+1}\frac{2\Delta p}{\mu bL\lambda_m^3\cosh(\lambda_m a)}$$

The final expression for the one-dimensional velocity profile through rectangular channels is;

$$v_z(x,y) = \frac{b^2 \Delta p}{2\mu L}\left[\left\{1-(y/b)^2\right\} + 4\sum_{n=0}^{\infty} \frac{(-1)^{n+1}}{(\lambda_n b)^3 \cosh(\lambda_n a)} \cosh(\lambda_n x)\cos(\lambda_n y)\right]$$

$$\lambda_n b = (2n+1)\frac{\pi}{2}$$

If one defines a *dimensionless* z-component of the fluid velocity vector via division of $v_z(x,y)$ by the average velocity $\langle v_z \rangle_{Average}$, then it is necessary to evaluate the volumetric flowrate Q through the rectangular channel by integrating the previous expression for v_z over the entire flow cross-section. Since all four quadrants behave similarly via symmetry, it is sufficient to focus on one quadrant only (i.e., $0 \le x \le a$, $0 \le y \le b$). Hence;

$$Q = 4ab\langle v_z \rangle_{Average} = \int_{x=-a}^{a}\int_{y=-b}^{b} v_z(x,y)\,dxdy = 4\int_{x=0}^{a}\int_{y=0}^{b} v_z(x,y)\,dxdy$$

$$\langle v_z \rangle_{Average} = \int_{x^*=0}^{1}\int_{y^*=0}^{1} v_z(x^*,y^*)\,dx^*dy^*$$

In terms of dimensionless spatial variables in the flow cross-section, x*=x/a and y*=y/b, one obtains the following result for the dimensionless velocity profile;

$$v_z^*(x^*,y^*) = \frac{v_z(x^*,y^*)}{\langle v_z \rangle_{Average}} = \frac{2\left[\left\{1-(y^*)^2\right\} + 4\sum_{n=0}^{\infty} \frac{(-1)^{n+1}}{M_n^3 \cosh(M_n A_r)} \cosh(M_n A_r x^*)\cos(M_n y^*)\right]}{\frac{4\mu L}{b^2 \Delta p}\int_{x^*=0}^{1}\int_{y^*=0}^{1} v_z(x^*,y^*)\,dx^*dy^*}$$

$$M_n = (2n+1)\frac{\pi}{2}$$

Page#619 4 lines up from the bottom of the page:
(2) Rate of depletion of reactants due to *heterogeneous surface-catalyzed* chemical reaction ...

Page#620 4 lines down from the beginning of **Section 23-3.2:**
transverse to the primary flow direction. (Catalyst poisoning introduces some dependence of $k_{1,Surface}$ on z). Hence;

Page#633 just above ***Self-Consistent Check of the Numerical Solution:***

Where the *fitting parameter* λ characterizes the spatial rate of decrease of reactant bulk molar density on semi-logarithmic axes. Appropriate ransformation of the dimensionless axial variable ξ (see equations 23-80, 23-81, and 23-82), which includes the aspect ratio and the Damkohler number, allows one to develop universal correlations for all rectangular duct reactors with uniform catalyst activity (Hatton & Quarmby, 1962).

Page#639 just above Section 23-6.3:
... understood. However, if one were designing an experimental reactor to measure the kinetics of heterogeneous surface-catalyzed chemical reactions, then a tube-wall reactor with circular cross-section would eliminate nonuniform reactant accessibility to the catalytic surface in the problematic corner regions.

Page#652 replace W(x) by W(χ) three lines above the last equation on this page.

Page#653 ***Problem 23-8***

Use some of the numerical methodology discussed in this chapter to solve the steady state microscopic mass transfer equation for convective diffusion in heterogeneous catalytic "tube-wall" reactors with circular cross-section in the laminar flow regime for incompressible Newtonian fluids. Chemical reaction at the catalytic surface (i.e., r=R) is irreversible and first-order with respect to reactant A. Let the tube radius R be the characteristic length in the definitions of the Damköhler (i.e., β) and mass transfer Peclet (i.e., Pe_{MT}) numbers, and consider the regime where Pe_{MT} is large enough to justify the neglect of axial diffusion.

Answer:

The appropriate mass transfer equation is given in *Step#5* of the previous problem at the bottom of page#649, and the laminar flow velocity profile is provided in *Step#7* on page#650. Hence, the primary objective of this exercise is to calculate the molar density of reactant A, $C_A(r,z)$, from the following partial differential equation and its boundary conditions in cylindrical coordinates, with variable coefficients and chemical reaction at the boundary of the flow configuration;

$$2\langle v_z\rangle_{Average}\left\{1-\eta^2\right\}\frac{\partial C_A}{\partial z}=D_A\frac{1}{r}\frac{\partial}{\partial r}\left\{r\frac{\partial C_A}{\partial r}\right\}=D_A\left\{\frac{\partial^2 C_A}{\partial r^2}+\frac{1}{r}\frac{\partial C_A}{\partial r}\right\}$$

$$C_A=C_{A,inlet}\ @\ z=0, r<R$$

$$\left\{\frac{\partial C_A}{\partial r}\right\}_{r=0}=0;-D_A\left\{\frac{\partial C_A}{\partial r}\right\}_{r=R}=k_{1,Surface}C_A\left(r=R,z\right)$$

The zero-flux boundary condition along the tube axis at r=0 is a consequence of symmetry, and the *radiation* boundary condition at the catalytic surface (i.e., r=R) represents a balance between diffusion and chemical reaction. Radial and axial positions are dimensionalized using tube radius R. Hence, $\eta = r/R$ and $\zeta = z/R$. Reactant molar density is dimensionalized via the inlet condition, $\Psi_A(\eta,\zeta) = C_A(r,z)/C_{A,inlet}$. In terms of the important dimensionless numbers that govern the solution to this problem;

$$Damkohler\#;\beta = \frac{k_{1,Surface}R}{D_{A,ordinary}}$$

$$Peclet\#;Pe_{MT} = \frac{\langle v_z \rangle_{Average}R}{D_{A,ordinary}}$$

the mass transfer equation and its boundary conditions can be written as follows using dimensionless variables;

$$2Pe_{MT}\left\{1-\eta^2\right\}\frac{\partial\Psi_A}{\partial\zeta} = \frac{\partial^2\Psi_A}{\partial\eta^2} + \frac{1}{\eta}\frac{\partial\Psi_A}{\partial\eta}$$

$$\Psi_A = 1 @ \zeta = 0, \eta < 1$$

$$\left\{\frac{\partial\Psi_A}{\partial\eta}\right\}_{\eta=0} = 0; \left\{\frac{\partial\Psi_A}{\partial\eta}\right\}_{\eta=1} = -\beta\Psi_A\left(\eta=1,\zeta\right)$$

Problem 23-7 provides an asymptotically exact mass transfer boundary layer solution for $C_A(r,z)$ in the inlet region (i.e., z>0) for heterogeneous catalytic tubular reactors (see *Step#16* on page#652). A much simpler approach is adopted below to initiate the numerical algorithm by applying the radiation boundary condition at z=0 and r=R (or ζ=0 and η=1) to estimate the molar density of reactant A at the wall near the inlet plane. For example;

$$\left\{\frac{\partial\Psi_A}{\partial\eta}\right\}_{\eta=1} \approx \frac{\Psi_A\left(\eta=1,\zeta=0\right)-1}{\Delta\eta} = -\beta\Psi_A\left(\eta=1,\zeta=0\right)$$

$$\Psi_A\left(\eta=1,\zeta=0\right) \approx \frac{1}{1+\beta\Delta\eta}$$

which exhibits the correct trend, because reactant molar density at the catalytic surface decreases when the rate of reaction is faster and the Damköhler number increases. In an effort to check the validity of the finite-difference solutions to the microscopic mass

transfer equation, one poses the following question; *Do the microscopic results satisfy the quasi-macroscopic mass balance?* Hence, it is necessary to evaluate the bulk molar density of reactant A at each axial position, given by equation (23-19), explicitly for tubular reactors. Analogous to equation (23-51) for rectangular ducts, the dimensionless bulk reactant molar density in tubular reactors is;

$$C_{A,bulk}(z) = \frac{\iint_S v_z(r) C_A(r,z) r dr d\Theta}{\pi R^2 \langle v_z \rangle_{Average}} = 4 \int_{\eta=0}^{1} C_A(r,z)\{1-\eta^2\}\eta d\eta$$

$$\Psi_{A,bulk}(\xi) = 4 \int_{\eta=0}^{1} \Psi_A(\eta,\xi)\{1-\eta^2\}\eta d\eta$$

Finally, the quasi-macroscopic mass balance for heterogeneous catalytic reactors with first-order irreversible chemical reaction at the boundary, as described on pages 634-636, is analyzed completely for uniform catalyst activity on the inner wall of tubes in Problem 23-6 on pages 647-648. Hence, the second equation on page#648 is dimensionalized as follows;

$$\langle v_z \rangle_{Average} \pi R^2 \left\{ -\frac{dC_{A,bulk}}{dz} \right\} = 2\pi R k_{1,Surface} C_A(r=R,z)$$

$$-\frac{d\Psi_{A,bulk}}{d\xi} = \frac{2\beta}{Pe_{MT}} \Psi_A(\eta=1,\xi)$$

These equations are analyzed via the following finite-difference algorithm that can be implemented in conjunction with a linear equation solver. A nonlinear equation solver is required if the chemical kinetics are not first-order.

Important parameters that govern the solution to the convective diffusion mass transfer equation for laminar flow tube-wall reactors

$\beta = 150$	Damköhler number; heterogeneous reaction rate wrt diffusion rate
$Pe_{MT} = 25$	Mass transfer Peclet number; rate of convection wrt diffusion rate

Numerical grid parameters that determine the total number of grid points and mesh size

$N_R = 101$	number of discretized points in the radial direction
$\Delta\eta = 1/(N_R-1)$	step size in the radial direction
$\Delta\xi = 0.001$	step increment in axial position

Establish the dimensionless inlet molar density profile of reactant A

$\Psi_A(j,k=0) = 1;\ 1 \le j \le N_R - 1$ no conversion in the feed stream at $\zeta=0$

$\Psi_A(N_R,k=0) = 1/(1+\beta\Delta\eta)$ approximate molar density at the wall via the BC at $\eta=1$

Evaluate the dimensionless laminar flow velocity profile at each radial mesh point

$\eta(j) = (j-1)\Delta\eta;\ 1 \le j \le N_R$

$v^*_z(j) = 2\{1-[\eta(j)]^2\}$

Initiate a counter and calculate the dimensionless axial position

k=1

***$\zeta = k\Delta\zeta$ use a loop and return to this statement each time counter k is incremented

Symmetry boundary condition at the center of the tube (i.e., $\eta=0$)
Second-order-correct forward difference representation for first derivatives, Eq. (23-35)

$$\frac{1}{2\Delta\eta}\left\{-\Psi_A(3,k) + 4\Psi_A(2,k) - 3\Psi_A(1,k)\right\} = 0$$

Radiation boundary condition at the catalytic wall (i.e., $\eta=1$)
Second-order-correct backward difference representation for first derivatives, Eq. (23-40)

$$\frac{1}{2\Delta\eta}\left\{3\Psi_A(N_R,k) - 4\Psi_A(N_R-1,k) + \Psi_A(N_R-2,k)\right\} = -\beta\Psi_A(N_R,k)$$

Implicit finite-difference representation of the convective diffusion mass transfer equation within the tube; 1st derivative with respect to axial position ζ is first-order correct; 1st and 2nd spatial derivatives with respect to radial position η are second-order correct, Eq. (23-24)

$$2 \le j \le N_R - 1$$

$$Pe_{MT} v_z^*(j) \frac{\Psi_A(j,k) - \Psi_A(j,k-1)}{\Delta\zeta} = \frac{\Psi_A(j+1,k) - 2\Psi_A(j,k) + \Psi_A(j-1,k)}{(\Delta\eta)^2} + \frac{\Psi_A(j+1,k) - \Psi_A(j-1,k)}{\eta(j)2\Delta\eta}$$

Calculate the bulk molar density of reactant A via the trapezoidal rule

$$\Psi_{A,bulk}(k) = 2\left\{\frac{\Delta\eta}{2}\right\}\sum_{j=2}^{N_R-1} 2\eta(j) v_z^*(j) \Psi_A(j,k)$$

Verify that the finite-difference solution of the microscopic convective diffusion equation also satisfies the quasi-macroscopic mass balance, using the trapezoidal rule

$$\frac{\Psi_{A,bulk}(k-1)-\Psi_{A,bulk}(k)}{\Delta\zeta}=\frac{2\beta}{Pe_{MT}}\Psi_{A}(N_R,k)$$

*Increment the counter, return to the step denoted by 3 asterisks ***, solve the system of linear algebraic equations at the next axial step, calculate the bulk molar density of reactant A and verify that the finite-difference solution also satisfies the quasi-macroscopic mass balance*

k = k+1

Go To ***

Calculate the dimensionless tube length ζ = z/R that is required to achieve 50% conversion of reactant A to products when the Damköhler number is 150 and the mass transfer Peclet number is 25. Hint: Graph $\Psi_{A,bulk}$ vs. ζ to obtain the answer.

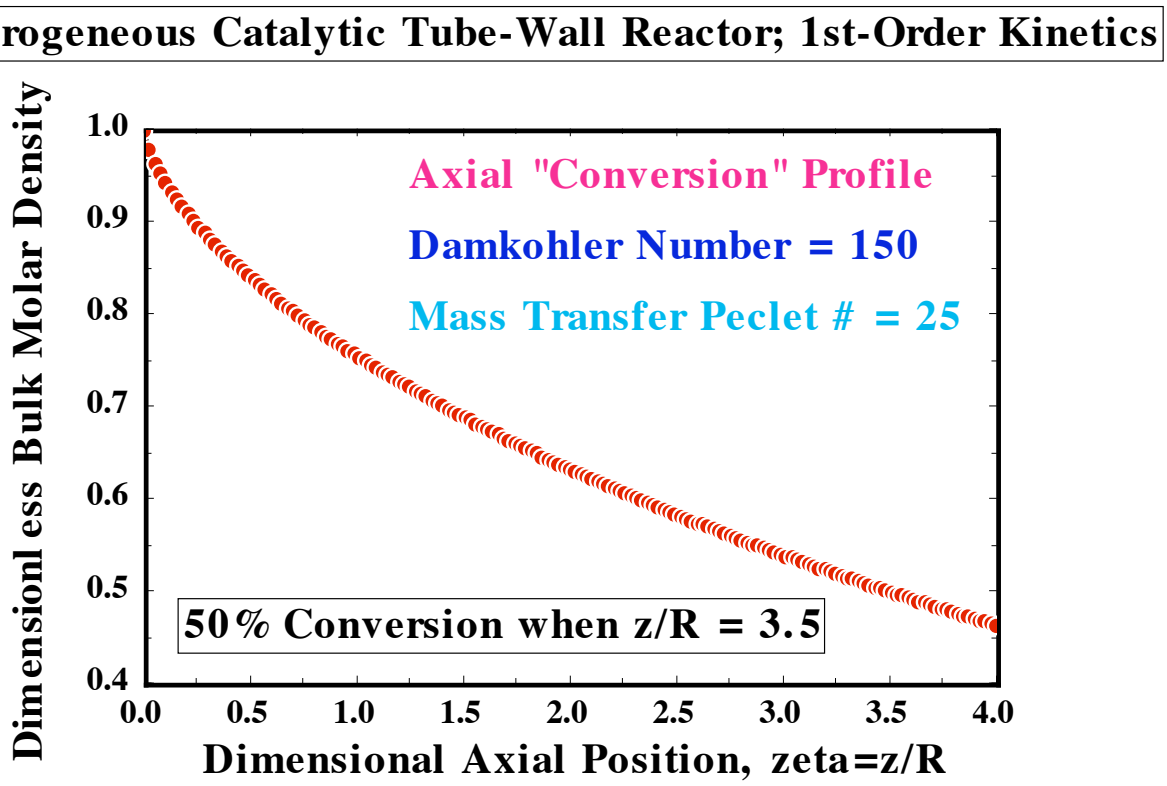

Predict the thickness of the mass transfer boundary layer $\delta_{MTBLT}(\zeta)$, measured inward from the catalytically active surface toward the centerline of the tube,

as a fraction of the tube radius R when ζ = 1, β = 150, and Pe_{MT} = 25. Hint: Graph $\Psi_A(\eta,\zeta=1)$ vs. η. Within the mass transfer boundary layer; $\Psi_A(R-\delta_{MTBLT},\zeta=1) \leq 0.98$

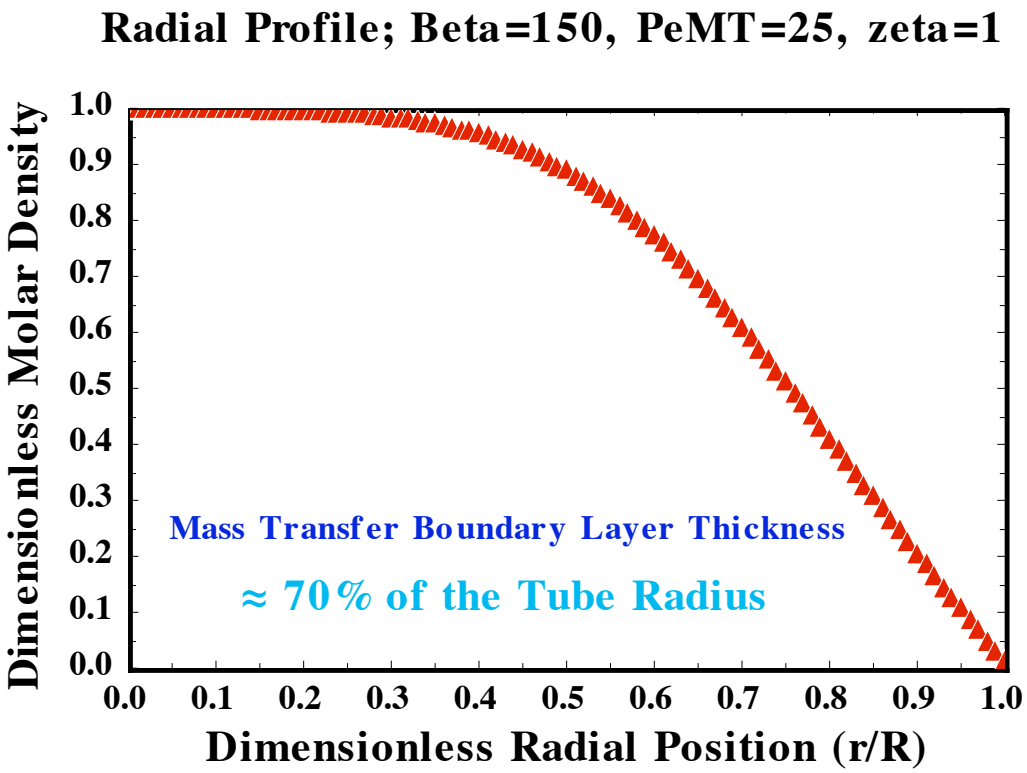

(24) Multicomponent Gas-Liquid CSTR's

Page#672 the reference for covalent and van der Waals radii in Table 24-1 is;
General Chemistry, by Linus Pauling, 3rd edition, WH Freeman (1970)

Page#683 **Problem 24-10** (last problem in the chapter on reactive distillation)

Pure liquid B is flowing at steady state from left to right across a perforated tray in a distillation column and bubbles of gas A rise through the liquid. Gas A is soluble in liquid B, and A reacts irreversibly with B only in the liquid phase. Due to the high concentration of B in the liquid phase, the "method of excess" suggests that the kinetic rate law is pseudo-first-order with respect to the liquid phase molar density of solubilized gas A. The rising motion of the bubbles produces a "well-stirred" liquid mixture of A and B, but the two streams do not leave the tray in equilibrium with each other. At most, equilibrium is established at the spherical gas-liquid interface.

(a) Consider mass transfer rate processes and their corresponding time constants to describe the conditions that must exist if the outlet liquid stream contains a significant fraction of species A, realizing that the inlet stream contains pure liquid B. Do not use any equations.

Answer:
The time constant for interphase mass transfer of species A must be significantly smaller than either of the time constants for (i) chemical reaction in the liquid phase or (ii) convective mass transfer of the liquid phase across the tray in the distillation column (i.e., residence time).

(b) In the diffusion-limited regime, perform a macroscopic balance on the liquid phase and obtain an algebraic equation that relates the outlet liquid phase molar density of reactant A, $C_{A,outlet}$, to the following quantities;

$C_{A,equilibrium}$	equilibrium molar density of species A on the liquid side of the gas-liquid interface (i.e., equilibrium solubility of gas A in liquid B, g-mol/cm^3)
$D_{A,Liquid}$	diffusion coefficient of species A in liquid B, (cm^2/sec)
k_1	pseudo-first-order kinetic rate constant in the liquid phase, (1/sec)
q	volumetric flow rate of the liquid, (cm^3/sec)
V_L	liquid phase volume on the tray, (cm^3)
τ	liquid phase residence time on the tray, V_L/q (sec)
a_L	interfacial area per unit volume of liquid, (1/cm)

Answer:
The liquid phase can be analyzed as a well-mixed CSTR operating at steady state. Hence, one equates rates of input to rates of output for reactant A in its liquid phase mass balance. Since the inlet liquid stream contains pure component B, there is no contribution from convective mass transfer across the inlet plane.

Rate of input due to interphase mass transfer = $\{k_1 D_{A,Liquid}\}^{1/2}[C_{A,equilibrium} - C_{A,outlet}]a_L V_L$
(using a chemical-reaction-enhanced mass transfer coefficient in the diffusion-limited regime, where curvature effects are negligible for thin mass transfer boundary layers)

Rate of output due to convective mass transfer = $qC_{A,outlet}$

Rate of disappearance of reactant A due to 1st-order irreversible reaction = $k_1 C_{A,outlet} V_L$

The steady state liquid-phase CSTR mass balance for reactant A, with dimensions of moles per time, is;

$$\sqrt{k_1 D_{A,Liquid}}\left(C_{A,equilibrium} - C_{A,outlet}\right)a_L V_L = qC_{A,outlet} + k_1 C_{A,outlet} V_L$$

$$C_{A,outlet} = C_{A,equilibrium}\frac{a_L\sqrt{k_1 D_{A,Liquid}}}{a_L\sqrt{k_1 D_{A,Liquid}} + k_1 + \frac{1}{\tau}}$$

(c) The Arrhenius activation energy for diffusion of solubilized gas A in liquid B, $E_{ac/Diffusion}$, is much smaller than the Arrhenius activation energy for the chemical reaction, $E_{act/ChemicalReaction}$. Hence,

$$E_{act/Diffusion} << E_{act/Chemical\,Reaction}$$

$$\frac{d}{dT}\ln D_{A,Liquid} = \frac{E_{act/Diffusion}}{RT^2} > 0$$

$$\frac{d}{dT}\ln k_1 = \frac{E_{act/Chemical\,Reaction}}{RT^2} > 0$$

Describe how a <u>decrease</u> in temperature T will affect the outlet liquid phase molar density of reactant A. Will C_A increase, decrease, remain unchanged, or is it too complex to determine how C_A will change?

Part 6
Thermodynamics and Nonisothermal Reactor Design

(25) Non-Equilibrium Thermodynamics of Multicomponent Mixtures: Formalism and the Stokes-Einstein Diffusion Equation

(26) Molecular Flux of Thermal Energy in Multicomponent Mixtures

(27) Thermal Energy Balances and Non-Isothermal Effectiveness Factors

Page#748 insert an *Appendix* just before the PROBLEMS section;

Appendix:

Effects of the Collision Integral, Thermal Diffusion, and the Prater Number on Maximum Temperature in Macroporous Catalysts with Exothermic Chemical Reaction in the Diffusion-Controlled Regime

Overview. The classic Prater equation is useful to estimate intrapellet temperatures in packed catalytic tubular reactors when the dimensionless Prater number β is relatively small (i.e., the magnitude of $\beta \leq 0.5$). However, for strongly exothermic chemical reactions, both thermal diffusion and the temperature dependence of important physicochemical properties of reactive gas mixtures should be included in the analysis of coupled heat and mass transfer within isolated catalytic pellets. In the diffusion-limited regime, intrapellet temperature increases could be much greater than those predicted by the Prater equation. The analysis herein for Lennard-Jones gases reveals that steady state predictions for exothermic reactions might not be possible when the Prater number is on the order of unity, because core temperatures are more than one order-of-magnitude larger than temperatures on the external catalytic surface. For reference, the Prater equation predicts that the maximum intrapellet temperature is 2-fold larger than that on the external catalytic surface when β=1, which severely underestimates realistic temperature increases by a factor of 5 or 6 (i.e., when β=1) for the synthesis of methanol from carbon monoxide and hydrogen. The largest increases in intrapellet temperature occur when all of the following conditions are satisfied; (i) chemical reactions are strongly exothermic, (ii) physicochemical properties of the reactive gas mixture exhibit temperature dependence, (iii) the Prater number approaches unity, and (iv) Soret diffusion enhances the molar flux of C≡O (i.e., $MW_{CO} < MW_{\text{"B"}}$ in pseudo-binary mixtures) into the central core of macroporous catalysts as a consequence of negative thermal diffusion coefficients.

Introduction. The classic Prater equation [1-4] relates temperature and reactant molar density in porous catalysts when (i) only one chemical reaction occurs, (ii) all physicochemical properties of the reactive mixture exhibit no temperature dependence, and (iii) thermal diffusion is not considered. When catalysts operate in the diffusion-controlled regime at large intrapellet Damköhler numbers [5], the Prater equation suggests that there is a simple linear relation between maximum intrapellet temperatures near the central core of the catalyst and the Prater number β, where β is defined in Equation [15]. This relation between maximum intrapellet temperature and the Prater number exhibits significant deviations from linearity when the analysis of coupled heat and mass transfer in macroporous catalysts includes thermal diffusion and temperature-dependent physicochemical properties of the reactive gas mixture. Numerical analysis is required, in general, to obtain the desired nonlinear relation between maximum intrapellet temperature

and the Prater number β, which reveals that β has a practical upper limit for steady state simulations to prevent core temperatures from increasing by several orders of magnitude relative to conditions on the external catalytic surface. This restriction on the magnitude of the Prater number for exothermic chemical reactions is not obvious from the original Prater equation, and there are very few publications in the Web of Science™ database that focus on maximum temperature in porous catalysts with exothermic chemical reaction. There seems to be a dearth of publications that address intrapellet coupled heat and mass transfer with exothermic chemical reaction in the presence of thermal diffusion (i.e., the Soret effect). The next two sections consider steady state analysis of the microscopic mass transfer equation and the thermal energy balance with one chemical reaction in porous catalysts. Convective transport in neglected. Equation [10] is valid in the presence or absence of thermal diffusion, whereas thermal diffusion is neglected in Equation [13]. These two equations and their dimensionless analogs provide the starting point for numerical analysis of maximum intrapellet temperature in the diffusion-controlled regime where the central core of the catalyst is starved of reactants.

Theoretical Considerations

Stoichiometry and the steady state mass balance with diffusion and chemical reaction in porous catalytic pellets. Contributions from convective transport are negligible in porous catalysts. Hence, one begins with the steady state microscopic mass transfer equation [6] for species *i* that includes pseudo-homogeneous diffusion and multiple pseudo-volumetric chemical reactions;

$$\frac{\partial C_i}{\partial t} + v \bullet \nabla C_i \underset{\substack{neglibible \\ convective \\ transport}}{\overset{steady\ state}{\Rightarrow}} 0 = -\nabla \bullet \left\{ \frac{j_{i,pellet}}{MW_i} \right\} + \sum_{\substack{k \\ reactions}} \upsilon_{ik} R_k \qquad [1]$$

where C_i is the molar density of component *i* with molecular weight MW_i, $\mathbf{j}_{i,pellet}$ represents the intrapellet diffusional mass flux of species *i* with respect to a reference frame that translates at the mass-average velocity $\mathbf{v} \approx 0$ of the reactive mixture, υ_{ik} is the stoichiometric coefficient of species *i* in reaction *k*, and R_k is the intrinsic rate of the k^{th} chemical reaction. Stoichiometric relations are exceedingly complex in the presence of multiple chemical reactions [7]. In light of this complexity, the current problem is addressed for only one chemical reaction on the internal catalytic surface. Now, subscript *k* is not required, and the previous mass balance with intrapellet diffusion and one chemical reaction yields the following stoichiometric relation [6] that is the *same for each component in the reactive mixture,* regardless of the consideration or neglect of thermal diffusion;

$$\frac{1}{\upsilon_i MW_i}\nabla \bullet j_{i,pellet} = \frac{1}{\upsilon_A MW_A}\nabla \bullet j_{A,pellet} = R \qquad [2]$$

Stoichiometric relations are generated from the mass balance by isolating all quantities that are *species specific* (i.e., containing subscript i). Equation [2] is integrated over an arbitrary control volume V within the catalytic pores via Gauss' law, yielding equation [3];

$$\int_V \left\{ \frac{1}{\upsilon_i MW_i}\nabla \bullet j_{i,pellet} - \frac{1}{\upsilon_A MW_A}\nabla \bullet j_{A,pellet} \right\} dV = \int_S \left\{ \frac{1}{\upsilon_i MW_i}\underline{n} \bullet j_{i,pellet} - \frac{1}{\upsilon_A MW_A}\underline{n} \bullet j_{A,pellet} \right\}_{@S} dS = 0$$

where $\underline{n}$ is a unit normal vector directed *outward* from the surface of the control volume. Since there are many choices for control volume V and surface S that surrounds this volume element, the integrand of the surface integral must vanish. Hence;

$$\frac{1}{\upsilon_i MW_i}\left\{ \underline{n} \bullet j_{i,pellet} \right\}_{@S} = \frac{1}{\upsilon_A MW_A}\left\{ \underline{n} \bullet j_{A,pellet} \right\}_{@S} \qquad [4]$$

It should be emphasized that this stoichiometric relation generated from the microscopic mass transfer equation with diffusion and one chemical reaction is valid at any surface S that surrounds control volume V within the pellet.

Intrapellet temperature. The primary objective of this section is to relate temperature and molar density within porous catalysts. This is accomplished from steady state analysis of coupled heat and mass transfer in an isolated pellet, where one pseudo-volumetric chemical reaction converts reactants to products. The thermal energy balance is written in terms of specific internal energy *u* for an N-component mixture, prior to invoking any assumptions [6];

$$\frac{\partial \rho u}{\partial t} + \nabla \bullet \rho v u = -\nabla \bullet \underline{q}_{pellet} - p\nabla \bullet v - \tau : \nabla v + \sum_{i=1}^{N} j_{i,pellet} \bullet g_i \qquad [5]$$

The molecular flux of thermal energy in this N-component gas mixture is [6];

$$\underline{q}_{pellet} = -k_{effective}\nabla T_{pellet} + \sum_{i=1}^{N} \frac{\overline{H_i}}{MW_i} j_{i,pellet} \qquad [6]$$

Fourier's law with effective intrapellet thermal conductivity $k_{effective}$ describes the first term on the right side of Equation [6], and the inter-diffusional flux that contains products of partial molar enthalpy and diffusional mass flux of each component in the summation accounts for the most important coupling between heat and mass transfer. The diffusion-thermo (i.e., Dufour) effect is neglected in Equation [6] for the molecular flux of thermal energy. The following intrapellet rate processes are neglected in the microscopic thermal energy balance [6] (i.e., Equation [5]);

(i) reversible exchange between internal and kinetic energies (i.e., $p\ \nabla \bullet \mathbf{v} \Rightarrow 0$),

(ii) irreversible conversion of kinetic energy to internal energy (i.e., $\tau : \nabla \mathbf{v} \Rightarrow 0$),

(iii) external force field effects (i.e., $\sum_{1 \le i \le N} \mathbf{j}_{i,pellet} \bullet \mathbf{g}_i \Rightarrow 0$)

Hence, the rather complex thermal energy balance given by Equation [5] is simplified considerably for steady state analysis with negligible intrapellet convective fluxes;

$$\nabla \bullet \underline{q}_{pellet} = 0 \qquad [7]$$

Integration of Equation [7] over an arbitrary control volume V within porous catalysts, via Gauss' law, yields;

$$\int_V \left\{ \nabla \bullet \underline{q}_{pellet} \right\} dV = \int_S \left[\underline{n} \bullet \underline{q}_{pellet} \right]_{@S} dS = 0 \qquad [8]$$

where $\underline{\mathbf{n}}$ is defined in the previous section. Since there are many choices for control volume V and surface S that surrounds this intrapellet volume element, the integrand of the surface integral vanishes. Hence;

$$\left[\underline{n} \bullet \underline{q}_{pellet} \right]_{@S} = \left[\underline{n} \bullet \left\{ -k_{effective} \nabla T_{pellet} + \sum_{i=1}^{N} \frac{\overline{H_i}}{MW_i} j_{i,pellet} \right\} \right]_{@S} = 0 \qquad [9]$$

Equation [9] is evaluated on the external surface of the catalyst, where $\underline{\mathbf{n}}$ represents a unit normal vector directed <u>into</u> the pellet. Then, one invokes stoichiometry, via Equation [4], to relate intrapellet diffusional molar fluxes when only one chemical reaction occurs. Equation [9] is manipulated as follows;

$$\left[\underline{n}\bullet\left\{k_{effective}\nabla T_{pellet}\right\}\right]_{\substack{External\\Surface}}=\sum_{i=1}^{N}\upsilon_i\overline{H_i}\frac{1}{\upsilon_i MW_i}\left\{\underline{n}\bullet j_{i,pellet}\right\}_{\substack{External\\Surface}}$$

$$=\frac{1}{\upsilon_A MW_A}\left\{\underline{n}\bullet j_{A,pellet}\right\}_{\substack{External\\Surface}}\sum_{i=1}^{N}\upsilon_i\overline{H_i}\underset{\upsilon_A=-1}{\Rightarrow}\frac{1}{MW_A}\left\{\underline{n}\bullet j_{A,pellet}\right\}_{\substack{External\\Surface}}\left(-\Delta H_{\mathrm{Re}action}\right) \qquad [10]$$

where the stoichiometric coefficient of reactant A is –1. The summation of products of stoichiometric coefficients and partial molar enthalpies, over all species in the reactive mixture, is an exact representation of the enthalpy change for chemical reaction, $\Delta H_{Reaction}$, on a molar basis [8]. Intermolecular interactions and non-ideal heats of solution are also included in;

$$\sum_{i=1}^{N}\upsilon_i\overline{H_i}=\Delta H_{\mathrm{Re}action}\approx\Delta H^{0}_{Rx,298K}+\sum_{i=1}^{N}\upsilon_i\int_{298K}^{T}C_{p,i}(T)dT \qquad [11]$$

because the summation on the left side of Equation [11] contains partial molar enthalpies. In practice, one estimates $\Delta H_{Reaction}$ using literature values for standard state enthalpies of formation at 298K and temperature polynomials for pure-component specific heats [9]. This approximation is exact for ideal solutions because partial molar enthalpies reduce to pure-component molar enthalpies under ideal conditions. The diffusional molar flux of reactant A in the direction of $\underline{\mathbf{n}}$ is expressed in terms of a molar density gradient within the pellet and an effective intrapellet diffusivity, $D_{A,effective}$ (i.e., thermal diffusion is considered later in this *Appendix*) Hence;

$$\frac{1}{MW_A}\left\{\underline{n}\bullet j_{A,pellet}\right\}=-D_{A,effective}\frac{\partial C_{A,pellet}}{\partial n} \qquad [12]$$

where *n* is a spatial coordinate that increases in the direction of $\underline{\mathbf{n}}$, and the temperature dependence of $D_{A,effective}$ is governed by pore size, as described in the following section. The intrapellet conductive and diffusional fluxes are evaluated in the normal coordinate direction, relative to the external surface of the catalyst. The desired relation between temperature and reactant molar density is applicable to multi-dimensional transport throughout porous catalysts of any geometry, but the stoichiometric condition among diffusional mass fluxes limits this analysis to one chemical reaction [6]. As illustrated by Equation [13], which is applicable everywhere throughout an isolated pellet, spatial coordinate *n* does not appear in the final result;

$$\underline{n} \bullet \left\{ k_{effective} \nabla T_{pellet} \right\} = k_{effective} \frac{\partial T_{pellet}}{\partial n} = -\left(-\Delta H_{Reaction} \right) D_{A,effective} \frac{\partial C_{A,pellet}}{\partial n}$$

$$\frac{\partial T_{pellet}}{\partial C_{A,pellet}} = \frac{-\left(-\Delta H_{Reaction} \right) D_{A,effective}}{k_{effective}} \qquad [13]$$

Maximum temperature in macroporous catalysts with exothermic chemical reaction in the diffusion-controlled regime. For isolated pellets, dimensionless variables (i.e., Θ and $\Psi_{A,pellet}$) are introduced using the characteristic temperature $T_{Surface}$ and reactant molar density $C_{A,Surface}$ on the external surface of the catalyst. Hence;

$$\Theta = \frac{T_{pellet}}{T_{Surface}}; \Psi_{A,pellet} = \frac{C_{A,pellet}}{C_{A,Surface}} \qquad [14]$$

The thermal energy generation parameter β, also known as the Prater number [1-4,6], strongly influences temperature profiles within the catalyst. If one accounts for the temperature dependence of effective intrapellet diffusivities and the enthalpy change for chemical reaction, then dimensional analysis of Equation [13] yields;

$$\frac{\partial \Theta}{\partial \Psi_{A,pellet}} = \frac{-D_{A,effective}\left(T_{Surface}\right) C_{A,Surface} \left\{ -\Delta H_{Reaction}\left(T_{Surface}\right) \right\}}{T_{Surface} k_{effective}} \left[\frac{D_{A,effective}\left(T_{pellet}\right)}{D_{A,effective}\left(T_{Surface}\right)} \right] \left\{ \frac{\Delta H_{Reaction}\left(T_{pellet}\right)}{\Delta H_{Reaction}\left(T_{Surface}\right)} \right\}$$

$$= -\beta \varepsilon(\Theta) \zeta(\Theta) \qquad [15]$$

$$\beta = \frac{D_{A,effective}\left(T_{Surface}\right) C_{A,Surface} \left\{ -\Delta H_{Reaction}\left(T_{Surface}\right) \right\}}{T_{Surface} k_{effective}} = \text{Prater\#}$$

The Prater number β, which is positive for exothermic reactions [1-4], should be calculated using conditions on the external catalytic surface [6]. $\varepsilon(\Theta)$ represents a ratio of effective intrapellet diffusivities at intrapellet temperature T_{pellet} relative to temperature on the external surface of the catalyst, and $\zeta(\Theta)$ is the ratio of the enthalpy change for chemical reaction at intrapellet temperature T_{pellet} relative to $\Delta H_{Reaction}$ at the external catalytic surface temperature. The product of the Prater number and the intrapellet Damköhler number (i.e., $\beta\Lambda^2_{A,intrapellet}$, the intrapellet Damköhler number is defined by Equation [27] in the Epilogue) essentially represents a ratio of the rate of thermal energy generation due to chemical reaction relative to the rate of conductive transport within the catalyst. In the diffusion-limited regime at large values of the intrapellet Damköhler number [5], the central core of the catalyst is reactant-starved (i.e., $\Psi_{A,pellet} \Rightarrow 0$ as the dimensionless spatial coordinate $\eta \Rightarrow 0$) and significant temperature increases occur within the catalyst when the reaction is

exothermic. Under these conditions, the Prater equation [1-4,6] provides a *zeroth-order* prediction for the maximum dimensionless temperature, $\Theta_{max} \approx 1+\beta$, near the center of the catalyst when the temperature dependencies of (i) effective intrapellet diffusivities and (ii) the enthalpy change for chemical reaction are neglected [i.e., $\varepsilon(\Theta) \approx 1$, $\zeta(\Theta) \approx 1$]. When simple temperature dependence of intrapellet diffusion coefficients is considered [i.e., $\varepsilon(\Theta) \approx \Theta^m$, with m=0.5 for nanopores and m=1.5 for macropores], a better prediction for the maximum dimensionless temperature is obtained via integration of Equation [15] for Θ vs. $\Psi_{A,pellet}$, when $\Psi_{A,pellet} \Rightarrow 0$ as $\eta \Rightarrow 0$ for diffusion-controlled operation [6]. Hence;

$$\frac{\partial \Theta}{\partial \Psi_{A,pellet}} = -\beta\varepsilon(\Theta) \approx -\beta\Theta^m$$
$$\Theta_{\max}^{1-m} \approx 1+(1-m)\beta\left\{1-\Psi_{A,pellet}(\eta=0)\right\} \Rightarrow 1+(1-m)\beta \qquad [16]$$

Now, the upper limit for the thermal energy generation parameter is $\beta < 2$ in the macropore regime, because steady state predictions of Θ_{max} tend toward infinity when $\varepsilon(\Theta) \approx \Theta^{1.5}$, m=3/2, and β=2. The kinetic theory of dilute gases [10-13] describes the complete temperature dependence of ordinary molecular diffusion coefficients;

$$D_{A,ordinary} \approx \frac{T^{3/2}}{p\sigma^2\Omega_D(T)}$$
$$D_{A,effective} = \frac{\varepsilon_{p,\text{int}rapellet}}{\tau_{or}} D_{A,ordinary} \qquad [17]$$

The internal structure of the catalytic pores is described by an intrapellet void volume fraction $\varepsilon_{p,intrapellet}$ and tortuosity factor τ_{or}, where the former represents an average over pore size and the latter averages the orientation of *parallel pores* [3,6]. Equation [17] contains the dominant resistance to intrapellet mass transfer in macroporous catalysts where the average pore size is typically greater than 1 μm. The collision integral Ω_D, which quantitatively summarizes the dynamics of molecular trajectories and binary collisions for dilute gas mixtures [10], provides a correction to the *hard sphere intermolecular potential energy* because realistic molecules do not collide like hard spheres when the repulsive part of the potential exhibits some degree of *softness*. Since diffusion is inherently a "mixture property", collision cross-sections and collision integrals for diffusion, which scale as $1-\cos\chi$ where χ is the deflection angle in a collision, are slightly smaller than those for viscosity and thermal conductivity of pure materials, which scale as $1-\cos^2\chi$, at least as a first-order approximation for these isotropic transport properties [10-12]. Relative to rigid spheres with collision diameter σ for low-energy collisions, *Lennard-Jones molecules* have a slightly

smaller cross-section for high-energy collisions that are almost *head-on*, due to strong repulsive forces. The influence of attractive forces when intermolecular separations are greater than their equilibrium values is responsible for the fact that collision cross-sections for diffusion can be almost 6-fold larger than the corresponding rigid-sphere cross-sections for low-energy "grazing" collisions [10]. Numerical simulations in this section include temperature dependence of the collision integral Ω_D for diffusion in $\varepsilon(\Theta)$, as proposed by Neufeld et al. [14] for molecules that follow the Lennard-Jones 6-12 potential energy of interaction;

$$\Omega_D\left(T^*\right) \approx A\left\{T^*\right\}^{-B} + C\exp\left\{-DT^*\right\} + E\exp\left\{-FT^*\right\} + G\exp\left\{-HT^*\right\}$$
$$T^* = \frac{k_{Boltzmann}T_{Surface}\Theta}{\varepsilon_{Lennard-Jones}}; A = 1.06036; B = 0.15610; C = 0.19300 \qquad [18]$$
$$D = 0.47635; E = 1.03587; F = 1.52996; G = 1.76474; H = 3.89411$$

in addition to the three-halves power of dimensionless temperature for large pores. There are no distinguishable differences between the previous empirical equation and tabulated values of the diffusion collision integral from *Transport Phenomena,* by Bird, Stewart, and Lightfoot [13], for dimensionless temperatures T* between 0.30 and 100. As a consequence of including Ω_D in the ratio of effective intrapellet diffusivities, there is an additional dimensionless parameter that affects the maximum temperature rise in adiabatic pellets with exothermic chemical reaction (i.e., $k_{Boltzmann}T_{Surface}/\varepsilon_{Lennard\text{-}Jones}$). The maximum depth of the Lennard-Jones potential energy function, or the maximum energy of attraction when molecules reside at their equilibrium separation distance [i.e., $\sigma(2)^{1/6}$], is given by $\varepsilon_{Lennard\text{-}Jones}/k_{Boltzmann}$ with dimensions of absolute temperature, where $k_{Boltzmann}$ is Boltzmann's constant. Now, one must integrate the following equation, with $\zeta(\Theta) \approx 1$;

$$\frac{\partial\Theta}{\partial\Psi_{A,pellet}} = -\beta\varepsilon\left(\Theta\right) \approx -\beta\Theta^{1.5}\left\{\frac{\Omega_D\left(\Theta=1\right)}{\Omega_D\left(\Theta\right)}\right\} \qquad [19]$$

numerically from the external surface, where dimensionless temperature Θ and molar density $\Psi_{A,pellet}$ are unity, *inward* toward the center of the catalyst where the molar density of reactant A tends toward zero in the diffusion-controlled regime at large values of the intrapellet Damköhler number. It is necessary to transform the independent variable from dimensionless molar density $\Psi_{A,pellet}$ to $1-\Psi_{A,pellet}$, so that the new independent variable begins at zero on the external surface and achieves a value of 1 at the center of the pellet, as required by numerical ODE solvers. No singularity exists at the center of catalysts with cylindrical or spherical symmetry. As a consequence of this change in independent variable

from $\Psi_{A,pellet}$ to $1-\Psi_{A,pellet}$, it is necessary to remove the negative sign in Equation [19]. A second-order predictor-corrector algorithm was implemented with automatic step-size adjustment that is useful for integrating stiff differential equations. As a general rule, the effect of the collision integral for diffusion and its temperature dependence on the maximum temperature near the center of the catalyst is insignificant for thermal energy generation parameters (i.e., Prater numbers) $\beta < 0.5$. Under these conditions (i.e., $\beta < 0.5$), $\Theta_{max} \approx \{1 - \beta/2\}^{-2}$ provides reasonably accurate estimates of the temperature increase due to exothermic chemical reaction in macroporous catalysts [6]. This claim is based on comparisons of Θ_{max}, with and without the ratio of collision integrals in Equation [19] at various Prater numbers [15]. Froment and Bischoff [3] calculate typical Prater numbers for ten exothermic catalytic reactions, and only the dissociation of N_2O is characterized by $\beta > 0.5$ (actually $\beta = 0.64$). For example, macroporous alumina catalysts with effective thermal conductivities of 1.6×10^{-3} J/cm-sec-K, surface temperatures near 350K, and reactant molar densities estimated via the ideal gas law at $T_{Surface}$ and ambient pressure require enthalpy changes for chemical reaction on the order of 120 kJ/mol (i.e., ≈29 kcal/mol) to achieve a Prater number of unity [6]. Hence, intrapellet temperatures are not predicted to increase significantly in many cases because large effective thermal conductivities (i.e., $k_{effective}$) of metallic or metal-coated ceramic porous catalysts produce efficient intrapellet heat transfer. This is one of the primary reasons why typical Prater numbers do not exceed unity. For example, the strongly exothermic hydrogenation of benzene to cyclohexane over a supported-nickel catalyst [7,16] is described by Prater numbers that approach 0.95 (i.e., $\Delta H_{Reaction} \approx 50$ kcal/mol). When temperature dependence of the collision integral Ω_D for diffusion is considered, numerical simulations reveal that it is difficult to predict steady state temperature profiles in macroporous catalysts with exothermic chemical reaction when the thermal energy generation parameter β achieves values between 1.25 and 1.35. This upper limit of β for realistic predictions depends on the ratio of the catalytic surface temperature $T_{Surface}$ to the Lennard-Jones characteristic temperature (i.e., $T_{Lennard\text{-}Jones}$), where the latter is defined by the ratio of the maximum potential well depth $\varepsilon_{Lennard\text{-}Jones}$ to Boltzmann's constant $k_{Boltzmann}$. The upper limit of β is larger (i.e., $\beta \Rightarrow 1.35$) for reasonable predictions of Θ_{max} when $T_{Surface}/T_{Lennard\text{-}Jones}$ increases. Obviously, Θ_{max} increases when β is larger and $T_{Surface}/T_{Lennard\text{-}Jones}$ remains constant. However, Θ_{max} decreases when $T_{Surface}/T_{Lennard\text{-}Jones}$ is larger at constant Prater number. These trends are illustrated below in Figure#1 for intrapellet diffusion of carbon monoxide (i.e., $T_{Lennard\text{-}Jones} \approx 110$K) [10] when the external catalytic surface temperature, $T_{Surface}$, is either 300K, 400K, or 900K.

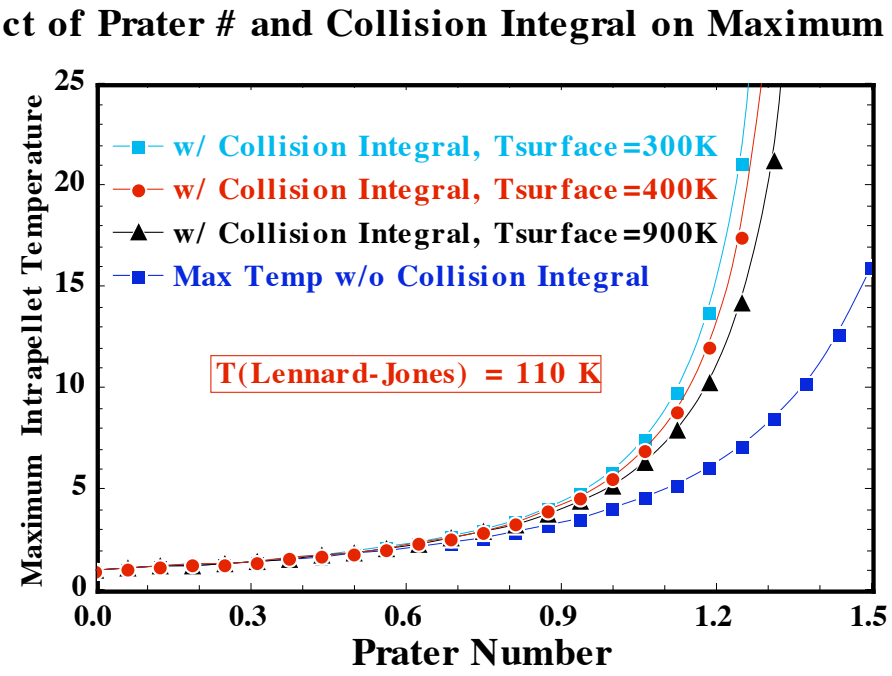

Figure#1

Effect of the Prater number and the collision integral for ordinary molecular diffusion on the maximum intrapellet temperature of macroporous catalysts in the diffusion-limited regime at large values of the intrapellet Damköhler number. Calculations are presented for carbon monoxide, whose maximum intermolecular energy of attraction is described by a Lennard-Jones temperature (or potential well depth, divided by Boltzmann's constant) of 110K. The Lennard-Jones temperature and the temperature on the external catalytic surface represent additional parameters that appear in the collision integral. For Prater numbers β greater than 1, there are significant differences between the maximum intrapellet temperature when the collision integral is included in the analysis, relative to the lowest curve that excludes the collision integral. Maximum temperature predictions without the collision integral correspond to $\Theta_{max} \approx \{1-\beta/2\}^{-2}$. Predictions from the original Prater equation yield $\Theta_{max} \approx 1+\beta$.

Effect of temperature-dependent enthalpy changes for exothermic chemical reaction on the maximum temperature in macroporous catalysts in the diffusion-controlled regime. *Production of methanol from a moderately high-pressure stoichiometric feed of carbon monoxide and hydrogen.* This specific example illustrates how the maximum intrapellet temperature for exothermic reactions is affected by including temperature dependence in $\Delta H_{Reaction}$, such that $\zeta(\Theta) \neq 1$ in Equations [15] and [19]. The synthesis of methanol from C≡O and H_2 in gas-phase packed catalytic tubular reactors is industrially important. Consequently, a large amount of experimental data is available to characterize this reaction over a wide range of operating pressures [17-21]. Since there are no H-H bonds in the final product, 5-site Langmuir-Hinshelwood chemical reaction

on zinc chromite catalysts (i.e., ZnO/Cr_2O_3) [6,17,18] is considered to be the rate-limiting step for $CO+2H_2 \Leftrightarrow CH_3OH$, with non-preferential dissociative adsorption of atomic hydrogen (i.e., H) on adjacent active sites. The synthesis of methanol over Cu-based catalysts [19] seems to occur exclusively by CO_2 hydrogenation at lower operating pressures. Equations [15], [17], [18], and [19] with $\zeta(\Theta) \neq 1$ provide the starting point for analysis of coupled heat and mass transfer in macroporous catalysts with temperature-dependent physicochemical properties, like $D_{A,effective}(T_{pellet})$ contained in $\varepsilon(\Theta)$ and $\Delta H_{Reaction}(T_{pellet})$ in $\zeta(\Theta)$;

$$\frac{\partial \Theta}{\partial \Psi_{A,pellet}} = -\beta \varepsilon(\Theta)\zeta(\Theta)$$

$$\zeta(\Theta) \approx \frac{\Delta H^0_{\mathrm{Re}action,298K} + \sum_{i=1}^{N} \upsilon_i \int_{298K}^{T=\Theta T_{Surface}} C_{p,i}(T')dT'}{\Delta H^0_{\mathrm{Re}action,298K} + \sum_{i=1}^{N} \upsilon_i \int_{298K}^{T_{Surface}} C_{p,i}(T')dT'} \qquad [20]$$

$$C_{p,i}(T) \approx a_i + b_i T + c_i T^2 + d_i T^3$$

The standard state enthalpy change at 298K, $\Delta H^0_{Reaction,298K}$, for the synthesis of methanol from carbon monoxide and hydrogen is –21.7 kcal/mol. The maximum energy of attraction for this Lennard-Jones ternary gas mixture, $\varepsilon_{ABC}/k_{Boltzmann}$, is estimated from a geometric average of pure-component potential well depths [6,10,13] when molecules reside at their equilibrium separation distances;

$$\frac{\varepsilon_{ABC}}{k_{Boltzmann}} \approx \frac{\sqrt[3]{\varepsilon_{C\equiv O}\varepsilon_{H_2}\varepsilon_{CH_3OH}}}{k_{Boltzmann}} \approx 123K \qquad [21]$$

Equation [21] is essentially an empirical *mixture rule* that allows one to estimate force constants between dissimilar molecules via force constants for pure gases [10]. Hence, the Lennard-Jones characteristic temperature for mixtures of $C\equiv O$, H_2, and CH_3OH is approximately 123K in Equation [18] for the diffusion collision integral. Following the numerical procedures described in the previous section, integration of Equation [20] from the external catalytic surface to the central core yields predictions of maximum dimensionless temperature that depend on the Prater number, as illustrated in Figure#2. It is assumed that the temperature polynomials [9] for pure-component specific heats $C_{p,i}(T)$ are valid at reasonably high temperatures near the center of the pellet.

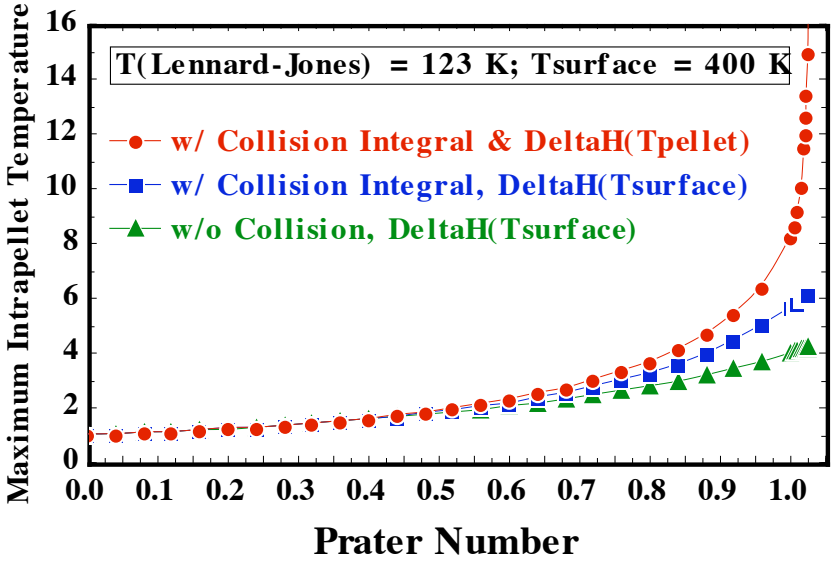

Figure#2

Effect of the Prater number, the collision integral for ordinary molecular diffusion, and temperature dependence of the exothermic enthalpy change for chemical reaction on the maximum intrapellet temperature of macroporous catalysts in the diffusion-limited regime. Calculations are presented for; $CO + 2H_2 \Leftrightarrow CH_3OH$. The Lennard-Jones temperature (or potential well depth, divided by Boltzmann's constant) of 123K represents a geometric average of $\varepsilon_i/k_{Boltzmann}$ for all three components in the gas mixture (see Equation [21]). Simulations are presented when temperature on the external catalytic surface is 400K. Inclusion of the collision integral and temperature dependence of the enthalpy change for chemical reaction in the analysis of coupled heat and mass transfer reveals that steady state simulations in macroporous catalysts might not be possible when the Prater number approaches unity for the synthesis of methanol.

Consideration of thermal diffusion in pseudo-binary mixtures. The preceding analysis of coupled heat and mass transfer in macroporous catalysts with exothermic chemical reaction in the diffusion-controlled regime suggests that predictions of maximum intrapellet temperatures could be significantly larger than those calculated from the Prater equation (i.e., $\Theta_{max} \approx 1+\beta$) when the Prater number, defined by Equation [15], is greater than 0.50. Furthermore, steady state analysis of the methanol synthesis from carbon monoxide and hydrogen is not a reasonable assumption when the Prater number approaches unity because maximum intrapellet temperatures could be more than an order of magnitude greater than $T_{Surface}$. The extreme upper limit of the Prater number for realistic steady state intrapellet simulations decreases from 2.0 to 1.25-1.35 to < 1.0, respectively, as the temperature dependencies of ordinary molecular diffusion coefficients for hard spheres (i.e.,

$T^{3/2}$), the collision integral $\Omega_D(T)$, and the enthalpy change for chemical reaction $\Delta H^0_{Reaction}(T)$ are systematically included in the analysis. Further modifications in the prediction of maximum intrapellet temperature for exothermic reactions in macroporous catalysts include contributions from thermal diffusion [6,10,13] to the diffusional mass flux vector (i.e., Equation [12]) when steep temperature gradients exist within the catalyst;

$$\frac{1}{MW_A} j_{A,pellet} \approx -D_{A,effective} \left\{ \nabla C_{A,pellet} + \frac{\rho}{MW_A} \left[k_T\right]_A \nabla \ln T_{pellet} \right\} \qquad [22]$$

Thermal diffusion has been neglected entirely in the classic treatise of reaction and diffusion in permeable catalysts by Aris [7]. In Equation [22], $[k_T]_A$ is the thermal diffusion ratio for species *A*, which characterizes the relative importance of thermal diffusion with respect to ordinary molecular diffusion. In binary mixtures of rigid spheres, where the molar masses of both components are very similar, the thermal diffusion ratio for species *A* is given by [10];

$$\left\{\left[k_T\right]_A\right\}_{\substack{Rigid \\ Sphere}} = \frac{105}{118} \left\{ \frac{MW_A - MW_B}{MW_A + MW_B} \right\} y_A y_B \qquad [23]$$

where y_i is the mole fraction of component i. The thermal diffusion ratio $\varphi_A(T^*)$ for Lennard-Jones molecules, relative to the corresponding ratio for rigid spheres, given by Equation [23], is defined as;

$$\varphi_A\left(T^*\right) = \frac{\left\{\left[k_T\left(T^*\right)\right]_A\right\}_{Lennard-Jones}}{\left\{\left[k_T\right]_A\right\}_{\substack{Rigid \\ Sphere}}} \qquad [24]$$

Figure#3 illustrates the universality of $\varphi_A(T^*)$ vs. $T^* = T/T_{Lennard\text{-}Jones}$ for binary isotopic mixtures whose intermolecular forces can be described by the Lennard-Jones 6-12 potential.

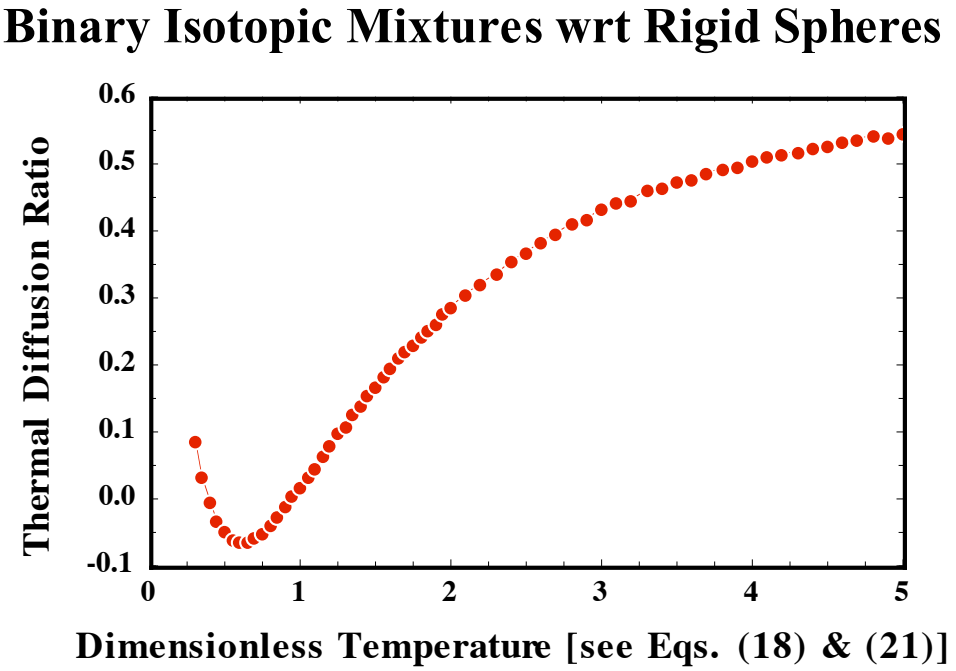

Figure#3

Universal temperature dependence of the thermal diffusion ratio for Lennard-Jones gases, relative to the corresponding ratio for rigid spheres (Eq. [23]), in binary isotopic mixtures. The dimensionless function $\varphi(T^*)$, defined by Equation [24], is plotted vs. dimensionless temperature for Lennard-Jones molecules (Eq. [18]), as required for the appropriate collision integrals. These data were obtained from pp.#528,543,1126-1129,1131 in *Molecular Theory of Gases & Liquids* [10].

Inversion temperatures exist when $\varphi_A(T^*)=0$ for $T^*\approx0.40$ and $T^*\approx0.95$. As temperature increases through these inversion points, the direction in which species *A* diffuses in response to temperature gradients changes. For example, if molecule *A* is the larger species in binary isotopic mixtures (i.e., $MW_A>MW_B$), then its rigid-sphere thermal diffusion ratio is greater than zero, via Equation [23], and *A* diffuses toward lower temperature when $T^* < 0.40$ and $T^* > 0.95$. If $MW_A < MW_B$, then the rigid-sphere thermal diffusion ratio for species *A* is negative and molecules of type *A* diffuse toward lower temperature when T^* is between 0.40 and 0.95. This is a crude approximation to the rigorous thermal diffusion ratio of carbon monoxide in ternary gas mixtures with hydrogen and methanol. Equation (8.2-50) in *Molecular Theory of Gases and Liquids* [10] for binary mixtures is expanded in powers of $(MW_A-MW_B)/(MW_A+MW_B)$ and truncated after the linear term when the molar masses of both components are similar. The universal model illustrated in Figure#3 for Lennard-Jones molecules is valid [22] when $(MW_A-MW_B)/(MW_A+MW_B) < 0.15$. The analog of Equation [13] in the presence of thermal diffusion is a considerably modified Prater equation that, upon numerical integration, yields more sophisticated predictions of maximum intrapellet temperatures relative to the results in Figures 1 and 2. Stoichiometry among intrapellet diffusional fluxes, as described by Equation [4] for only one chemical reaction, remains valid

when thermal diffusion is operative. Hence, the appropriate dimensional equation that describes intrapellet temperature changes is obtained by substituting Equation [22] into Equation [10]. Upon rearrangement, one obtains;

$$\frac{\partial T_{pellet}}{\partial C_{A,pellet}} = \frac{-D_{A,effective}\left(T_{pellet}\right)\left\{-\Delta H_{\mathrm{Re}action}\left(T_{pellet}\right)\right\}}{k_{effective}\left\{1+\frac{\rho}{MW_A T_{pellet}} D_{A,effective}\left(T_{pellet}\right)\left\{-\Delta H_{\mathrm{Re}action}\left(T_{pellet}\right)\right\}\frac{\left[k_T\left(T^*\right)\right]_A}{k_{effective}}\right\}} \quad [25]$$

Dimensional analysis of Equation [25] proceeds via the same methodology illustrated in Equation [15]. Hence, with assistance from the universal temperature-dependent thermal diffusion ratio $\varphi_A(T^*)$ for binary isotopic mixtures, illustrated in Figure#3, one predicts maximum intrapellet temperatures via numerical integration of Equation [26] from the external catalytic surface to the central core;

$$\frac{\partial \Theta}{\partial \Psi_{A,pellet}} = \frac{-\beta\varepsilon(\Theta)\zeta(\Theta)}{1+\left\{\frac{\rho}{MW_A C_{A,Surface}}\right\}\frac{1}{\Theta}\beta\varepsilon(\Theta)\zeta(\Theta)\varphi_A\left(T^*\right)\left\{\left[k_T\right]_A\right\}_{\substack{Rigid\\Sphere}}} \quad [26]$$

Simulations are presented in Figure#4, for $MW_A < MW_B$, and Figure#5, for a wide range of MW_B, to investigate the effect of *thermal diffusion inversion* in pseudo-binary isotopic mixtures on the maximum temperature within macroporous catalysts in the diffusion-controlled regime. When carbon monoxide is the smaller of the two components in pseudo-binary isotopic mixtures, C≡O migrates toward higher temperature regions in the central core of porous catalysts with exothermic chemical reaction for dimensionless temperatures $T^* > 0.95$ (i.e., see Equations [18], [23], and Figure#3). These conditions are simulated in Figure#4, revealing that the enhanced molar flux of C≡O toward the central core via thermal diffusion, together with temperature dependence for all physicochemical parameters in Equation [26], yields the largest prediction of maximum intrapellet temperatures. Relative to simulations that only account for temperature dependence of effective intrapellet diffusivities and $\Delta H_{Reaction}$, consideration of thermal diffusion (i.e., $MW_A < MW_B$) on maximum intrapellet temperatures in Figure#4 is insignificant unless the Prater number is very close to unity.

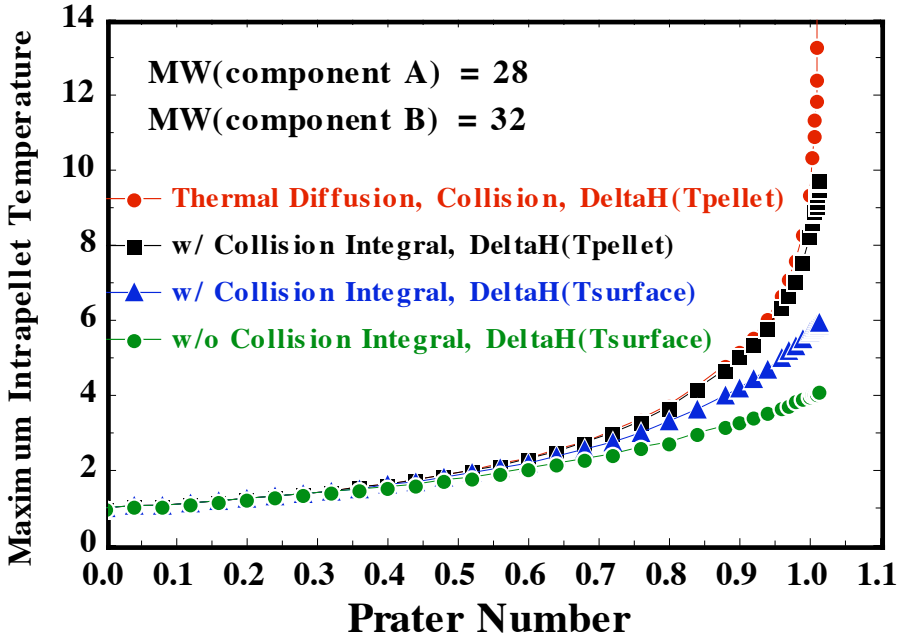

Figure#4

Effect of the Prater number, thermal diffusion, the collision integral for ordinary molecular diffusion, and temperature dependence of the exothermic enthalpy change for chemical reaction on the maximum intrapellet temperature within macroporous catalysts in the diffusion-limited regime. Calculations are presented for; $CO + 2H_2 \Leftrightarrow CH_3OH$. The Lennard-Jones temperature (or potential well depth, divided by Boltzmann's constant) of 123K represents a geometric average of $\varepsilon_i/k_{Boltzmann}$ for all three components in the gas mixture (see Equation [21]). Simulations are presented when temperature on the external catalytic surface is 400K, and the molecular weight of component A (i.e., MW_{CO} = 28 daltons) is less than that of "component B" (i.e., MW_B = 32 daltons) in pseudo-binary mixtures.

In contrast, when C≡O is the larger of the two components in pseudo-binary mixtures, it migrates toward lower temperatures near the external catalytic surface for T* > 0.95, impeding the *net diffusional flux* of C≡O toward the central core. Simulations in Figure#5 for exothermic chemical reaction and Prater numbers greater than 0.75 indicate that maximum intrapellet temperatures in the presence of thermal diffusion with $MW_A > MW_B$ are *less* than those predicted by Equation [20] when thermal diffusion is neglected (i.e. $MW_A = MW_B = 28$ daltons in Figure#5), but all other physicochemical parameters exhibit temperature dependence.

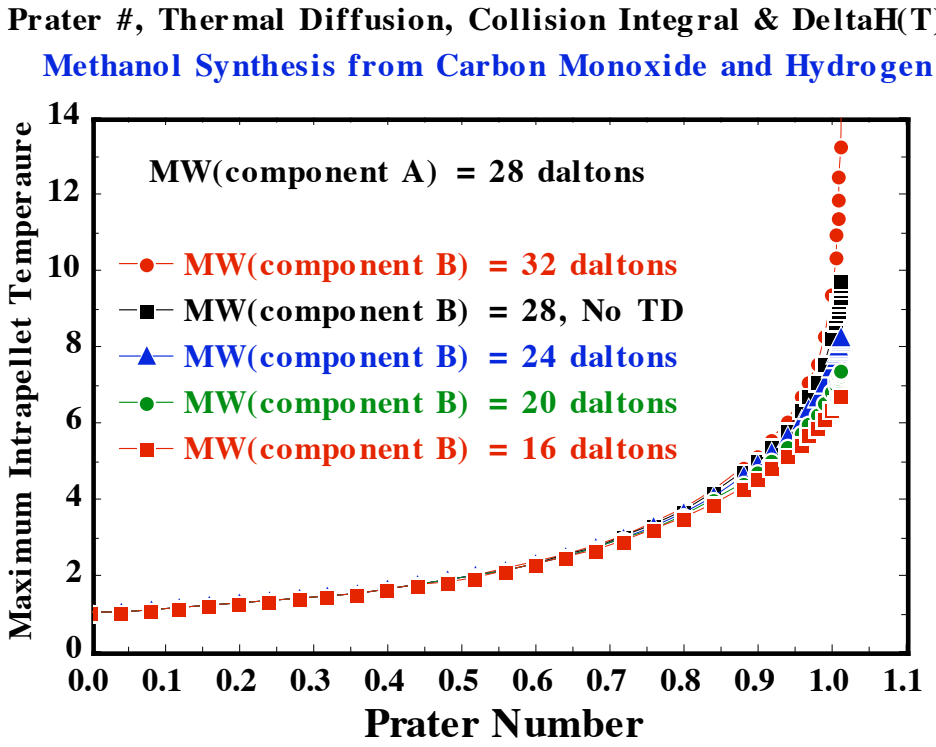

Figure#5

Effect of the Prater number, thermal diffusion, the collision integral for ordinary molecular diffusion, and temperature dependence of the exothermic enthalpy change for chemical reaction on the maximum intrapellet temperature within macroporous catalysts in the diffusion-limited regime. Calculations are presented for; $CO + 2H_2 \Leftrightarrow CH_3OH$. The Lennard-Jones temperature (or potential well depth, divided by Boltzmann's constant) of 123K represents a geometric average of $\varepsilon_i/k_{Boltzmann}$ for all three components in the gas mixture (see Equation [21]). Simulations are presented when temperature on the external catalytic surface is 400K, and the molecular weight of component A (i.e., C≡O) is 28 daltons. The effect of the molecular weight of "component B" in pseudo-binary mixtures is indicated in the legend. Thermal diffusion does not affect these simulations when the molecular weights of both components are the same (see Equation [23]).

Summary. The simulations described in this contribution are based on an analysis of coupled heat and mass transfer for Lennard-Jones gases in macroporous catalysts with exothermic chemical reaction in the diffusion-controlled regime. Numerical results suggest that predictions of maximum intrapellet temperatures could be significantly larger than those calculated from the Prater equation (i.e., $\Theta_{max} \approx 1+\beta$) when the Prater number, defined by Equation [15], is greater than 0.50. Steady state analysis of the methanol synthesis from carbon monoxide and hydrogen is not a reasonable assumption when the Prater number approaches unity, because core temperatures are more than one order-of-magnitude larger than temperatures on the external catalytic surface. The extreme upper limit of the Prater number for realistic steady state intrapellet simulations decreases from

2.0 to 1.25–1.35 to < 1.0, respectively, as the temperature dependencies of ordinary molecular diffusion coefficients for hard spheres (i.e., $T^{3/2}$), the collision integral $\Omega_D(T)$, and the enthalpy change for chemical reaction $\Delta H^0_{Reaction}(T)$ are systematically included in the analysis. The largest increases in intrapellet temperature occur when all of the following conditions are satisfied; (i) chemical reactions are strongly exothermic, (ii) physicochemical properties of the reactive gas mixture exhibit temperature dependence, (iii) the Prater number approaches unity, and (iv) Soret diffusion enhances the molar flux of C≡O (i.e., MW_{CO} < $MW_{\text{"B"}}$ in pseudo-binary mixtures) into the central core of macroporous catalysts as a consequence of negative thermal diffusion coefficients.

Epilogue. The intrapellet Damköhler number represents a dimensionless ratio of the pseudo-volumetric rate of n^{th}-order chemical reaction relative to the rate of intrapellet diffusion. If $S_m\rho_{apparent}k_{n,Surface}$ is a temperature-dependent n^{th}-order pseudo-volumetric kinetic rate constant, with dimensions of $(volume/mol)^{n-1}$ per time, for pseudo-volumetric rates of reaction (i.e., dimensions of moles per pellet volume per time) that are expressed using molar densities on the external surface of the catalyst, then for reactant *A*;

$$\Lambda^2_{A,\text{int}\,rapellet} = \frac{S_m \rho_{apparent} k_{n,Surface} d^2_{equivalent} C^{n-1}_{A,Surface}}{D_{A,effective}} \qquad [27]$$

where the effective intrapellet diffusion coefficient for reactant *A* is defined by Equation [17].

Nomenclature

$C_{A,pellet}$	molar density of reactant *A* within a porous catalytic pellet
C_i	molar density of species *i*
$C_{i,Surface}$	molar density of gaseous species *i* near the external surface of a catalytic pellet
$C_{p,i}$	specific heat of pure component *i*, expressed as a polynomial in T
$D_{A,effective}$	effective intrapellet diffusivity of reactant *A* in porous catalysts
$D_{A,ordinary}$	ordinary molecular diffusion coefficient for reactant *A*
$d_{equivalent}$	equivalent diameter of irregular-shaped pellets, = $6V_{catalyst}/S_{external}$
$\mathbf{g}_i$	external body force per unit mass acting on species i in a mixture
H_i	partial molar enthalpy of species i in a mixture
$\mathbf{j}_{i,pellet}$	diffusional mass flux of species *i* within a porous catalytic pellet
$k_{Boltzmann}$	Boltzmann's constant; 1.38066 *x* 10^{-23} Joule/K
$k_{effective}$	effective intrapellet thermal conductivity of a porous catalyst
$k_{n,Surface}$	n^{th}-order kinetic rate constant with dimensions of $(vol/mol)^{n-1}$(length/time) for heterogeneous chemical reaction on the catalytic surface, where the reaction

rate is expressed via molar densities and has dimensions of moles per internal catalytic surface area per time

$[k_T]_A$ ratio of the thermal diffusion coefficient to the ordinary molecular diffusion coefficient in Equation [22] for diffusional mass flux of species *A*

MW_i molecular weight of species *i*

m exponent for the temperature dependence of effective intrapellet diffusion coefficients in macropores (i.e., m=1.5) and nanopores (i.e., m=0.5)

$\mathbf{n}$ outward directed unit normal vector on surface S that surrounds a chosen volume element V

n independent spatial variable measured in the direction of $\mathbf{n}$

p gas phase pressure

$\mathbf{q}_{pellet}$ molecular flux of thermal energy in multicomponent gas mixtures

R_k pseudo-volumetric kinetic rate law for the k^{th} independent chemical reaction

R pseudo-volumetric kinetic rate law when only one chemical reaction occurs

S surface element over which integration occurs via Gauss' law

$S_{external}$ external surface area of one porous catalytic pellet

S_m internal catalytic surface area per unit mass of catalyst

t time

T temperature in the thermal energy balance

T* dimensionless temperature in the diffusion collision integral, Equation [18]

T_{pellet} temperature within porous catalytic pellets

$T_{Surface}$ temperature near the external surface of the catalytic pellets

u specific internal energy of the gas phase mixture

$\mathbf{v}$ mass-average velocity vector of a multicomponent reactive mixture

V volume element over which integration occurs

$V_{catalyst}$ total volume of one porous catalytic pellet

y_i mole fraction of component *i*

Greek Symbols:

β Prater number, defined in Equation [15]

∇ gradient operator

$\Delta H_{Reaction}$ molar enthalpy change for the chemical reaction at temperature T

$\Delta H^0_{Rx,298K}$ standard state molar enthalpy change for the chemical reaction at 298K

$\varepsilon(\Theta)$ ratio of effective intrapellet diffusivities for reactant *A*, defined in Equations [15] and [19]

$\varepsilon_{Lennard\text{-}Jones}$ maximum energy of attraction for Lennard-Jones molecules, or maximum depth of the potential well when molecules reside at their equilibrium separation distance

$\varepsilon_{p,intrapellet}$ intrapellet porosity, or void volume fraction, of an isolated catalytic pellet

$\Lambda^2_{A,intrapellet}$ intrapellet Damköhler number of reactant *A*, defined in Equation [27]

υ_{ik} stoichiometric coefficient of species i in the k^{th} chemical reaction

υ_i stoichiometric coefficient of species i when there is only 1 reaction

η dimensionless intrapellet radial coordinate in porous spherical catalysts

$\varphi_A(T^*)$ thermal diffusion ratio for Lennard-Jones gases relative to that for hard spheres, illustrated as a function of dimensionless temperature T* in Figure#3 for binary isotopic mixtures

$\rho_{apparent}$ apparent density of a porous catalytic pellet, including occupied and void volume

ρ total mass density of the gas phase mixture

Θ dimensionless intrapellet temperature in porous catalysts

Θ_{max} maximum dimensionless intrapellet temperature near the center of porous catalysts

σ collision diameter for the Lennard-Jones 6-12 intermolecular potential

τ viscous stress tensor (i.e., molecular momentum flux)

τ_{or} intrapellet tortuosity factor, representing an average over pore orientation

$\Psi_{A,pellet}$ dimensionless intrapellet molar density of reactant A in porous catalysts

$\Psi_{A,Surface}$ dimensionless molar density of reactant *A* near the external surface of a catalytic pellet

Ω_D collision integral for diffusion, parameterized by Equation [18]

$\zeta(\Theta)$ dimensionless ratio of molar enthalpy changes for chemical reaction, defined by Equations [15] and [20]

χ deflection angle for binary molecular collisions in dilute gas mixtures

Literature References

1) CD Prater; *Chemical Engineering Science,* **8**, 284 (1958).

2) PB Weisz, & JS Hicks; *Chemical Engineering Science,* **17**, 265-275 (1962).

3) GF Froment, & KB Bischoff; *Chemical Reactor Analysis and Design,* 2nd edition, Wiley: New York (1990), pp. 184 & 497.

4) ME Davis, & RJ Davis; *Fundamentals of Chemical Reaction Engineering,* McGraw Hill: New York (2003), pp. 213-218 & 317.

5) G Damköhler; *Z. Physical Chemistry,* **A193**, 16 (1943).

6) LA Belfiore; *Transport Phenomena for Chemical Reactor Design,* Wiley: Hoboken, NJ (2003), Chapters 9, 15, 21, 26, 27 30.

7) R Aris; *The Mathematical Theory of Diffusion and Reaction in Permeable Catalysts; Theory of the Steady State,* Volume#1, Oxford University Press: Bristol (1975), pp. 53, 96, and Chapter#5.

8) JW Tester, & M Modell; *Thermodynamics and its Applications"*, 3rd edition, Prentice-Hall: Upper Saddle River, NJ (1997), pp. 769-770.

9) OA Hougen, KM Watson, & RA Ragatz; *Chemical Process Principles, Part 2, Thermodynamics,* Wiley: New York (1964), Appendix 27-28.

10) JO Hirschfelder, CF Curtiss, & RB Bird; *Molecular Theory of Gases and Liquids,* Wiley: New York (1954), pp. 527-8, 542-3, 558,567,1110-1112, 1126-9,1131.

11) DA McQuarrie; *Statistical Mechanics,* University Science Books: Sausalito, CA (2000), Chap. 19.

12) P Resibois, & M de Leener; *Classical Kinetic Theory of Fluids,* Wiley: New York (1977), pp. 141-2, 372-3.

13) RB Bird, WE Stewart, & EN Lightfoot; *Transport Phenomena,* 2nd edition, Wiley: Hoboken, NJ (2002), pp. 441, 686.

14) PD Neufeld, AR Janzen, & RA Aziz; *Journal of Chemical Physics,* **57**, 1100 (1972).

15) LA Belfiore, JJ Way & L Zhang, **Simultaneous Heat and Mass Transfer in Packed Catalytic Tubular Reactors with External Transport Resistances**, *Kirk-Othmer Encyclopedia of Chemical Technology, 5th edition;* Wiley: New York, submitted for publication, January (2006).

16) Irving, JP, & Butt, JB; *Chemical Engineering Science,* **22**, 1859-1873 (1967).

17) K Klier, V Chatikavanij, RG Herman, & GW Simmons; *Journal of Catalysis,* **74** (2), 343-360 (1982).

18) G Natta; in *Catalysis,* PH Emmett, editor; Vol. 3; Reinhold: New York (1955), pp. 349-411.

19) AY Rozovskii, & GI Lin; *Topics in Catalysis,* **22** (3-4), 137-150 (2003).

20) IK Gamwo, JS Halow, D Gidaspow, & R Mostofi; *Chemical Engineering Journal,* **93** (2), 103-112 (2003).

21) VE Leonov, MM Karavaev, EN Tsybina, & GS Petrishcheva; *Kinet. Katal.,* **14**, 970-975 (1973).

22) ERS Winter; *Transactions of the Faraday Society,* **46**, 81 (1950).

(28) Statistical Thermodynamics of Ideal Gases

Page#761 need consistency between dW in eq. (28-27) and dw in eq. (29-5)

(29) Thermodynamic Stability Criteria for Single Phase Homogeneous Mixtures

Page#786 need consistency between dW in eq. (28-27) and dw in eq. (29-5)

(30) Coupled Heat and Mass Transfer in Packed Catalytic Tubular Reactors that Account for External Transport Limitations

Page#826 the right side of equation (30-17) needs a lowercase p in $j_{i,pellet}$

Page#834-835 just above *Step 3 and Step 5.* ...at prevailing values of $C_{A,Surface}$ and $T_{Surface}$. The characteristic length L in the definition of the intrapellet Damköhler number is the radius of spherical catalytic pellets for the correlation given by Equation (20-57) for 1st-order irreversible chemical kinetics. The heat and mass transfer correlations contain the Reynolds number, which is based on particle dimensions and the interstitial fluid velocity. The Schmidt and Sherwood numbers require ordinary molecular diffusion coefficients in the dimensionless mass transfer correlations for interphase mass transfer coefficients, not interpellet axial dispersion coefficients.

Page#838 just below equation (30-64); which reduces to $\Psi_{A,surface} = \Psi_{A,bulk\ gas}$ via (i) equation (30-63) when α=0, or (ii) application of l'Hôpital's rule in equation (30-64) when the external resistance to mass transfer is negligible (i.e., α=0 and β=0). Equation (30-64) for ...

Page#846 4 lines up from R_{PFR} = 10 cm, need a space between 0.25 and $(atm)^{-1}$

Page#848 3 lines up from the bottom; ... constants are 0.25 atm^{-1} [see equations 22-42, 22-54, and Figure 22-1 on pages 576-579])

Page#850 Last equation before section 30-6.1; add dz in the integral expression for $T_{BulkGas}$

Page#852 add ***Section 30-6.3***

Numerical simulations of temperature and molar density profiles in the bulk fluid phase and on the external surface of porous catalysts for moderately high-pressure syntheses of methanol from carbon monoxide and hydrogen in non-adiabatic PFRs

The complete strategy for ideal nonisothermal packed catalytic tubular reactors. When porous pellets are packed in tubular reactors and the external resistances to both heat and mass transfer cannot be neglected, it is necessary to predict temperature $T_{Surface}$ and reactant molar density $C_{A,Surface}$ on the external catalytic surface. The appropriate initial guesses are based on bulk conditions at the reactor inlet. With assistance from effectiveness factor correlations, the rate of reactant consumption is averaged volumetrically throughout the catalyst by evaluating heterogeneous rate laws using conditions on the external catalytic surface. Hence, the appropriate sequence of calculations is; (i) predict $C_{A,Surface}$ and $T_{Surface}$ via coupled heat and mass transfer principles discussed earlier in this chapter, (ii) calculate the intrapellet Damköhler number for reactant A on the external catalytic surface, (iii) estimate the effectiveness factor via dimensionless correlations that consider catalyst geometry and the kinetic rate law, (iv) predict a volumetric average of the rate of reactant consumption throughout the catalyst, and (v) solve coupled plug-flow differential mass and thermal energy balances to estimate changes in temperature and reactant molar density within the bulk gas phase. The mathematical description of this strategy is summarized below;

(1) Use bulk conditions at the reactor inlet, $C_{A,BulkGas}(z=0)$ and $T_{BulkGas}(z=0)$, to estimate the intrapellet Damköhler number $\Lambda^2_{A,intrapellet}$ and the corresponding effectiveness factor E via dimensionless correlations that account for catalyst geometry and the appropriate kinetic rate law (i.e., n^{th}-order kinetics). The characteristic length L in the definition of the intrapellet Damköhler number is the radius of spherical catalytic pellets for the analytical correlations described in *Chapter#20* for 1^{st}-order irreversible chemical kinetics. If the kinetics are not zeroth-order or first-order, then numerical methods are required to calculate the effectiveness factor.

(2) Since $C_{i,BulkGas}$ at the reactor inlet is known via the nature of the feed stream, one should obtain an iterative solution to the following set of coupled non-linear algebraic equations to predict $C_{A,Surface}$, $C_{i,Surface}$, and $T_{Surface}$ *near* the reactor inlet;

$$k_{A,MTC}\left(C_{A,BulkGas}-C_{A,Surface}\right)S_{external}=ES_m\rho_{apparent}k_{n,Surface}C_{A,Surface}^{n}V_{catalyst}$$

$$\frac{1}{\upsilon_i}k_{i,MTC}\left(C_{i,Surface}-C_{i,BulkGas}\right)=k_{A,MTC}\left(C_{A,BulkGas}-C_{A,Surface}\right)$$

$$h_{HTC}\left\{T_{Surface}-T_{BulkGas}\right\}=\left(-\Delta H_{\mathrm{Re}action}\right)k_{A,MTC}\left\{C_{A,BulkGas}-C_{A,Surface}\right\}$$

$$\Lambda^2_{A,\mathrm{int}rapellet}=\frac{S_m\rho_{apparent}k_{n,Surface}\left(T_{Surface}\right)R^2_{sphere}C^{n-1}_{A,Surface}}{D_{A,effective}\left(T_{Surface}\right)}$$

$$E=f\left(\Lambda^2_{A,\mathrm{int}rapellet};n,CatalystGeometry\right)$$

All of these expressions have been discussed earlier in this chapter. Each iteration requires a recalculation of the intrapellet Damköhler number and the effectiveness factor (i.e., analytical or numerical) at the prevailing values of $C_{A,Surface}$ and $T_{Surface}$. Gas-phase mass transfer coefficients for species *A* (i.e., $k_{A,MTC}$) and species *i* (i.e., $k_{i,MTC}$) in the first three equations above should be evaluated via equation (22.3-43) or (22.3-44) in *Transport Phenomena, 2nd edition,* by Bird, Stewart, & Lightfoot. For creeping flow around solid spheres, the Sherwood number for mass transfer scales as the one-third power of the particle-based mass transfer Peclet number (i.e., $Pe_{particle}$), which incorporates the equivalent diameter of a single catalytic pellet, the average interstitial fluid velocity through the packed bed, and ordinary molecular diffusion coefficients at bulk-gas temperatures in the external gas-phase boundary layer adjacent to spherical gas-solid interfaces. The corresponding heat transfer coefficient (i.e., h_{HTC}) in the third equation above should be evaluated using equation (14.5-2) or (14.5-6) in BSL's 2nd edition of *Transport Phenomena*. All of these heat and mass transfer correlations are consistent with two-dimensional creeping flow of incompressible fluids adjacent to high-shear, no-slip interfaces.

(3) When convergence is obtained for $C_{A,Surface}$, $C_{i,Surface}$, and $T_{Surface}$ near the reactor inlet, it is possible to (i) use the current value of the effectiveness factor, (ii) predict the volumetric rate of consumption of reactant A throughout the pellets via effectiveness factor formalism, and (iii) employ numerical methods like the Runge-Kutta-Gill 4th-order-correct integration algorithm to solve coupled *dimensional* mass and thermal energy balances for ideal gas-phase plug-flow tubular reactors that include the effectiveness factor in the kinetic rate law. The first term on the right side of the one-dimensional thermal energy balance (i.e., 2nd equation below), which reduces the bulk gas temperature, represents heat transfer to the surroundings because the reactor is not insulated. The second term on the right side of the thermal energy balance represents heat generation due to exothermic chemical reaction. The primary

objective is to predict $C_{A,BulkGas}$, $C_{i,BulkGas}$, and $T_{BulkGas}$ at a small distance z downstream from their values at the reactor inlet.

$$q\frac{dC_{A,BulkGas}}{dV_{\mathrm{Re}actor}} = -\left(1-\varepsilon_{p,\mathrm{int}erpellet}\right)ES_m\rho_{apparent}k_{n,Surface}C^n_{A,Surface}$$

$$q\rho_{BulkGas}C_{p,mixture}\frac{dT_{BulkGas}}{dV_{\mathrm{Re}actor}} = \left\{\frac{dQ}{dV_{\mathrm{Re}actor}}\right\}_{@\,wall} + \left(-\Delta H_{Rx}\right)\left(1-\varepsilon_{p,\mathrm{int}erpellet}\right)ES_m\rho_{apparent}k_{n,Surface}C^n_{A,Surface}$$

$$C_{i,BulkGas} = C_{i,BulkGas,Inlet} + \upsilon_i\left\{C_{A,BulkGas,Inlet} - C_{A,BulkGas}\right\}$$

(4) Use values for $C_{A,Surface}$, $C_{i,Surface}$, and $T_{Surface}$ that were obtained from convergence in *step#2*, which includes the most up-to-date values of the intrapellet Damköhler number and the effectiveness factor, update bulk gas molar densities and temperature from the solution of coupled mass and thermal energy balances in *step#3*, and obtain another iterative solution to the coupled nonlinear algebraic equations in *step#2*. The primary objective is to predict $C_{A,Surface}$, $C_{i,Surface}$, and $T_{Surface}$ slightly downstream from their previous values.

(5) Repeat *step#3* and *step#4* to predict molar densities and temperatures in the bulk fluid phase and on the external surface of the catalyst from inlet to outlet of the packed catalytic tubular reactor.

There is some discrepancy in the Chemical Engineering textbook literature about the use of superficial (i.e., $\langle v_z \rangle_{superficial}$) vs. interstitial (i.e., $\langle v_z \rangle_{interstitial}$) average fluid velocity to describe convective transport in the coupled plug-flow mass and thermal energy balances (i.e., summarized in *step#3*) for packed catalytic tubular reactors.

Numerical analysis of pseudo-1st-order irreversible chemical kinetics in ideal packed catalytic tubular reactors when the external resistances to heat and mass transfer cannot be neglected. *Production of methanol from a moderately high-pressure stoichiometric feed of carbon monoxide and hydrogen.* This realistic example implements the complete strategy outlined in the previous section to simulate ideal reactor performance at high mass and heat transfer Peclet numbers, when reactants are consumed by approximate 1st-order irreversible kinetics on the internal surface of porous spherical pellets. The catalyst is distributed uniformly in a fixed-bed arrangement. The synthesis of methanol from C≡O and H_2 in gas-phase packed catalytic tubular reactors is industrially important. Consequently, a large amount of experimental data is available to characterize this reaction over a wide range of operating pressures. For simplicity, the effectiveness factor is calculated analytically via the classic isothermal expression in spherical coordinates, as developed in *Chapter#20.* The cgs system of units is employed in the following analysis.

Design parameters for ideal tubular reactor performance when external resistances to heat and mass transfer are considered. Most of the parametric values, summarized below, are self-explanatory. The interaction energy that governs molecular trajectories and binary collisions is assumed to follow the Lennard-Jones 6-12 potential function. The collision diameter σ and the depth of the potential well are required to calculate collision integrals for viscosity and ordinary molecular diffusion, as well as the important dimensionless numbers (i.e., Reynolds, Schmidt, Prandtl, and Damköhler) that are necessary to estimate interphase heat and mass transfer coefficients, and the effectiveness factor. An integral formulation of linear least squares regression for continuous objective functions, discussed in *Chapter#15* and implemented in *Chapter#22,* is employed to quantify *reversible* heterogeneous catalytic reactions using first-order irreversible rate laws [i.e., $k_{1,Pseudo\text{-}Volumetric}C_{A,inlet}(\xi_{equilibrium} - \xi)$], where $\xi_{equilibrium}$ is the equilibrium conversion of carbon monoxide (C≡O) that depends on the local external catalytic surface temperature $T_{Surface}$ and pressure at each axial position in the tubular reactor. Since there are no H-H bonds in the final product, 5-site Langmuir-Hinshelwood chemical reaction on zinc chromite catalysts (i.e., ZnO/Cr_2O_3) is considered to be the rate-limiting step for $CO+2H_2 \Leftrightarrow CH_3OH$ (i.e., see *Chapter#22*), with non-preferential dissociative adsorption of atomic hydrogen (i.e., H) on adjacent active sites. The synthesis of methanol over Cu-based catalysts seems to occur exclusively by CO_2 hydrogenation at lower operating pressures. Under non-ideal conditions, kinetic rate laws should be constructed using fugacities instead of molar densities or partial pressure, as suggested in the *Problems Section* of *Chapter#7*.

Length of the packed catalytic tubular reactor = 325 cm
Radius of the packed catalytic tubular reactor = 7 cm
Radius of each porous catalytic pellet (spherical) = 0.7 cm
Average catalytic pore radius = 10 nm
Approximate Lennard-Jones collision diameter σ for CO in the ternary gas mixture ≈ 3.5 Å
Approximate (i.e., geometric average) Lennard-Jones potential well depth for a ternary gas mixture of C≡O, H_2, and CH_3OH; $\varepsilon_{ABC}/k_{Boltzmann} \approx \{\varepsilon_{CO}\varepsilon_{H2}\varepsilon_{CH3OH}\}^{1/3}/k_{Boltzmann} \approx 123K$
Tortuosity factor for individual porous catalytic pellets = 2
Intrapellet porosity, or void volume fraction for each catalytic pellet = 0.60
Interpellet porosity, or void volume fraction of the entire packed bed = 0.35
Volumetric flowrate of bulk gas through the packed bed = 100 cm^3/sec (i.e., 6 Litre/min)
Average residence time = 175 seconds
Ambient temperature = 298K
Inlet bulk gas temperature = 498K (nonisothermal) or 528K (isothermal)
Inlet total pressure = 50 atmospheres
Standard state entropy change for $CO+2H_2 \Leftrightarrow CH_3OH$; $\Delta S^0_{Rx,298K} \approx -53$ cal/mol-K
Standard state enthalpy change (exothermic chemical reaction); $\Delta H^0_{Rx,298} \approx -21.7$ kcal/mol

Arrhenius activation energy for the forward reaction = 22.7 kcal/mol
Pre-exponential factor for pseudo-1st-order Arrhenius kinetic rate constant $\approx 3 \times 10^{6}$ sec^{-1}
Overall heat transfer coefficient (to the surroundings) = 6×10^{-4} cal/cm^2-sec-K
Stoichiometric feed (i.e., 1:2) of C≡O and H_2 at the reactor inlet
Axial step size for numerical integration = $\Delta\zeta_{PFR} = 10^{-4}$; $0 \leq \zeta_{PFR} = z/L_{PFR} \leq 1$

Comparison of analytical and numerical solutions for ideal isothermal tubular reactors. Numerical simulations were compared with the analytical solution (i.e., Equations 30-60 and 30-61) when the kinetics are 1st-order and irreversible, and heat effects due to chemical reaction are negligible. Hence, isothermal operation was simulated at 528K, with external mass transfer resistance included in the analysis, but no temperature gradients anywhere throughout the system. Analytical and numerical solutions for the predicted bulk-gas conversion of carbon monoxide are essentially indistinguishable, but the gas-phase molar density of C≡O near the external catalytic surface is slightly less than its corresponding bulk gas-phase molar density, as expected for reactants.

Nonisothermal tubular reactor performance. The influence of external resistances to heat and mass transfer was analyzed in ideal plug flow reactors without interpellet axial dispersion in the species mass balance or axial conduction in the thermal energy balance. The external resistance to heat transfer is proportional to the difference between bulk gas and surface temperatures. Analogously, external mass transfer resistance scales linearly with the difference between species molar density near the external catalytic surface and in the bulk gas phase. Using the parameters defined earlier in this section, temperature profiles in the bulk gas stream and near the external surface of the catalytic pellets are illustrated in Figure#30-4.

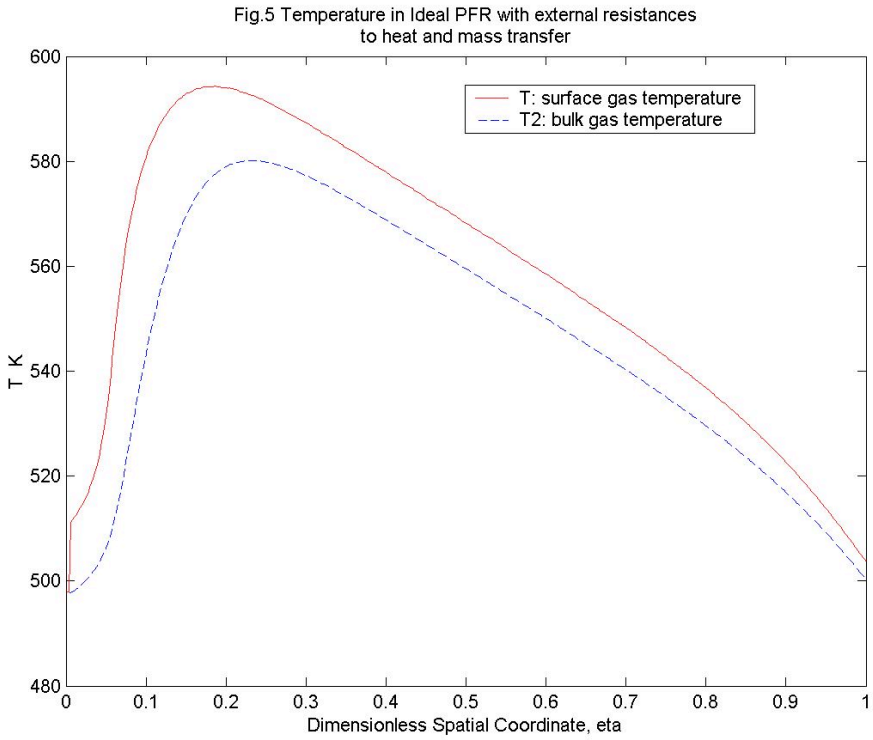

Figure#30-4

Temperature profiles in the bulk gas phase (i.e., dashed line; $T_{BulkGas}$) and near the external surface of porous catalytic pellets (i.e., solid line; $T_{Surface}$) for the production of methanol from carbon monoxide and hydrogen in ideal tubular reactors that are not insulated from the surroundings. The ≈80K increase in reactor temperature relative to $T_{BulkGas,Inlet}$, 20% of the reactor length downstream from the inlet, is attributed to exothermic chemical reaction. All simulation parameters are defined in the text. The horizontal coordinate ζ_{PFR} represents dimensionless axial position in the direction of bulk flow, measured from the reactor inlet.

The corresponding reactant (i.e., C≡O) molar densities are presented in Figure#30-5. C≡O conversion ξ is defined by *one minus dimensionless molar density in the bulk gas phase* (i.e., $\xi = 1 - \Psi_{A,BulkGas}$). Simulations reveal that the maximum difference between external catalytic surface temperature and bulk gas temperature [i.e., $(T_{Surface} - T_{BulkGas})_{max} \approx 40K$] occurs approximately 8% of the reactor length downstream from the inlet, whereas this temperature difference (i.e., $T_{Surface} - T_{BulkGas}$) is less than 10K much further downstream. As expected for exothermic reactions, temperatures within the porous pellets and near the external catalytic surface should be higher than those in the bulk gas stream. The interplay between the rate of thermal energy generation due to exothermic chemical reaction and the rate of thermal energy removal due to heat transfer across the lateral surface of the reactor governs the maximum temperature increase [$(T_{BulkGas} - T_{BulkGas,inlet})_{max} \approx 80K$ in Figure#30-4), the axial position where maximum temperature occurs, and the overall shapes of the profiles in Figure#30-4 and Figure#30-5.

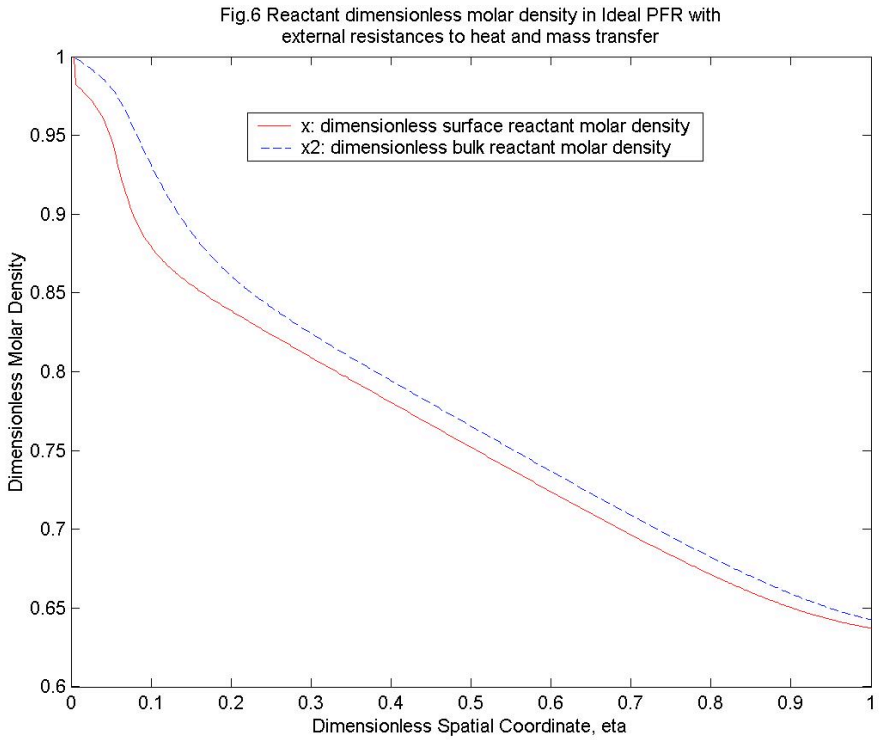

Figure#30-5

Dimensionless molar density profiles for carbon monoxide in the bulk gas phase (i.e., dashed line; $\Psi_{A,BulkGas}$) and near the external surface of porous catalytic pellets (i.e., solid line; $\Psi_{A,Surface}$) for the gas-phase production of methanol from a stoichiometric feed of C≡O and H_2 in ideal tubular reactors that are not insulated from the surroundings. Based on simulation parameters defined in the text, the maximum difference between $\Psi_{A,BulkGas}$ and $\Psi_{A,Surface}$ occurs approximately 8% of the reactor length downstream from the inlet [i.e., $(\Psi_{A,BulkGas} - \Psi_{A,Surface})_{max} \approx 0.07$ when $\zeta_{PFR} \approx 0.08$], and ≈35% final conversion of C≡O to CH_3OH is achieved (i.e., $\Psi_{A,BulkGas} \approx 0.65$ when $\zeta_{PFR}=1$). The horizontal coordinate ζ_{PFR} represents dimensionless axial position in the direction of bulk flow, measured from the reactor inlet.

The bulk gas temperature decreases when the rate of heat removal across the lateral surface of the reactor is greater than the generation rate due to exothermic chemical reaction, as described by the one-dimensional thermal energy balance for plug-flow reactors. Thermal runaway occurs when the generation rate significantly outweighs the rate of heat removal, producing steep increases in reactor temperature and *near-equilibrium* reactant conversions that might not be described adequately by steady state analyses. Practical strategies to prevent thermal runaway, summarized and implemented in *Chapter#4,* include (i) lowering the inlet temperature of the reactive fluid, (ii) diluting the feed stream with an inert carrier gas, (iii) increasing the surface-to-volume ratio of the reactor by decreasing its diameter, and (iv) increasing the flowrate and lowering the inlet temperature of a cooling

fluid that flows either cocurrently or countercurrently with respect to the reactive fluid. One might predict that an increase in bulk gas flowrate of the reactive fluid, which decreases the residence time τ_{PFR}, should reduce the overall temperature increase, $(T_{BulkGas} - T_{BulkGas,inlet})_{max}$, for exothermic reactions and decrease the final conversion of carbon monoxide. However, decreases in τ_{PFR} and subsequent increases in the mass transfer Peclet number Pe_{MT} reduce external heat and mass transfer resistances in the gas-phase boundary layers surrounding the catalytic pellets. Consequently, the diffusional flux of reactants toward the external catalytic surface increases, reaction rates increase because kinetic rate laws are evaluated at higher reactant molar densities near the external catalytic surface, more thermal energy is generated when reaction rates increase, and the flux of thermal energy from the pellets to the bulk gas phase increases. There is a restricted range of residence times and mass transfer Peclet numbers where all of these sequential effects produce larger increases in reactor temperature and higher conversion, even though shorter residence times suggest that there is less opportunity to convert reactants to products. Isothermally, the effect of residence time, or Pe_{MT}, on reactant conversion is illustrated in Figures 30-1 to 30-3 when the external resistance to mass transfer is important. The study of maximum conversion in nonideal packed catalytic tubular reactors, summarized in Table#30-2, is based on these results. Under nonisothermal conditions, both external resistances are significant near the reactor inlet, and they decrease in magnitude as one approaches the reactor outlet. External transport resistances vanish completely at steady state when there is no chemical reaction. This claim is supported by analyzing all of the coupled nonlinear algebraic equations in *step#2* of the overall strategy. In other words, $C_{A,BulkGas} = C_{A,Surface}$ and $T_{BulkGas} = T_{Surface}$ when $k_{n,Surface} = 0$. Pellet size, internal pore structure, reactor diameter, and volumetric flowrate represent important design parameters that influence the relative magnitude of external transport resistances, and they should have significant effects on the temperature and molar density profiles illustrated in Figure#30-4 and Figure#30-5.

Page#857 ***Problem 30-7(i):***

Include the necessary corrections from part (h) in the expression for the dimensionless bulk molar density of reactant A;

$$\Psi_{A,bulk}(z) = \frac{C_{A,bulk}(z)}{C_{A,inlet}} = \exp\left\{-8\phi \frac{\Lambda_A^2}{Pe_{MT}} \frac{z}{d_{effective}}\right\}$$

and verify that the universal correlation for duct reactors with rectangular cross-section, given by equations (23-80) and (23-81), is reasonable for "tube-wall" catalytic channels with circular cross-section. The dimensionless axial coordinate ξ is given by equation (23-49), the mass transfer Peclet number is

defined in equation (23-50), and the Damköhler number is given by equation (23-18) when the equivalent diameter of circular channels is 2R.

Answer:

Let's focus on the argument of the exponential function in the problem statement for part (h) and use the expression for *external mass transfer resistance parameter* ϕ from part (b) of this same problem. Then, rewrite the (1) mass transfer coefficient in terms of the Sherwood number, and (2) the heterogeneous first-order kinetic rate constant (i.e., reaction velocity constant) via the Damköhler number. One obtains the following result;

$$\Psi_{A,bulk}(\xi) = \exp\left\{-\frac{k_{A,MTC}}{k_{A,MTC}+k_{1,surface}}8\Lambda_A^2\xi\right\} = \exp\left\{-\frac{\frac{D_{A,ordinary}}{2R}Sh}{\frac{D_{A,ordinary}}{2R}Sh+\frac{D_{A,ordinary}}{R}\Lambda_A^2}8\Lambda_A^2\xi\right\} = \exp\left\{\frac{-8\Lambda_A^2\xi}{1+\frac{2\Lambda_A^2}{Sh(\xi)}}\right\}$$

Steps 13 and 17 of Problem 23-7 provide an expression for the local Sherwood number near the tube inlet via mass transfer boundary layer analysis. The local Sherwood number is also known as the *Nusselt number for mass transfer,* and Sh_{Local}, which varies inversely with the dimensionless mass transfer boundary layer thickness δ_{MTBLT} (i.e., see *Step 17 of* Problem 23-7), decreases in the flow direction because $\delta_{MTBLT}(\xi)$ scales as the cube root of dimensionless axial position ξ measured from the inlet. Notice that there is a *factor of 2* difference between the definition of ξ in equation (23-49) and the dimensionless axial coordinate ζ that appears in the dimensionless boundary layer thickness in *Steps 12 & 13* of Problem 23-7 on page#651-652. In other words, $\xi = \zeta/2$. Hence;

$$Sh(\xi) \approx 2\Gamma\left(\tfrac{2}{3}\right)\left\{\frac{1}{9\xi}\right\}^{1/3};\ \Psi_{A,bulk}(\xi) = \exp\left\{\frac{-8\Lambda_A^2\xi}{1+\frac{2\Lambda_A^2}{Sh(\xi)}}\right\} \Rightarrow \exp\left\{\frac{-8\Lambda_A^2\xi}{1+\frac{\Lambda_A^2(9\xi)^{1/3}}{\Gamma\left(\frac{2}{3}\right)}}\right\}$$

where $\Gamma(2/3)$ is the gamma function evaluated at argument 2/3, and the previous reactor correlations for $Sh(\xi)$ and $\Psi_{A,bulk}(\xi)$ are valid for small ξ near the tube inlet.

Page#857 ***Problem 30-7(j):***

Modify this analysis of heterogeneous catalysis in ideal plug-flow tubular reactors with expensive metal catalyst coated on the inner wall (i.e., $r=R_{PFR}$) of the flow channel and significant mass transfer resistance for *zeroth-order* kinetics. Consider the realistic situation where the catalytic surface is *reactant-*

starved in the diffusion-limited regime at large values of the Damköhler number relative to the mass transfer Peclet number or, analogously, small chemical reaction time constants relative to the time constant for convective mass transfer (i.e., residence time τ_{CMT}). Formulate a reactor design strategy to calculate the realistically useful upper limit for τ_{CMT} and the corresponding final conversion of reactants to products that should be expected.

Answer:

Begin with the quasi-macroscopic plug flow mass balance in ideal tubular reactors with uniform activity at the catalytic surface, as described by the answer to part (a) of this problem on page#854. Upon modifying the *reaction rate term* in the mass balance to account for heterogeneous zeroth-order kinetics, one obtains;

$$\pi R_{PFR}^2 \left\langle v_z \right\rangle_{Avg} \frac{dC_{A,bulk}}{dz} = -2\pi R_{PFR} k_{0,surface}$$

where $k_{0,surface}$ is the heterogeneous zeroth-order kinetic rate constant with dimensions of moles per *area* per time. Even though zeroth-order heterogeneous rate laws do not depend on reactant molar densities in the vicinity of the catalytic surface, it is extremely important to relate surface and bulk molar densities of each species in the reactive mixture for the following reason. Zeroth-order rate laws are mathematically simple, but they do not provide accurate descriptions of realistic situations when the catalytic surface is reactant-starved because the reaction rate proceeds at a non-zero temperature-dependent "constant" that must be *turned-off* when reactants are totally depleted. This problem is not encountered when rate laws depend on reactant molar densities, because reaction rates vanish when reactants are not present. Accurate reactor design models that simulate zeroth-order kinetics at the catalytic surface must monitor surface molar densities of the reactants and manually *turn-off* the rate of conversion of reactants to products when reactants are totally depleted. This is accomplished by (i) analytically solving the plug-flow mass balance for bulk molar density as a function of axial position z within the tube, (ii) relating bulk and surface molar densities via the balance between diffusion and reaction at the catalytic surface, (iii) identifying the *critical axial coordinate* $z_{critical}$ where surface molar densities of reactants vanish, and (iv) designing the reactor such that its length L_{PFR} is less than $z_{critical}$ because reactants cannot be converted to products beyond $z_{critical}$ if the surface is void of reactants. If mass transfer resistance is significant, then the catalytic surface could be completely reactant-starved while the bulk fluid phase contains residual reactants that cannot be converted to products as a consequence of *rate-limiting* radial diffusion relative to the rate of chemical reaction. Hence, one should not expect to achieve 100% conversion for irreversible heterogeneous reactions in exceedingly long tubes because no reaction occurs beyond $z_{critical}$. Analytical solution of the plug-flow mass balance for $C_{A,bulk}$ is obtained rather

quickly, because the profile is described by a linear decrease from $C_{A,inlet}$ at z=0 to $C_{A,bulk}(z)$ at axial position z downstream from the inlet;

$$C_{A,bulk}(z) = C_{A,inlet} - \frac{2k_{0,surface}}{R_{PFR}\langle v_z \rangle_{Avg}} z$$

The next step in the reactor design strategy requires the establishment of a steady state balance between the rate of radial diffusion of reactant A toward the catalytic surface, expressed via Fick's first law of diffusion using *mass-transfer-coefficient* formalism, and the rate of consumption of reactants via heterogeneous reaction on the surface, where each rate process has dimensions of moles per *area* per time. This balance at the reaction site provides a relation between surface and bulk molar densities of reactant A;

$$-D_A \left\{ \frac{\partial C_A(r,z)}{\partial r} \right\}_{r=R_{PFR}} = k_{A,MTC}\left(C_{A,bulk} - C_{A,surface}\right) = k_{0,surface}$$

$$C_{A,surface}(z) = C_{A,bulk}(z) - \frac{k_{0,surface}}{k_{A,MTC}}$$

One identifies the critical axial coordinate $z_{critical}$ where reactant molar densities vanish by substituting the *linear molar density profile* for $C_{A,bulk}(z)$ into the previous equation and requiring that $C_{A,surface} \Rightarrow 0$. The important reactor design criterion for zeroth-order heterogeneous catalysis on the inner wall of empty tubes is formulated as follows when the Damköhler number is greater than the mass transfer Peclet number;

$$C_{A,surface}(z_{critical}) = C_{A,inlet} - \frac{2k_{0,surface}}{R_{PFR}\langle v_z \rangle_{Avg}} z_{critical} - \frac{k_{0,surface}}{k_{A,MTC}} \Rightarrow 0$$

$$\frac{z_{critical}}{L_{PFR}} = \frac{\langle v_z \rangle_{Avg}}{L_{PFR}} \frac{R_{PFR}}{2k_{0,surface}} \left\{ C_{A,inlet} - \frac{k_{0,surface}}{k_{A,MTC}} \right\} = \frac{1}{\tau_{CMT}} \left(\lambda_{ChemRx} - \Theta_{RadialDiffusion} \right) \geq 1$$

There are three important mass transfer rate processes that must be considered for accurate design of heterogeneous catalytic reactors with expensive metal catalyst coated on the inner walls of the flow channels. The characteristic time constants for these rate processes are (i) τ_{CMT} for convective mass transfer in the primary flow direction, (ii) λ_{ChemRx} for n^{th}-order irreversible chemical reaction at the catalytic surface, and (iii) $\Theta_{RadialDiffusion}$ for radial diffusion of reactants from the bulk fluid to the wall at $r=R_{PFR}$. The previous criterion

identifies an *upper limit* on reactor length L_{PFR}, or residence time τ_{CMT}, to avoid the embarrassing situation where the catalytic surface is completely void of reactants. In terms of mass transfer time constants;

$$\tau_{CMT} \leq \lambda_{ChemRx} - \Theta_{RadialDiffusion}$$

$$\tau_{CMT} = \frac{L_{PFR}}{\langle v_z \rangle_{Avg}}$$

$$\lambda_{ChemRx} = \frac{1}{k_{n,PseudoVolumetric} C_{A,inlet}^{n-1}} \overset{\substack{n=0 \\ Tubes}}{\Longrightarrow} \frac{R_{PFR} C_{A,inlet}}{2k_{0,surface}}$$

$$\Theta_{RadialDiffusion} = \frac{R_{PFR}}{2k_{A,MTC}}$$

Prediction of the upper limit for reactant conversion, when $L_{PFR} = z_{critical}$ and $\leq$ is replaced by an equal sign for τ_{CMT} ($= \lambda_{ChemRx} - \Theta_{RadialDiffusion}$), is obtained by (i) evaluating the bulk molar density of reactant A at $z = z_{critical} = L_{PFR}$;

$$C_{A,bulk}\left(z = z_{critical} = L_{PFR}\right) \geq C_{A,inlet} - \frac{2k_{0,surface}}{R_{PFR}\langle v_z \rangle_{Avg}} L_{PFR}$$

and (ii) defining reactant conversion χ_A with respect to $C_{A,inlet}$ using bulk molar density, not surface molar density, even though heterogeneous reaction rates require nonzero species molar densities in the vicinity of the catalytic surface. Hence, the upper limit for the final conversion of reactant A is predicted to be;

$$\chi_{A,final} \leq 1 - \frac{C_{A,bulk}\left(z = z_{critical} = L_{PFR}\right)}{C_{A,inlet}} = \frac{2k_{0,surface}}{R_{PFR} C_{A,inlet}} \frac{L_{PFR}}{\langle v_z \rangle_{Avg}}$$

$$= \frac{\tau_{CMT}}{\lambda_{ChemRx}} = 1 - \frac{\Theta_{RadialDiffusion}}{\lambda_{ChemRx}} = 1 - \frac{k_{0,surface}}{k_{A,MTC} C_{A,inlet}}$$

which approaches 100% for irreversible chemical reactions when the time constant for radial diffusion is much shorter than the time constant for chemical reaction. Under these conditions with negligible mass transfer resistance (i.e., $\Theta_{RadialDiffusion} << \lambda_{ChemRx}$), the catalytic surface will not be *reactant-starved* until the residence time τ_{CMT} approaches the time constant for chemical reaction and 100% conversion of reactants to products is achieved.

Page#857 ***Problem 30-7(k):***
Calculate a ***numerical value*** for the conversion of reactant A in the exit stream of a 4-cm inner diameter (i.e., R_{PFR} = 2 cm) isothermal PFR at 30^0C with one ***zeroth-order irreversible*** surface-catalyzed chemical reaction on the inner wall at $r=R_{PFR}$, where the heterogeneous temperature-dependent rate law is; $R_{Surface} = k_{0,surface}$, with dimensions of moles per catalytic surface area per time. The time constant for zeroth-order irreversible chemical reaction λ is 2 minutes and the average residence time for convective mass transfer is 1.5 minutes. There is significant mass transfer resistance between the bulk fluid phase and the catalytic surface, characterized by the following mass transfer coefficient for reactant A; $k_{A,MTC}$ = 1 cm/minute.

Answer:
Begin by calculating the time constant for radial diffusion of reactant A toward the catalytic surface at $r=R_{PFR}$. Hence, $\Theta_{RadialDiffusion}$ = 1 minute, and the useful upper limit for τ_{CMT} is 1 minute (i.e., $\tau_{CMT} \leq \lambda_{ChemRx} - \Theta_{RadialDiffusion}$), which implies that the catalytic surface becomes reactant-starved 67% of the reactor length from the inlet [i.e., $z_{critical}/L_{PFR} = 0.67$, because $\lambda_{ChemRx} - \Theta_{RadialDiffusion}$ = 1 minute and τ_{CMT} = 1.5 minutes]. Now, calculate reactant conversion χ_A via the useful upper limit for τ_{CMT}, not the actual residence time (i.e., 1.5 minutes), because no chemical reaction occurs in the latter third of the tube where reactant molar densities have vanished in the vicinity of the catalytic surface and radial diffusion toward the heterogeneous reaction site is not fast enough to replenish the surface with reactants. Hence, 50% conversion is achieved in the presence of significant mass transfer resistance, when residual reactants exist in the bulk fluid phase but the catalytic surface is reactant-starved. One predicts 75% conversion if bulk and surface molar densities are indistinguishable, such that chemical reaction occurs when reactants are present in the bulk fluid and it is possible to achieve 100% conversion if τ_{CMT} is the same as λ_{ChemRx} (i.e., $\Theta_{RadialDiffusion} \Rightarrow 0$).

Page#857 ***Problem 30-7(m):***
Sketch the conversion of reactant A vs. residence time τ from τ=0 to τ=1.5 minutes at two different temperatures, 30^0C (λ = 2 minutes) and 50^0C (λ = 1.5 minutes). Obviously, the time constant for chemical reaction decreases at higher temperature because the reaction rate increases, but the mass transfer coefficient that characterizes diffusion of reactant A toward the catalytic surface is essentially temperature-independent at 1 cm/minute. Be quantitative on both axes.

Answer:
Use the same logic that was discussed in the answer to the previous part of this problem to identify the useful upper limit of τ_{CMT} and the maximum conversion of reactants to products

that occurs when the catalytic surface becomes reactant-starved. Faster rates of chemical reaction at higher temperature will produce more severe diffusion-controlled conditions because reactants cannot reach the catalytically active sites on the tube wall at a rate that is fast enough in comparison with the rate at which they are consumed. Typically, more conversion is achieved at higher temperatures when the apparent activation energy is positive in multiple-reaction sequences with rate-limiting steps. However, faster kinetics at higher temperatures create reactant-starved conditions closer to the tube inlet, and a larger fraction of the catalytic reactor is not useful to convert reactants to products when the rate law is described by zeroth-order kinetics. Since the time constant for radial diffusion toward the catalytic surface is not a strong function of temperature for liquids, the useful upper limit of τ_{CMT} is reduced from 60 seconds at 30^{0}C to 30 seconds at 50^{0}C. The corresponding final conversion of reactant A decreases from 50% at 30^{0}C to 33% at 50^{0}C. This is a consequence of mathematically simple, but conceptually difficult, zeroth-order rate laws that convert reactants to products faster at higher temperature when the surface is not reactant-starved. In this particular example, the slope of χ_A vs. τ_{CMT} is steeper at 50^{0}C relative to 30^{0}C, but the latter two-thirds of the reactor cannot convert reactants to products at 50^{0}C compared to the latter one-third of the reactor being extremely inefficient at 30^{0}C. This analysis suggests that the two curves (actually linear relations) for χ_A vs. τ_{CMT} intersect when $\tau_{CMT} \approx 40$ seconds. The reactor operating at 50^{0}C already achieved 33% conversion at $\tau_{CMT} = 30$ seconds and the catalytic surface has been reactant-starved for the last 10 seconds. The reactor operating at 30^{0}C continues to convert reactants to products at a slower rate for an additional 20 seconds (i.e., beyond $\tau_{CMT} = 40$ seconds) because surface molar densities of reactants have not vanished at the point of intersection.

Page#857 Third line of **Problem 30-8**; reactor without external mass transfer resistance (i.e., $\alpha = 0$)

A few more problems on the last few pages of Chapter#30; **Problem 30-12**

Zeroth-Order Chemical Kinetics in Packed Catalytic Tubular Reactors; With and Without Interpellet Axial Dispersion

Consider the differential design equation for packed catalytic tubular reactors with zeroth-order chemical kinetics. When interpellet axial dispersion is negligible at large mass transfer Peclet numbers, one must solve the following 1st-order dimensionless ODE;

$$Pe_{MT} \frac{d\Psi_{A,ideal}}{d\zeta} = -E(\Lambda_{A,\text{int}ra})\left\{1-\varepsilon_{p,\text{int}er}\right\}\Lambda^2_{A,\text{int}er} \qquad (1)$$

subject to the boundary condition that the dimensionless molar density $\Psi_{A,ideal}$ of reactant A under ideal conditions is, by definition, unity at the reactor inlet where ζ=0. Since the reaction rate is independent of molar density for zeroth-order chemical kinetics, equation (1) is valid for ideal tubular reactors in which external mass transfer resistance is included or neglected, provided that the catalytic surface is not starved of reactants. If the product of the effectiveness factor, the catalyst filling factor, and the interpellet Damköhler number on the right side of equation (1) is denoted by Ω;

$$\Omega = E(\Lambda_{A,\mathrm{int}ra})\left\{1-\varepsilon_{p,\mathrm{int}er}\right\}\Lambda^2_{A,\mathrm{int}er} \qquad (2)$$

then the solution to equation (1) is;

$$\Psi_{A,ideal} = 1-\left\{\frac{\Omega}{Pe_{MT}}\right\}\zeta \qquad (3)$$

When interpellet axial dispersion is important at low mass transfer Peclet numbers, the differential design equation for nonideal reactors corresponds to a 2nd-order ODE;

$$Z = \frac{d\Psi_{A,nonideal}}{d\zeta}$$

$$\frac{dZ}{d\zeta} = Pe_{MT}Z + E(\Lambda_{A,\mathrm{int}ra})\left\{1-\varepsilon_{p,\mathrm{int}er}\right\}\Lambda^2_{A,\mathrm{int}er} \qquad (4)$$

The homogeneous analytical solution for the dimensionless axial reactant concentration gradient in nonideal reactors is;

$$Z_{\mathrm{hom}ogeneous} = \left\{\frac{d\Psi_{A,nonideal}}{d\zeta}\right\}_{\mathrm{hom}ogeneous} = C_1\exp\left(Pe_{MT}\zeta\right) \qquad (5)$$

The particular solution, which is the same as the complete axial concentration gradient in ideal packed catalytic tubular reactors with zeroth-order kinetics, is;

$$Z_{particular} = \left\{\frac{d\Psi_{A,nonideal}}{d\zeta}\right\}_{particular} = -\frac{\Omega}{Pe_{MT}} \qquad (6)$$

The Danckwerts boundary condition in the exit stream (i.e., Z=0 when ζ=1) is satisfied when;

$$C_1 = \frac{\Omega}{Pe_{MT}} \exp\left(-Pe_{MT}\right) \qquad (7)$$

The final expression for the dimensionless axial reactant concentration gradient in nonideal reactors is obtained by adding the homogeneous and particular solutions for Z;

$$Z = \left\{\frac{d\Psi_{A,nonideal}}{d\zeta}\right\} = -\frac{\Omega}{Pe_{MT}}\left\{1 - \exp\left[-Pe_{MT}(1-\zeta)\right]\right\} \qquad (8)$$

Equation (8) is integrated analytically to obtain the molar density profile of reactant A for zeroth-order chemical kinetics in nonideal packed catalytic tubular reactors in which interpellet axial dispersion is important. If the catalytic surface is not starved of reactants, then the following expression is valid when external mass transfer resistance is either included or neglected, because reactant molar density does not appear in the rate law for zeroth-order kinetics;

$$\Psi_{A,nonideal}(\zeta) = C_2 - \frac{\Omega}{Pe_{MT}}\left\{\zeta - \frac{1}{Pe_{MT}}\left[\left\{\exp\left(Pe_{MT}\zeta\right) - 1\right\}\exp\left(-Pe_{MT}\right)\right]\right\} \qquad (9)$$

The boundary condition at the reactor inlet governs the value of integration constant C_2 in equation (9). For example, if one employs the definition of dimensionless reactant molar density, which requires that $\Psi_{A,nonideal}$ = 1 at ζ = 0, then C_2 = 1. However, the Danckwerts boundary condition at the reactor inlet (i.e., interpellet axial dispersion is important for ζ > 0, but it is nonexistent prior to the inlet plane) suggests that;

$$\Psi_{A,nonideal}(\zeta = 0) - \frac{1}{Pe_{MT}}\left\{\frac{d\Psi_{A,nonideal}}{d\zeta}\right\}_{\zeta=0} = 1 \qquad (10)$$

Now;

$$C_2 = 1 - \frac{\Omega}{Pe_{MT}^2}\left\{1 - \exp\left(-Pe_{MT}\right)\right\} \qquad (11)$$

The final expression for the reactant molar density profile, that satisfies Danckwerts boundary conditions at the inlet and outlet, is;

$$\Psi_{A,nonideal}(\zeta) = \Psi_{A,ideal}(\zeta) - \frac{\Omega}{Pe_{MT}^2}\left\{1 - \exp\left[-Pe_{MT}(1-\zeta)\right]\right\} \qquad (12)$$

If one evaluates equations (3), (9), and (12) in the exit stream (i.e., ζ=1) and compares the final conversion of reactant A {i.e., 1 – $\Psi_A(\zeta=1)$} for real and ideal packed catalytic tubular reactors with zeroth-order chemical kinetics, then the following results are obtained;

(1) If $\Omega \leq Pe_{MT}$, then Ω/Pe_{MT} represents the final conversion that one should achieve under ideal conditions via equation (3) when the mass transfer Peclet number is larger than its critical value, such that interpellet axial dispersion is negligible. Reactants have not been consumed completely and mass transfer resistance between the bulk fluid phase and the external surface of the catalyst is not an important factor for reactor design.

(2) Equation (12) indicates that *nonideal* reactors which satisfy both Danckwerts boundary conditions achieve the same final conversion (i.e., at ζ=1) that is predicted by the ideal design equation.

(3) Equation (9) suggests that *nonideal* reactors which satisfy the Danckwerts boundary condition in the exit stream and the ideal reactor boundary condition at the inlet, based on the definition of dimensionless reactant molar density, achieve less conversion than ideal reactors, because $\Psi_{A,nonideal}(\zeta=1)$ is larger than $\Psi_{A,ideal}(\zeta=1)$;

$$\Psi_{A,nonideal}(\zeta = 1) = \Psi_{A,ideal}(\zeta = 1) + \frac{\Omega}{Pe_{MT}^2}\left\{1 - \exp\left(-Pe_{MT}\right)\right\} \qquad (13)$$

When the mass transfer Peclet number is *large enough* (i.e., larger than its critical value that increases at higher interpellet Damköhler numbers), the second term on the right side of Equation (13) is negligible and the PFR behaves ideally.

Addendum: Zeroth-order kinetics in non-ideal heterogeneous catalytic tubular reactors with mass transfer resistance

Modify the previous analysis of heterogeneous catalysis in *nonideal* plug-flow tubular reactors with expensive metal catalyst coated on the inner wall (i.e., r=R_{PFR}) of the flow channel and significant mass transfer resistance for *zeroth-order* kinetics. There are no porous pellets packed in this "tube-wall" reactor. Consider the realistic situation where the

catalytic surface is *reactant-starved* in the diffusion-limited regime at large values of the Damköhler number relative to the mass transfer Peclet number or, analogously, small chemical reaction time constants relative to the time constant for convective mass transfer (i.e., residence time τ_{CMT}). Formulate a reactor design strategy to calculate the realistically useful upper limit for τ_{CMT} and the corresponding final conversion of reactants to products that should be expected for non-ideal PFRs that obey (i) Danckwerts boundary conditions at the inlet and outlet, vs. (ii) the ideal boundary condition at the inlet and the Danckwerts boundary condition in the exit stream.

Answer:

For specific numerical values of the mass transfer Peclet number and all three important mass transfer time constants discussed in *Problem 30-7(j),* numerical techniques are required to calculate the critical value of the dimensionless axial coordinate $\zeta_{critical}$ at which the molar density of reactants vanishes on the catalytic surface. When non-ideal PFRs obey Danckwerts boundary conditions at the inlet and outlet, the bulk molar density profile for reactant A is given by Equation (12) in *Problem 30-12 when the effectiveness factor is unity and the catalyst filling factor is not an issue*;

$$\Psi_{A,bulk}(\zeta) = 1 - \frac{\Lambda_A^2 \zeta}{Pe_{MT}} - \frac{\Lambda_A^2}{Pe_{MT}^2}\left\{1 - \exp\left[-Pe_{MT}(1-\zeta)\right]\right\}$$

In terms of the ideal PFR boundary condition at the inlet and the Danckwerts boundary condition in the exit stream, the non-ideal bulk molar density profile for reactant A is given by Equation (9) with C_2=1 in *Problem 30-12 when the effectiveness factor is unity and the catalyst filling factor is not an issue;*

$$\Psi_{A,bulk}(\zeta) = 1 - \frac{\Lambda_A^2 \zeta}{Pe_{MT}} + \frac{\Lambda_A^2}{Pe_{MT}^2}\left[\left\{\exp\left(Pe_{MT}\zeta\right) - 1\right\}\exp\left(-Pe_{MT}\right)\right]$$

The steady state balance between the rate of radial diffusion of reactant A toward the catalytic surface, expressed via Fick's first law of diffusion using *mass-transfer-coefficient* formalism, and the rate of consumption of reactants via heterogeneous catalysis, where each rate process has dimensions of moles per *area* per time was considered in *Problem 30-7(j).* Hence, the relations between surface and bulk molar densities for reactant A are given below in dimensional and dimensionless form;

$$C_{A,surface}(z) = C_{A,bulk}(z) - \frac{k_{0,surface}}{k_{A,MTC}}$$

$$\Psi_{A,surface}(\zeta) = \Psi_{A,bulk}(\zeta) - \frac{\Theta_{RadialDiffusion}}{\lambda_{ChemRx}}$$

The critical dimensionless axial coordinate in the flow direction $\zeta_{critical}$ (= $z_{critical}/L_{PFR}$) is calculated from the previous dimensionless equation for surface molar density, such that $\Psi_{A,surface}(\zeta_{critical})=0$. The appropriate nonlinear equations, whose positive roots are desired, can be expressed as;

$$(i);1 - \frac{\Lambda_A^2 \zeta_{critical}}{Pe_{MT}} - \frac{\Lambda_A^2}{Pe_{MT}^2}\left\{1 - \exp\left[-Pe_{MT}(1-\zeta_{critical})\right]\right\} - \frac{\Theta_{RadialDiffusion}}{\lambda_{ChemRx}} = 0$$

$$(ii);1 - \frac{\Lambda_A^2 \zeta_{critical}}{Pe_{MT}} + \frac{\Lambda_A^2}{Pe_{MT}^2}\left[\left\{\exp\left(Pe_{MT}\zeta_{critical}\right) - 1\right\}\exp\left(-Pe_{MT}\right)\right] - \frac{\Theta_{RadialDiffusion}}{\lambda_{ChemRx}} = 0$$

where the ratio of the Damköhler number to the mass transfer Peclet number (i.e., Λ^2_A/Pe_{MT}) is equivalent to the ratio of the residence time τ_{CMT} to the time constant for zeroth-order chemical reaction λ_{ChemRx}. The following trends are appropriate for zeroth-order kinetics in non-ideal PFRs with significant mass transfer resistance. The catalytic surface is reactant-starved when $0 \le \zeta_{critical} \le 1$, which implies that the latter section of the reactor cannot convert reactants to products even though reactants are present in the bulk fluid phase. An efficient reactor design strategy corresponds to $L_{PFR} \le z_{critical}$, or $\zeta_{critical} \ge 1$, because reactants are never totally depleted on the catalytic surface within the reactor. Hence, an important design criterion identifies physically realistic ranges for the dimensionless numbers (i.e., Λ^2_A and Pe_{MT}) and mass transfer time constants where $\zeta_{critical} \ge 1$ in the previous two equations that characterize the surface molar density of reactants in non-ideal PFRs, subject to two different sets of split boundary conditions. $\zeta_{critical}$ decreases and approaches zero, which is extremely undesirable, when (i) the Damköhler number increases, (ii) the mass transfer Peclet number decreases, (iii) the residence time τ_{CMT} increases, (iv) the chemical reaction time constant λ_{ChemRx} decreases, and (v) the time constant for radial diffusion $\Theta_{RadialDiffusion}$ increases. When $\Theta_{RadialDiffusion}$ is comparable to, or greater than, λ_{ChemRx}, the previous two equations reveal that non-ideal heterogeneous catalytic tubular reactors with zeroth-order kinetics cannot convert reactants to products. For example, when $\Theta_{RadialDiffusion} = \lambda_{ChemRx}$, equation (ii) predicts $\zeta_{critical}=0$ and equation (i) predicts $\zeta_{critical}<0$. This situation must be avoided.

Problem 30-13

A packed catalytic tubular reactor (radius R_{PFR} and length L_{PFR}) contains porous spherical catalysts (radius R_{sphere}) and operates at the following values of the important dimensionless numbers that govern reactor performance. The reaction kinetics are second-order irreversible (i.e., n = 2) and the rate law depends only on the molar density of reactant A on the external surface of the catalyst [i.e., $k_2(C_{A,surface})^2$].

Intrapellet Damkohler number (characteristic length is R_{sphere}), $\Lambda^2_{A,intrapellet} = 4$
Interpellet Damkohler number, $\Lambda^2_{A,interpellet} = 14$
Mass transfer Peclet number, $Pe_{MT} = 3$
Simple particle-based Peclet number, $Pe_{simple} = 50$
Interpellet porosity, $\varepsilon_{p,interpellet} = 0.5$

(a) Predict reactant conversion in the PFR exit stream.

Answer:

Calculate the chemical reaction coefficient = $(1-\varepsilon_{p,interpellet})\Lambda^2_{A,interpellet}E \approx 5$ (actually 4.97). Then, use Table 30-1 on page#841 for a non-ideal reactor [i.e., Pe_{MT} is 10-fold smaller than $(ReSc)_{critical} \approx 30$] with significant external mass transfer resistance because $\alpha \approx 2.5$. Based on the definition of dimensionless reactant molar density, final conversion is given by $\chi_{final} = 1 - \Psi_{A,BulkGas,real}(\zeta=1) = 20\%$ (i.e., 0.20).

(b) Explain why it is or is not possible to obtain an analytical solution to the ideal reactor problem with second-order irreversible chemical reaction [i.e., $k_2(C_{A,surface})^2$] and significant external mass transfer resistance.

Answer:

With assistance from the appropriate variable transformations and integration tables, it might be possible to integrate the ideal mass transfer equation analytically. However, numerical methods are the "technique of choice" because one must relate $C_{A,Surface}$ and $C_{A,BulkGas}$ via a quadratic equation when the external resistance to mass transfer is significant. Then one requires $C^2_{A,Surface}$ to account for the rate of disappearance of reactant A via second-order chemical kinetics in the mass balance.

(c) The reactor length is tripled (i.e., three-fold increase in L_{PFR}) while maintaining the same pellet packing density. How do the five dimensionless numbers listed in the problem statement above change?

Answer:

The particle-based dimensionless numbers are not affected by an increase in the length of the reactor. Hence, the intrapellet Damkohler number, the effectiveness factor, and the particle-based mass transfer Peclet number do not change. The interpellet porosity of the

packed bed remains constant according to the problem statement. The mass transfer Peclet number scales as L_{PFR} and the interpellet Damkohler number scales as the square of L_{PFR}. If reactor length increases by a factor of 3, then Pe_{MT} = 9 (i.e., increases by a factor of 3) and $\Lambda^2_{interpellet}$ = 126 (i.e., increases by a factor of 9).

(d) Does α, the dimensionless number that governs the importance of external mass transfer resistance, increase, decrease, remain unchanged, or is it too difficult to determine how α changes for second-order irreversible kinetics when the reactor length increases by a factor of three?

Answer:

There is no change in α, which remains constant at a numerical value of 2.5 as the reactor length increases by a factor of 3. In general, α is independent of reactor length. Equation (30-76) on page#841 reveals that α scales as the ratio of the chemical reaction coefficient to the square of the mass transfer Peclet number. The chemical reaction coefficient is directly proportional to the interpellet Damkohler number. Hence, both the chemical reaction coefficient and the square of the mass transfer Peclet number scale as L^2_{PFR}, yielding no dependence of α on L_{PFR}. There are no other dimensionless numbers in the definition of α in equation (30-76) that depend on $L_{PFR.}$

(e) Predict conversion in the exit stream of an ideal PFR after the three-fold increase in reactor length if the kinetics are 1st-order irreversible [i.e., $k_1 C_{A,surface}$], not 2nd-order. Do not neglect external mass transfer resistance.

Answer:

According to equation (30-61) on page#837, one predicts 77% final conversion for first-order irreversible chemical kinetics in ideal packed catalytic tubular reactors when external mass transfer resistance cannot be neglected. Alpha remains constant at 2.8 for first-order kinetics as L_{PFR} increases by a factor of 3. The only difference between α = 2.5 for second-order kinetics and α = 2.8 for first-order kinetics is due to the effectiveness factor in spherical catalytic pellets (E = 0.71 for n=2 vs. E = 0.81 for n=1 when $\Lambda^2_{A,intrapellet}$ = 4).

(f) The volumetric flowrate is tripled (i.e., three-fold increase in q) while maintaining the same pellet packing density. How do the five dimensionless numbers listed in the problem statement above change?

Answer:

The intrapellet Damkohler number and the effectiveness factor are not affected by a change in volumetric flowrate. According to the problem statement, the interpellet porosity of the packed bed remains constant. The other three dimensionless numbers change. The particle-based mass transfer Peclet number increases by a factor of 3 because it is defined in terms of the average interstitial fluid velocity between the catalytic pellets. As Pe_{simple} increases from 50 to 150, the correlation coefficient that relates interpellet axial dispersion

to Pe_{simple} increases from 1 to 2. Hence, the mass transfer Peclet number decreases by a factor of 2, from 3 to 1.5, because the interpellet axial dispersion coefficient appears in the denominator of Pe_{MT}. There is no other effect of flowrate on Pe_{MT} because the interstitial fluid velocity in the dimensional scaling factor for convective mass transfer (i.e., in the numerator of Pe_{MT}) cancels the effect of an increase in flowrate on the interpellet axial dispersion coefficient. Since interpellet axial dispersion coefficients increase by a factor of 6 (i.e., 3-fold increase in the interstitial fluid velocity and a 2-fold increase in the correlation coefficient from the dimensional analysis of *flow through porous media*), the interpellet Damkohler number decreases from 14 to 2.33 when the volumetric flowrate triples.

(g) Does α, the dimensionless number that governs the importance of external mass transfer resistance, increase, decrease, remain unchanged, or is it too difficult to determine how α changes for second-order irreversible kinetics when the volumetric flowrate increases by a factor of three?

Answer:

Since α is proportional to β, equations (30-57), (30-62) and (30-63) reveal that an increase in volumetric flowrate causes the mass transfer coefficient to increase as the gas-phase resistance decreases in the boundary layer external to the catalytic pellets. Both α and β decrease as the external mass transfer resistance decreases at higher gas-phase volumetric flowrate. Interpellet axial dispersion coefficients scale linearly with q via their dependence on the interstitial fluid velocity between the catalytic pellets, and interpellet Damkohler numbers scale inversely with q. In the creeping flow regime, mass transfer coefficients in the gas-phase boundary layer scale as the one-third power of the particle-based Reynolds number, which includes the interstitial fluid velocity. Equation (30-76) on page#841 reveals that α scales as $q^{-1/3}$ for creeping flow. Hence, if q increases 3-fold, then α decreases by $3^{1/3}$, or 1.4, which agrees with the actual decrease in α from part (h), even though the correlation coefficient for interpellet axial dispersion from *flow in porous media* increases from 1 to 2 when the volumetric flowrate triples and the particle-based mass transfer Peclet number increases from 50 to 150.

(h) Predict conversion in the exit stream of an ideal PFR after the three-fold increase in volumetric flowrate if the kinetics are 1st-order irreversible [i.e., $k_1 C_{A,surface}$], not 2nd-order. Do not neglect external mass transfer resistance.

Answer:

According to equation (30-61) on page#837, one predicts 19% final conversion for first-order irreversible chemical kinetics in ideal packed catalytic tubular reactors when external mass transfer resistance cannot be neglected. Reactant conversion is governed primarily by a 3-fold decrease in residence time. Alpha actually decreases from 2.8 to 2.0 when the kinetics are first-order irreversible and the volumetric flowrate triples. This agrees with $\alpha \approx q^{-1/3}$.

(i) The spherical pellet diameter is reduced by a factor of two (i.e., two-fold decrease in R_{sphere}) while maintaining the same pellet packing density. How do the five dimensionless numbers listed in the problem statement above change?

Answer:

Both the particle-based and vessel-based dimensionless numbers are affected when the size of the pellets changes. The interpellet porosity remains unchanged, according to the problem statement. Since the intrapellet Damkohler number scales as the square of the pellet radius, a 2-fold decrease in R_{pellet} produces a 4-fold decrease in $\Lambda^2_{intrapellet}$ from 4 to 1, and a corresponding increase in the effectiveness factor from 0.71 to 0.89 as summarized in Table 18-1 on page#488 for second-order irreversible chemical kinetics. Since particle diameter for spherical catalysts represents the characteristic length in Pe_{simple}, the particle-based mass transfer Peclet number decreases 2-fold from 50 to 25, and the correlation coefficient for interpellet axial dispersion remains constant at $\varphi_{correlation} = 1$. The mass transfer Peclet number scales inversely with particle size, so Pe_{MT} increases 2-fold from 3 to 6. Interpellet axial dispersion coefficients scale linearly with particle size, so a 2-fold decrease in pellet diameter produces a 2-fold decrease in interpellet axial dispersion coefficients and a corresponding 2-fold increase in the interpellet Damkohler number from 14 to 28.

(j) Does α, the dimensionless number that governs the importance of external mass transfer resistance, increase, decrease, remain unchanged, or is it too difficult to determine how α changes for second-order irreversible kinetics when the spherical catalytic pellet size is reduced by a factor of two?

Answer:

Equation (30-76) on page#841 reveals an approximate dependence of α on particle size. This is only an estimate of how α depends on $d_{equivalent}$ because the effectiveness factor scales inversely with $d_{equivalent}$ only in the diffusion-limited regime (i.e., $E \approx 1/\Lambda_{intrapellet}$) at large values of the intrapellet Damkohler number. In general, interpellet axial dispersion coefficients scale linearly with $d_{equivalent}$ and the mass transfer Peclet number scales inversely with $d_{equivalent}$. Hence, in the diffusion-limited regime, the chemical reaction coefficient scales inversely with $d^2_{equivalent}$ via the effectiveness factor and the interpellet Damkohler number. Now, the effects of $d_{equivalent}$ on α via the chemical reaction coefficient and the mass transfer Peclet number cancel [see equation (30-76)] and the only remaining dependence of α on $d_{equivalent}$ is due to the particle-based mass transfer Peclet number, so $\alpha \approx (d_{equivalent})^{2/3}$ because Pe_{simple} scales linearly with $d_{equivalent}$. When particle size decreases by a factor of 2, the previous scaling law in the diffusion-limited regime suggests that α decreases by $2^{2/3}$, or 1.6. If one neglects the effect of particle size on the effectiveness factor in the extreme reaction-rate-controlled regime at very small values of the intrapellet Damkohler number (i.e., $E \approx 1$, isothermally), then the chemical reaction coefficient scales inversely with $d_{equivalent}$

via the interpellet Damkohler number, the ratio of the chemical reaction coefficient to Pe^2_{MT} scales linearly with $d_{equivalent}$, and $\alpha \approx (d_{equivalent})^{5/3}$. When particle size decreases 2-fold, this scaling law suggests that α decreases by $2^{5/3}$, or 3.2. Actual calculations for first-order irreversible kinetics in part (k) indicate that α decreases by a factor of 2.8, from 2.8 to 1.0, when $d_{equivalent}$ decreases 2-fold, the intrapellet Damkohler number $\Lambda^2_{intrapellet}$ decreases 4-fold, and the effectiveness factor increases from E = 0.81 when $\Lambda^2_{A,intrapellet} = 4$ to E = 0.94 when $\Lambda^2_{A,intrapellet} = 1$.

(k) Predict conversion in the exit stream of an ideal PFR after the two-fold decrease in size of the spherical catalytic pellets if the kinetics are 1st-order irreversible [i.e., $k_1 C_{A,surface}$], not 2nd-order. Do not neglect external mass transfer resistance.

Answer:

According to equation (30-61) on page#837, one predicts 66% final conversion for first-order irreversible chemical kinetics in ideal packed catalytic tubular reactors when external mass transfer resistance cannot be neglected. Alpha decreases from 2.8 to 1.0 when the kinetics are first-order irreversible and the diameter of the catalytic pellets decreases by a factor of two. The actual scaling law is somewhere between $\alpha \approx (d_{equivalent})^{5/3}$ at small intrapellet Damkohler numbers, and $\alpha \approx (d_{equivalent})^{2/3}$ at large intrapellet Damkohler numbers, which is consistent with the fact that $\Lambda^2_{intrapellet} = 1$.

(l) The tubular reactor diameter is doubled (i.e., two-fold increase in R_{PFR}) while maintaining the same pellet packing density. How do the five dimensionless numbers listed in the problem statement above change?

Answer:

The intrapellet Damkohler number and the effectiveness factor are not affected by a change in reactor diameter. According to the problem statement, the interpellet porosity of the packed bed remains constant because the pellet packing density does not change. The particle-based mass transfer Peclet number decreases 4-fold, from 50 to 12.5, because the average interstitial fluid velocity is 4-fold smaller if the volumetric flowrate remains constant and the flow cross-sectional area experiences a 4-fold increase. In this range of Pe_{simple}, the correlation coefficient that relates interpellet axial dispersion to Pe_{simple} does not change, and neither does the mass transfer Peclet number. Since the average interstitial fluid velocity experiences a 4-fold decrease, so does the interpellet axial dispersion coefficient, which causes the interpellet Damkohler number to increase by a factor of four, from 14 to 56, when the reactor diameter is doubled.

(m) Does α, the dimensionless number that governs the importance of external mass transfer resistance, increase, decrease, remain unchanged, or is it too difficult to determine how α changes for second-order irreversible kinetics when the reactor diameter increases by a factor of two?

Answer:
The primary reason that α increases is due to the fact that the average interstitial velocity decreases when the flow cross-sectional area increases and the volumetric flowrate remains constant. A few important dimensionless numbers are affected by $\langle v_z \rangle_{interstitial}$. The interpellet Damkohler number and the chemical reaction coefficient increase by a factor of four, due to a 4-fold decrease in the interpellet axial dispersion coefficient when $\langle v_z \rangle_{interstitial}$ decreases by a factor of four. The particle-based mass transfer Peclet number also decreases by a factor of four. The mass transfer resistance increases in the external gas-phase boundary layer when the interstitial fluid velocity decreases. In the creeping flow regime, mass transfer coefficients scale as the one-third power of the particle-based Reynolds number, which includes the interstitial fluid velocity. This effect is accounted for by the dependence of the particle-based Sherwood number on Pe_{simple} for creeping flow around submerged objects. Equation (30-76) on page#841 reveals that α scales as $(R_{PFR})^{2/3}$ for creeping flow, via consideration of the effect of R_{PFR} on the chemical reaction coefficient, or the interpellet Damkohler number, and Pe_{simple}. Hence, if R_{PFR} increases 2-fold, then α increases by $2^{2/3}$, or 1.6, which agrees with the actual increase in α from part (n), below.

(n) Predict conversion in the exit stream of an ideal PFR after the two-fold increase in reactor diameter if the kinetics are 1st-order irreversible [i.e., $k_1 C_{A,surface}$], not 2nd-order. Do not neglect external mass transfer resistance.

Answer:
According to equation (30-61) on page#837, one predicts 75% final conversion for first-order irreversible chemical kinetics in ideal packed catalytic tubular reactors, primarily because residence time increases by a factor of four with significant external mass transfer resistance. Part (e) above reveals that ideal packed catalytic tubular reactors achieve 77% conversion when L_{PFR} triples, which corresponds to a 3-fold increase in residence time with α = 2.8 and first-order irreversible kinetics. Relative to part (e), this example indicates that one achieves slightly less conversion (i.e., 75%) when residence time increases 4-fold because alpha increases from 2.8 to 4.5 when R_{PFR} is doubled. This agrees with $\alpha \approx (R_{PFR})^{2/3}$. Equation (30-76) on page#841 describes how α depends on some important dimensionless parameters that govern the performance of packed catalytic tubular reactors. The correlation is exact in the creeping flow regime. Several examples in this multi-part problem reveal an equivalent creeping-flow scaling law for α in terms of some important dimensional parameters, as discussed above;

$$\alpha \approx \frac{R_{PFR}^{2/3} d_{equivalent}^{\gamma}}{q^{1/3}} \neq f\left(L_{PFR}\right)$$

$$\frac{2}{3} < \gamma < \frac{5}{3}$$

where the exponent γ is a decreasing function of the intrapellet Damkohler number. For example, γ is slightly less than 5/3 when $\Lambda_{A,intrapellet}$ approaches zero in the extreme reaction-rate-controlled regime, and γ = 2/3 at very large values of the intrapellet Damkohler number in the diffusion-controlled regime where the effectiveness factor scales inversely with $\Lambda_{A,intrapellet}$.

References

Page#861 last reference on the page; Carslaw, H. S. , and ...

Page#863 Nijemeisland, M., and A. G. Dixon (2001). *Chemical Engineering Journal*, **82**, 231.

Index